Doctoral theses at NTNU, 2023:413

Krister Leonart Haugen

Scalable Regenerative Power Converters for Accelerator Magnets

Applications for high energy physics at CERN

Doctoral thesis

NTNU
Norwegian University of Science and Technology
Thesis for the Degree of Philosophiae Doctor
Faculty of Information Technology and Electrical Engineering
Department of Electric Power Engineering

NTNU
Norwegian University of Science and Technology

Krister Leonart Haugen

Scalable Regenerative Power Converters for Accelerator Magnets

Applications for high energy physics at CERN

Thesis for the Degree of Philosophiae Doctor

Trondheim, December 2023

Norwegian University of Science and Technology
Faculty of Information Technology and Electrical Engineering
Department of Electric Power Engineering

NTNU
Norwegian University of
Science and Technology

NTNU
Norwegian University of Science and Technology

Thesis for the Degree of Philosophiae Doctor

Faculty of Information Technology and Electrical Engineering
Department of Electric Power Engineering

ISBN 978-82-326-7526-5 (printed ver.)
ISBN 978-82-326-7525-8 (electronic ver.)
ISSN 1503-8181 (printed ver.)
ISSN 2703-8084 (online ver.)

Doctoral theses at NTNU, 2023:413

Printed by NTNU Grafisk senter

Abstract

Electromagnets are used at The European Centre for Nuclear Research (CERN) in high-energy physics experiments to direct the charged particle beams. They store significant amounts of energy in the magnetic fields and are cycled on and off with a cycling period in the order of seconds. Powerful power converters with peak power capability 10 times larger than the average power usage are used to push the electromagnet's energy in and out of the magnet before and after the physics operations. The loads having a significant amount of energy which can be recovered, and the cycling nature of the load and the long operating times, resulting in millions of thermal cycles for these devices.

This PhD thesis explores the possibilities of scalable converters for cycling electromagnetic loads with energy recovery. The thesis introduces the concept of a modular converter with separated storage and demonstrates how it can be used in a scalable way to achieve scalability in how the converter is configured and operated. It contains an investigation into the cost optimal design and a control structure for the converter's controller to handle the separated storage. The fundamental building modules, refereed to as bricks, can either be connected to the grid or to separate energy-storage components.

Splitting the converter in to bricks with separated energy storage can enhance the flexibility of the system by scaling for storage requirements, power capabilities and grid connecting more independently. By doing a sweep of the different semiconductor power modules, storage units and output voltages the cost optimal combination of such a converter has been investigated. By expanding the calculations to include lifetime cost of operating the converters, SiC MOSFETs has a significant cost saving compared to the IGBTs currently used.

The proposed modular converter enables independent power flow control among the bricks and five different strategies have been demonstrated. They manage the power flow and optimise the usage of the power converters in terms of cost, efficiency, reliability and precision. Energy recovery into the energy storage takes place by redistributing the current during inductive load ramp-down.

The performance of the proposed modular converter is validated experimentally on a full-scale lab prototype rated at 800 kW. It is shown that up to 30% cost savings can be achieved by eliminating converter components in the storage and in the grid connection, while the converter performance on the load is maintained and the same amount of energy is recycled. A laboratory verification shows that the converter can operate with independent currents delivered from the bricks while respecting the total voltage and current reference and that the system can manage

the losses of the converter without compromising the performance of the converter. The various strategies allows the converter to operate with different modes, for example, optimal utilisation of the energy storage systems, minimised current stress in the semiconductors or minimising the installed grid capacity.

Acknowledgements

Thanks are given to my supervisors, Kostas and Dimos. Both for their advice and guidance, but also for their patience during the difficult years. Thanks also to Panos, as a co-supervisor, but mostly as a good colleague during the first years when we where working together. And to Manuel, for his support and interest.

Thanks also to my girlfriend, friends and family, for giving an alternative to work and grounding my understanding of the world in reality and reminding me what is important. Your presence in my life has been invaluable. The great adventure I embarked on was in the end not such an adventure.

Nullius in Verba.

"Ford, there's an infinite number of monkeys outside who want to talk to us about this script for Hamlet they've worked out."

– Hitchhikers Guide to the Galaxy

This page is intentionally left blank.

This page was an accident.

Abbreviations and Symbols

BESS	Battery Energy Storage System
CERN	European Organisation for Nuclear Research
DAB	Dual-Active Bridge, a device providing galvanic isolation through a high-frequency link
DSP	Digital Signal Processor
ESS	Energy Storage System
FGC	CERN Function Generation Controller
IGBT	Insulated-Gate Bipolar Transistor
LHC	Large Hadron Collider
MMC	Modular Multilevel Converter
MOSFET	Metal–Oxide–Semiconductor Field-Effect Transistor
SiC	Silicon Carbide
SIRIUS	System for rapId Regulation with Internal controlled Unit of energy Storage, the CERN converter which the experiments were based on
SoC	System on a Chip
TT	Abbreviation used at CERN to denote Transfer lines between storage rings, sources and experiments
V_{mag}	Voltage across the electromagnet
I_{mag}	Current through the electromagnet
V_{bus}	Bus voltage on the converters internal DC-bus
V_{flat}	Flat-top voltage of the trapezoidal load current
I_{flat}	Flat-top current of the trapezoidal load current
L_{mag}	Inductance of the electromagnet
R_{mag}	Resistance of the electromagnet
$t_{flat-top}$	Duration of the flat-top for the trapezoidal load current

t_{rise} Duration of the ramp-up or rise-time for the trapezoidal load current

t_{fall} Duration of the ramp-down or fall-time for the trapezoidal load current

Contents

Chapter 1

Introduction

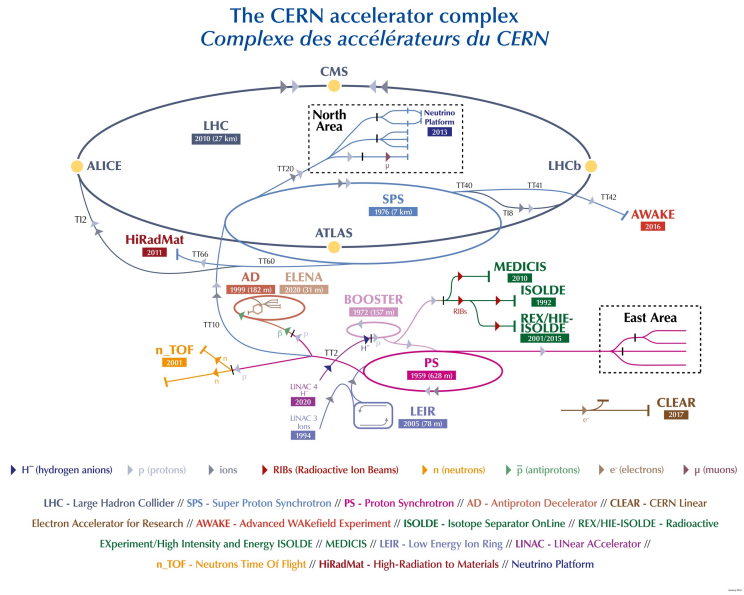

Figure 1.1: The CERN accelerator complex, layout in 2022.

The scientific accelerator complex at CERN for high energy physics consists of several storage rings, particle sources and experiments, all interconnected by transfer lines. An overview of the CERN Accelerator complex as of 2022 is presented in Figure 1.1. These lines are designed to deliver a specific magnetic field to accommodate the transfer of the particle beams, depending on the energy of the particular beam. These magnetic fields are created by sending currents to the electromagnets

in the transfer lines, these magnets are considered hot in the context of CERN, i.e. they are not cooled down to have superconducting properties.

The force used to control these particles is known as Lorentz Force, it can be derived from Maxwell's Equations and is presented in Equation 1.1 in a practical vector form. The electromagnetic force $\vec{F}$ on a charge depends on the charge q, the electric field vector $\vec{E}$, the velocity vector $\vec{v}$ and the magnetic field $\vec{B}$. This is the fundamental principle that the accelerator complex is built on.

$$\vec{F} = q(\vec{E} + \vec{v} \times \vec{B}) \tag{1.1}$$

The magnetic field is constructed with electromagnets where the field strength is determined by the current density in the coil winding and the number of turns. In Equation 1.2 the original form of Amperes Law is presented, where $\vec{B}$ is the magnetic field, μ_0 is the vacuum magnetic permeability and $\vec{J}$ is the current density in the coil winding.

$$\vec{\nabla} \times \vec{B} = \mu_0 \vec{J} \tag{1.2}$$

This PhD thesis focuses on the power electronic converters supplying the current to these electromagnets, and in particular to a sub-set of the hot electromagnets in the transfer lines between the storage rings and experimental areas. Hot magnets refer to non-super-cooled and non-super-conducting magnets.

1.1 Objectives

The primary objective of this PhD thesis is to propose a method for the design and operation of scalable power converters for supplying high-precision current to the accelerator magnets and recovering the energy at every cycle. The converter should allow for safe and stable operation on par with or exceed existing solutions. The main requirement, set out at the beginning of this research, is for the new converter topology to have a modularised approach and control the energy flow. Which enables the separation of function of supplying losses and cycling the stored energy. This enhances the ability to adapt to different loads and consequently to different ratios of peak to RMS power ratings and can thus be considered more scalable. These sub-modules, referred to as bricks, aim to both work in series, to increase voltage, and in parallel, to increase current.

The primary objective can be separated into the following sub-objectives:

1. Cost-effective scalable design. By having a brick with a simple design, it is

possible to keep maintenance simple and allow low-cost design on a large scale. The design should also allow for high utilisation of the capabilities of the converter, such as the storage elements.

2. Energy flow control scheme to allow for adapted operation. This is essential to allow the converter with separated storage to operate in an optimised way. It will also allow the system to utilise the capabilities of the converter better.

3. Show that utilisation of Silicon Carbide (SiC) Metal–Oxide–Semiconductor Field-Effect Transistor (MOSFET) modules can be cost-effective on a system level across multiple loads. The reduced losses will reduce the requirements on the cooling infrastructure, and the potentially increased switching frequency can give benefits for applications which require very high accuracy.

4. Re-use as much of the existing CERN's component designs as possible. To keep time to deployment low and compatibility with existing circuits as much as possible.

Potentially, this modular and scalable design could use a large number of sub-modules, which enables:

- A relatively low voltage rating for each module.
- It can utilise interleaving to improve output current ripple.
- High efficiency from transistor switching, such as Silicon Carbide (SiC) MOSFETs.
- Incorporate redundancy by having extra modules built-in and in the event of a module failure the failed module can be bypassed and replaced instantly.

This research has built on existing experience and knowledge of the power converters group (EPC) at CERN. A number of design objectives such as the standardisation of power bricks, the lifetime preservation by low thermal stressing of semiconductors and the several cost constraints have been kept in mind throughout the research, while a new direction such as the technical and economic impact of Silicon Carbide semiconductors in a large scale project has been examined.

1.2 Organisation of the thesis

The thesis is paper-based. The first chapter gives an introduction to the scientific objectives and contributions of the PhD project. The second chapter introduces

CERN and the electromagnets that the converters described in this thesis will work with. In particular, the electromagnets used in the CERN North Area, see Figure 1.1, have been used as reference magnets for the design and development work in this thesis. The third chapter gives a background on the state-of-the-art of converters with energy storage and converters used for high-energy physics.

The fourth chapter introduces the papers this thesis is based on, the scientific contribution of each paper and some relevant background and context on the thesis.

For the design of a power converter with energy recovery operation, a trade-off is related to the choice of the output and dc-link voltages, which, in turn, determines the choice of the blocking voltage capability of the semiconductor switches. In Section 4.1.2 it is shown how considering the purchasing and operating costs separately can yield different conclusions. It also highlights the effect of high precision requirements on the converter scalability and final cost. The concept has been demonstrated in a full-scale converter, presented in Section 4.1.4, and the benefits of using interleaving and increasing the switching frequency have been discussed in Section 4.1.6.

In Section 4.2.1 the full-scale prototype is introduced and used to demonstrate a method and an experimental setup of an energy management control scheme for controlling the energy flow in a modular and scalable DC/DC converter. The converter has a more scalable topology based on a fundamental building block and features energy recovery capabilities. The overall design configuration, control and optimised electrical operation are presented and tested. This constitutes a method for using the internal flexibility of a modular converter to achieve flexibility in operation. The concept has been demonstrated in a full-scale converter, presented in Section 4.2.2.

By combining the internal and external scalability, a more scalable and flexible converter for efficient maintenance is proposed. Incorporating modularised storage for increased safety, and also gives the converter a topology where a strategy of redundancy is more obtainable, which increases the availability of the system and enables the possibility for swapping out parts of the converters without stopping the operation.

1.3 Scientific contributions

1.3.1 Selected articles

The thesis is based on the work presented in the following articles:

I. K. L. Haugen, K. Papastergiou, P. Asimakopoulos, and D. Peftitsis *On di-*

mensioning the fundamental brick for a scalable DC-DC converter with energy recovery. Submitted to European Conference on Power Electronics and Applications (EPE'21 ECCE Europe), September 2021.

II. K. L. Haugen, K. Papastergiou, and D. Peftitsis *A scalable DC/DC converter topology with modularised energy storage for high energy physics applications.* Published by IEEE Journal on Emerging and Selected Topics in Power Electronics, April 2023.

III. K. L. Haugen, K. Papastergiou, P. Asimakopoulos, and D. Peftitsis, *High precision scalable power converter for accelerator magnets.* Published by Journal of Instrumentation, March 2022.

IV. K. L. Haugen, K. Papastergiou, P. Asimakopoulos, and D. Peftitsis *Energy flow control in a modular DC-DC converter with energy recovery.* Submitted to International Symposium on Power Electronics for Distributed Generation Systems (PEDG), June 2021.

V. K. L. Haugen, K. Papastergiou, and D. Peftitsis, *Adaptive system control of a modular converter with energy storage to optimise for different key metrics.* Submitted to IET Power Electronics for review, September 2023.

The results and main findings in these articles will be presented in Chapter 4.

1.3.2 The author's contribution to the selected articles

The author has performed the following work for each selected publication:

I. Haugen has developed the optimal procedure, and the Python script used for the calculations, primary writing of the paper and presentation at the conference. Dr. Papastergiou and Dr. Asimakopoulos have contributed detailed knowledge of the existing systems, providing scientific guidance and feedback on the manuscript. Prof. Peftitsis has provided scientific guidance and feedback on the manuscript.

II. Haugen has developed the controller, set up the lab experiment and carried out the experiments and primary writing of the paper. Haugen has also done the cost calculations and post-processing of the laboratory data. Dr. Papastergiou has contributed a detailed knowledge of the existing systems, providing scientific guidance and feedback on the manuscript. Prof. Peftitsis has provided scientific guidance and feedback on the manuscript.

III. Haugen has set up the converter designs, simulation models and completed the simulation results, primary writing of the paper and presentation at the

conference. Dr. Papastergiou and Dr. Asimakopoulos have contributed detailed knowledge of the existing systems, providing scientific guidance and feedback on the manuscript. Prof. Peftitsis has provided scientific guidance and feedback on the manuscript.

IV. Haugen has developed the controller to be compatible with the existing control structure and enable the new control of power flow. He has also found the four proposed strategies, set up the simulation models and completed the simulation results, primary writing of the paper and presentation at the conference. Dr. Papastergiou and Dr. Asimakopoulos have contributed detailed knowledge of the existing systems and provided scientific guidance and feedback on the manuscript. Prof. Peftitsis has provided scientific guidance and feedback on the manuscript.

V. Haugen has developed the controller, set up the lab experiment and carried out the experiments and primary writing of the paper. Haugen has also done the post-processing of the laboratory data. Dr. Papastergiou has contributed a detailed knowledge of the existing systems, providing scientific guidance and feedback on the manuscript. Prof. Peftitsis has provided scientific guidance and feedback on the manuscript.

1.3.3 Scientific contribution of the thesis

Based on the work presented in this thesis, the main scientific contribution of the thesis is highlighted here:

1. A scalable power converter for supplying high-precision current to the accelerator magnets and recovering the energy. The converter allows for safe and stable operation on par or exceeding existing solutions. Published in Paper I, II and III.

2. A method to find the most cost-effective switching technology and electrical characteristics of the proposed converter design for a given group of highly inductive cycling loads, including lifetime cost and other external targets. Published in Paper I.

3. Energy flow control scheme to allow for adapted operation of the scalable converter, increasing the utilisation of the hardware in an optimised way. Published in Paper VI and Paper V.

Chapter 2

Background

In this PhD thesis, the converter concept is combined with a substantial collection of large electromagnets and it aims to find the optimum balance between the usage of the capabilities of the individual components and the total system. The thesis develops a method for identifying the optimum current and voltage level for a new type of scalable power converters for high energy physics. The experiments considered in this thesis require a large current, in the range of 50-2000A in time scales varying from 1s pulses up to continuous DC-current. In order to supply a large number of different-sized electromagnets with different ratios of inductance to resistance (L/R-ratio) the desire is to have a power converter which is easily re-configurable and can utilise the optimum technology at any given time. At the same time, the number of converters in use requires the converters to have a strong similarity in order to enable easy maintenance and availability of parts.

- Best possible utilisation of semiconductor ratings
- Best possible utilisation energy storage capacitors
- Minimise investment and operation cost of power conversion at project level
- Allow scalability for wide range of peak/RMS output current
- Standardise a fundamental building block regardless of function (grid supply/storage bricks)

In this chapter, the converters currently in use at CERN, their load profiles and the connected electromagnetic loads are introduced. The first section covers the existing converters for high energy physics, then the load profile of the current pulse

is described, followed by an overview of the electromagnets and their parameters. The chapter ends with a short descriptions of the recent trends for power converters at CERN, showing where the inspiration for a modular and scalable converter is coming from.

2.1 Converters for high energy physics

The converters have two primary functions, firstly they must deliver a high-precision current with ppm accuracy in a reliable and repeatable way. Secondly, they should minimise the electricity consumption, both for environmental reasons and reduction in running costs such as electricity and cooling costs.

Some critical conditions for meeting these requirements is an ability to deliver current pulses to a wide range of electromagnets inductance and resistance following a given current ramp and level [1]. This forces a current and voltage to be supplied to each load independently. In addition, important considerations that are relevant to this PhD thesis are minimal downtime, ease of maintenance, long lifetime (20 years minimum), galvanic isolation between electromagnets and ability to withstand grid under/over-voltages. Naturally, there are many more requirements applicable, but they do not have an impact on the design at this development level, generally these overarching requirements will be simply referred to as the *CERN framework*. More details on relevant figures of merit have been discussed in [2].

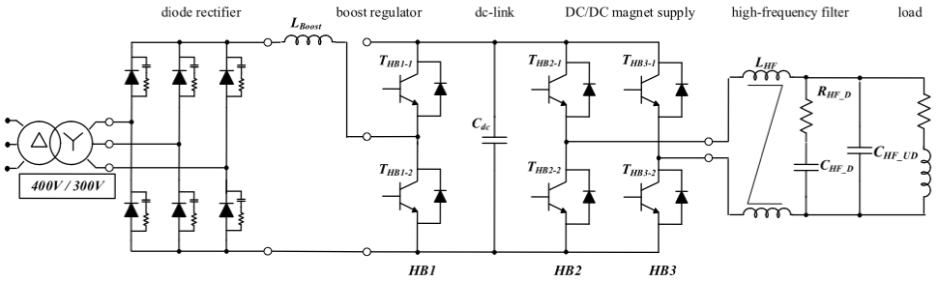

Figure 2.1: Circuit diagram of a current CERN power converter (SIRIUS).

The current converters supplying the loads considered in this thesis are comprised of 3 fundamental components in order to comply with all the given requirements of the application. A complete schematic of a present converter can be found in Figure 2.1. Working backwards from the output these components can be described as the following:

1. In order to supply the pulsed current, the converters should be able to deliver both positive and negative DC voltage while supplying a positive cur-

rent, thus the converters are based on a four-quadrant design using H-bridges to control the power delivered to the load as shown in Figure 2.2. The H-bridges also enable the precise control of the current required for the magnets [3]. In order to get the current accuracy in the ppm range, active filters are often used. The H-bridge is an important part of the overall converter cost and is part of the core of this PhD thesis.

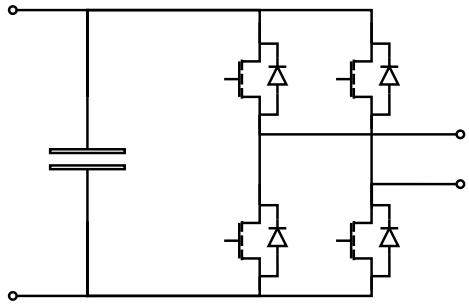

Figure 2.2: Output stage: H-bridge.

2. Inside the converters there is a DC-bus, which can be supplied by a DC-DC converter from the front-end, such as a boost-converter as shown in Figure 2.3. The boost DC-DC converter allows the complete converter system to operate even if the grid voltage is somewhat lower than the nominal, ensuring the operation is independent of the grid voltage quality (except blackouts). An energy storage solution can be connected to the DC-bus. This allows the converter to recover the energy stored in the magnetic field as the current pulse is ramped down, which in turn can be reused in the following cycle when the current is ramped up. This energy transfer process is referred to here as *power cycling*. This power flow poses several technical challenges [4]. Energy storage is an important part of the scalability of the converter and will be discussed further in the thesis.

3. The last part of the converter is the front-end shown in Figure 2.4, connecting the converter to the grid and supplying the power to the converter. The front-end is normally where the galvanic isolation requirement is preserved, as each magnet must be galvanically insulated from each other. This is typically utilising a 3-phase transformer per converter followed by a 3-phase diode rectifier.

Traditionally functions 1-3 are all met by each converter individually, the converter is designed to be functioning ideally from the perspective of a single converter

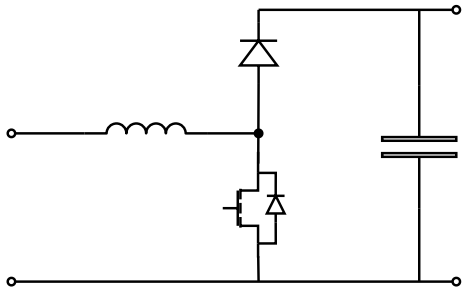

Figure 2.3: DC-bus: Energy storage and DC-DC booster.

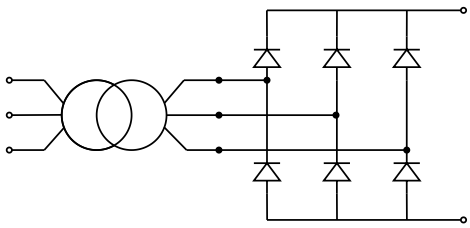

Figure 2.4: Front-end: Transformer and Diode rectifier.

given the constraints and the available switching technology. In order to ensure good availability of parts and ease of use, CERN desires only a single type of converter to be used for a given power range. This results in a functional converter, that has only one current and voltage level for the magnet. If a higher current or voltage is required, the converters have to be parallel or series connected respectively, or indeed both if the application requires higher voltage and current simultaneously. If any series or parallel connection is made, the converter is always scaled with the full capabilities of functions 1-3, even if only a higher capability in one of them was required. Inversely, if the current or voltage required is lower than the converter can deliver only a fraction of the capability is utilised.

Starting from the first principles the two primary functions of the power converter are separated and investigated, and from that the 3 parts of the converter are reassembled with scalability as a requirement. By separating the grid from the storage, the boost stage can be omitted. The functionality of this scalable power converter is demonstrated by simulation and different types of assembly are discussed. Then the scalable power converter is used as the basis for the calculations for choosing the optimum switches, storage and brick voltage level given various optimisation targets on a given family of electromagnets.

2.2 Current supplied to the electromagnets

The current supplied to the magnets can be broadly divided into 3 categories based on their duration. For all types the current starts at zero and at a certain time will ramp up, with some requirement on the total time this should take, referred to here as rise-time ($t_{rise-time}$), followed by a flat-top ($t_{flat-top}$) where the operation is essentially a DC-current mode. The duration of this part is what primarily separates the different types of pulses. The current level during this phase is known as the flat-top current (I_{flat}). The current is then ramped down to zero in a controlled manner, again with some requirement on the total time this should take ($t_{ramp-down}$) before the magnet is held at zero current until the end of the period (t_{pulse}). Combined these three intervals represents one cycle, which is followed by the next cycle. The duration of each cycle and the current at flat-top can be combined in different ways based on the application into a super-cycle, but for the simplicity of this discussion, the cycles will be kept identical if more than one is used. An example of one such current pulse is shown in Figure 2.5. And a table showing the typical load parameters for the loads from a recent consolidation project is presented in Table 2.1.

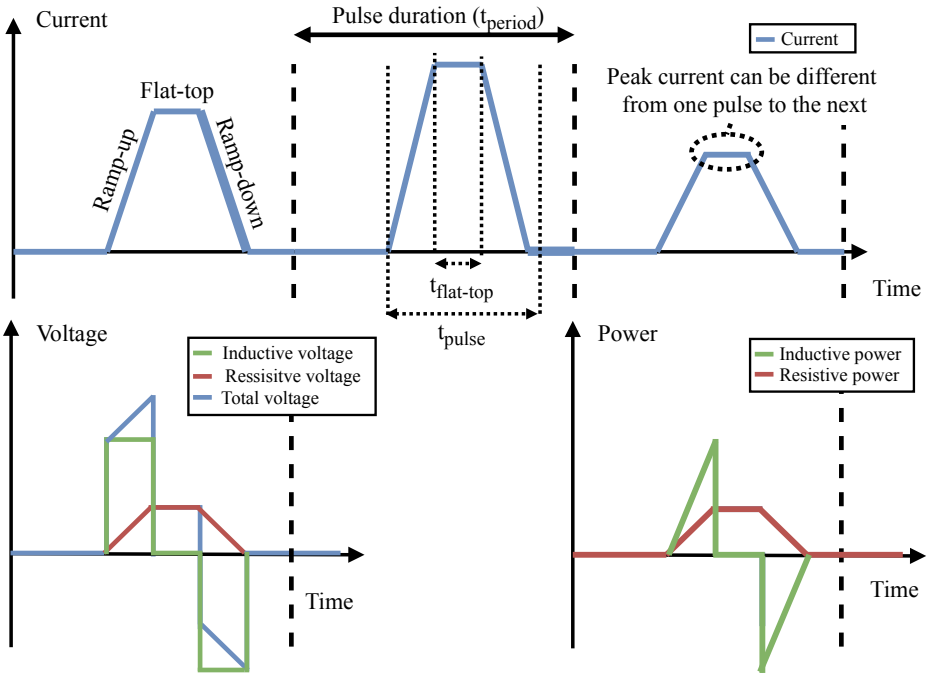

Figure 2.5: Example of pulsed current reference for the power converters, including the corresponding voltage and power.

The 3 types of pulsed current used by these types of converters are as follows:

1. Short pulses, the flat-top is less than 1s, typically in the range of 100ms. The total cycle time is in the range of 1-2s and typically 1.2s, with the ramp-up and ramp-down times typically in the range of 200ms. Figure 2.5 shows the general shape of such a cycle.
2. Medium pulses, the flat-top is now increased to 5s up to 10s, while total cycle time is 15-45s. The ramps are often the same as for the short pulses but can be larger if this is beneficial for the converter or the H-B magnetic curve in the electromagnet.
3. DC-mode, for some applications the magnets are supplied with a continuous current. In these applications, the considerations for ramps and energy recovery can be neglected.

A specific example and the calculations necessary to obtain the voltage for a given current reference are presented in Appendix A.1.

2.3 On the electromagnets

The electromagnets (or just magnets) used as the basis for the calculations in this PhD thesis are collected from a variety of families of magnets and application types. They all have in common the range of current required to supply them.

Figure 2.6 shows a plot of some of the magnet's total resistance (R_M) in Ohms and the total magnet inductance (L_M) in Henry's as a scatter plot. Each point is represented by a blob, where the blob size is the maximum current required during operation for each magnet. In this exemplary plot in total 350 magnets from the CERN North Area are considered. The variety of load characteristics and mission profiles shown in this figure, are the very reason for researching on scalable converter designs.

The energy stored in the magnets is given by Equation 2.1.

$$E_{magnet} = \frac{1}{2} L_{magnet} I^2_{magnet} \tag{2.1}$$

From the plot in Figure 2.6 some basic inferences can be observed. Since the maximum operating current can be assumed to be the flat-top of the current pulse, the blob size indicates both the total magnetic energy and the voltage required during the flat-top. The magnetic inductance in this data set is from 4mH to 2.9H and the resistance is from 0.02-1.7Ω, where the highest value is only a single

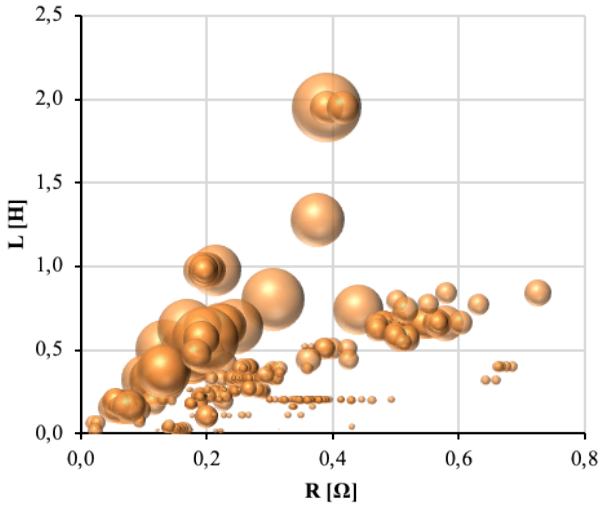

Figure 2.6: Scatter-plot of inductance and resistance for each electromagnet, with maximum current as the blob-size.

magnet at 2.9H and 2.7Ω which is not shown in the plot. The R to L ratio for these magnets are between 0.2 and 25, and the total energy stored in the magnet's electric field is between 10kJ and 670kJ with a median energy of about 20kJ.

2.4 Recent trends at CERN

Prior to the CERN LHC era, when accelerators were still relatively small machines, the power converters used to supply the electromagnets were in the past designed for each magnet individually, or as a type of converter for a relatively small magnet family. As the CERN accelerator complex has expanded with different magnets targeting different uses, a large number of very similar converters have been developed over time. Since the basic operating principles are the same, they typically have many of the same features, yet they might have small differences in their implementation. This has resulted in a challenge for operational stability, both to retain specific knowledge and competence to service and operate the converters over several decades and to keep sufficient stocks of spare parts.

Thus, the current trend has been to standardise the converters as much as possible and to consolidate as many converters as possible using a single converter family. This makes keeping spares and training technical staff a more reasonable task and has the added benefit of reducing costs through increased manufacturing numbers. It also enables a greater accumulation of experiences and ensures that the

Parameter	Typical values	Minimum	Maximum
Max current	450 A	50 A	1950 A
Current rise-time	300 ms		
Current fall-time	200 ms		
Restive load	200 mΩ	20 mΩ	1680 mΩ
Inductive load	130 mH	4 mH	2310 mH
Peak voltage	315 V	15 V	691 V
Peak power	150 kW	20 kW	800 kW
Recoverable energy	13.2 kJ	0.045 kJ	704 kJ

Table 2.1: Typical parameters for the load requirements at CERN North Area and TT20

converters have higher reliability.

The first standardisation exercise from 2000 to 2020 resulted in modular designs (such as various LHC converters; the SIRIUS family and others). The next standardisation wave is expected to add scalability to the modular design by adapting individually the energy storage capacity, the grid connection ratings and by control software. The standardisation has left the converters with a lot of oversizing, as the 3 functions mentioned in Section 2.1 are limited to a few discrete values depending on the type of function. If for example more grid power is needed, the only option is to add more storage and output current capability as well.

In addition to the trends in power electronics hardware, a recent trend is also to consolidate the control functions of the control electronics into a single System on a Chip (SoC). This will allow for greater signal integration, the converter will no longer have separated control functions in different hardware and limits in signal bandwidth and the number of signals will be reduced. Moreover, it will allow the converter to take more parameters into account when being controlled, such as the State-of-Charge of the energy storage components, energy stored in the magnet, future energy availability and various temperatures. Finally, it will free up more computing power, which will allow for more sophisticated algorithms to take all these parameters into account and enable higher switching frequencies to be used.

Bibliography

[1] B. L. M. Lamaille, F. Dragoni, S. Evrard, F. J. Harden, E. Harrouch, M. Lazzaroni, R. Lopez, and K. D. Papastergiou, "Study of the Energy Savings Resulting From the East Area Renovation," *10th Int. Partile Accelerator Conferance*, pp. 4023–4025, 2019. ISBN: 9783954502080.

[2] S. Maestri, R. G. Retegui, D. Carrica, S. Rossini, G. Le Godec, and K. Papas-

tergiou, “Figures of merit for the evaluation of regenerative power converters,” *2016 18th European Conference on Power Electronics and Applications, EPE 2016 ECCE Europe*, pp. 1–9, 2016. Publisher: Jointly owned by IEEE-PELS and EPE Association ISBN: 9789075815245.

[3] G. Kniegl, R. Weber, F. Bordry, and A. Dupaquier, “Four-quadrant converter [±600 A, ±12 V] prototype for LHC,” in *Proceedings of the IEEE Particle Accelerator Conference*, vol. 5, pp. 3740–3742, IEEE, 1999.

[4] P. Asimakopoulos, K. Papastergiou, T. Thiringer, M. Bongiorno, and G. Le Godec, “On Vce Method: In Situ Temperature Estimation and Aging Detection of High-Current IGBT Modules Used in Magnet Power Supplies for Particle Accelerators,” *IEEE Transactions on Industrial Electronics*, vol. 66, no. 1, pp. 551–560, 2019.

Chapter 3

Topologies, components and important considerations for converters with energy storage

Converters with Energy Storage Systems (ESS) combine switch mode circuits with electrical energy storage. These converters can either have the storage integrated into the converter or provide an interface between the storage and the rest of the system [1], enabling the converters to take a more active role in the grid [2]. Rather than just control for a voltage level, they can act as grid forming converters, controlling the frequency [3], act as voltage quality regulators (STATCOM) or compensate for longer-term power imbalance [4, 5, 2, 6].

The latter is generating a lot of interest in later years, as the grid is increasingly relying on renewable energy sources [7]. Such sources tend to be intermittent and more or less unpredictable [8], thus there has to be the ability for compensation in the grid to allow for a stable grid operation. This is a key requirement to ensure the successful integration of renewable energy sources into the grid [9], or in order to ease grid congestion [10, 11]. In more direct applications, such as automotive and traction, there is also a renewed interest in recycling the kinetic energy of the vehicle as the energy prices continue to increase [12, 13].

The converter topology presented in this thesis have characteristic similar to a Modular Multilevel Converter (MMC) [14, 15], while taking advantage of a full bridge module to ensure 4-quadrant operation [16]. Using modular converters provides many benefits in terms of scalability [17, 18] and by combining ESS with modular converters, a more flexible system emerges [19]. A modular system of

converters allows for high accuracy and high current [20], an application which is very relevant to the experimental facilities at CERN. In principle, any number of storage types can be used for a converter with ESS, at present the most used remains batteries [21]. It is, however, possible to use other storage types, such as capacitors, mechanical flywheels [22, 23] or super-capacitors depending on the amount of stored energy required, delivered power and storage time. It is also possible to combine different types of storage, intro Hybrid Energy Storage Systems (HESS) for increased flexibility [21, 24].

The following section will cover the main types of converters utilising some form of energy storage and a number of the key technologies to design these converters such as power semiconductors and energy storage components, where many of these solutions are of relevance to CERN. A discussion of the converter topologies when used in the CERN framework is presented in Section 3.4.2.

3.1 Power converter topologies

3.1.1 Modular Multilevel Converters - MMC/M2C

An area of interest for the next generation of converters for CERN is to create a modularized design. This can offer redundancy and easy replacement of damaged converter parts. Initially, a modular multilevel converter (MMC) would be the perfect topology to achieve higher scalability for high power and medium-/high-voltage energy conversion systems [17, 25]. The MMCs have good voltage and current scalability and exhibits advantages such as transformerless operation, reduced filter size, a reduced ripple of the output current for AC outputs, high efficiency, and relatively low installation cost on redundancy [18].

However, using only half-bridge on the output does not have the 4Q operation capability and fault blocking capability of the current converters, so a possible topology for the converters at CERN is to use Modular Multilevel Converter (M2C) topology. Developments in high-power semiconductors have enabled them to perform comparable to more traditional power converter designs [26].

An M2C design comprises a series of modules, namely sub-modules (SM). SMs are made with 2 (half bridge) switches and a capacitor [26, 27]. The capacitor functions both as a filter and energy storage and these SMs are connected in series [14].

It is also possible to create combinations of different hybrid multilevel converters with H-bridges or half-bridges and combine them in different arrangements of SM branches in leg or phase [28].

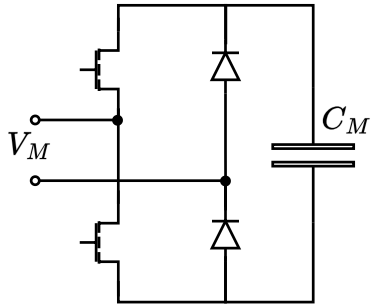

Figure 3.1: The Modular Multilevel Converter (MMC) sub-module, as proposed by [14].

This design gives several benefits which are of interest. Each SM acts as a voltage divider and is only subjected to a fraction of the total voltage. In principle the SM voltage V_m, see Figure 3.1, is the maximum converter voltage V_0 divided by the number of sub-modules n, see Equation 3.1. Allowing the SM to be assembled of relativity low voltage rated components. The independent voltage of each SM allows easy scalability with voltage and allows for built-in redundancy [25].

$$V_m = \frac{V_0}{n} \tag{3.1}$$

In this topology, the SMs can either be active (charge/discharge) or bypassed (inactive). In either case, all the current of the converter has to go through all the SMs, so they will contribute to the converter parasitic conductance and resistance, which is not desired in an inverter type application. Another disadvantage is that the capacitors can only be used in series or remain inactive, so for low voltage levels with many inactive SMs, the potential of the converter is not fully utilised. [25].

3.1.2 Modular Multilevel Series/Parallel Converter (M2SPC)

In an attempt to manage these disadvantages and provide better current delivery potential, [25] proposes a novel topology of M2C with possibilities of series and parallel connections. The topology with full-bridge for parallel connection capability is shown in Figure 3.2.

With two terminals, two going to each neighbour, the capacitor in the sub-module can now be connected in series or in parallel, depending on the operating needs [29]. Over time the SMs voltage on the capacitors tends to drift away from the expected given by Equation 3.1, resulting in a voltage difference between the two neighbours. In [25] the authors propose routinely connecting two SMs in parallel

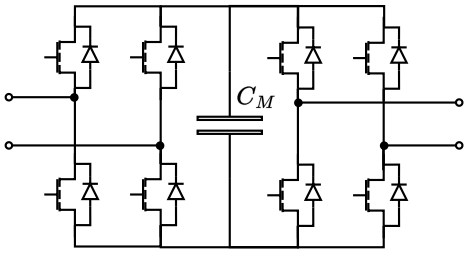

Figure 3.2: Modular Multilevel Converter (M2CPC) sub-module.

to equalise the voltage and minimise this instability, in order to avoid unexpected depletion or overloading of the capacitor.

The ability to connect SMs in parallel also enables the capacitors to be connected in parallel, providing more current. Unfortunately, this requires constant monitoring and calculations from the control interface. Several papers have built on this topology and proposed various strategies to adress these issues [30, 31, 32]. For example, in [30] the authors propose a strategy for controlling the M2SPCs which are distributed and can operate without voltage sensors.

3.1.3 Multiport converters and DAB

A multiport converter or power router is essentially a converter with more than two ports. This can be achieved either by a common DC bus or a common AC transformer. A typical AC transformer will have a solid-state transformer (SST) with three or more windings, enabling the power transfer. The Multiport converter will typically use a switching frequency above 5kHz, allowing the transformer to be relatively small, compact and efficient [33, 34, 35, 36, 37, 38]

A very interesting approach, which would have many benefits for CERN, is using Dual-Active Bridge (DAB) converters in combination with full bridge MMC as shown in Figure 3.3, similar to the method used in [39] to create an MMC with integrated battery storage. By replacing the transformer with an internal DAB, the galvanic isolation of the magnets is preserved, and the modules could more easily be adapted to different types of storage. High-efficiency switches with resonant operation would probably have lower losses than the existing solution, and the high-frequency transformer could facilitate a very compact design. In locations where the management of the generated heat is of high importance, a DAB-based design could utilise water cooling resulting in almost no ambient heat losses from the converter.

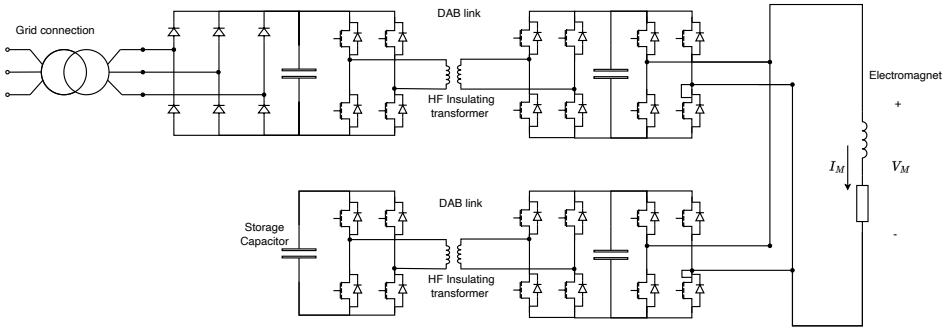

Figure 3.3: Dual Active Bridge based topology.

3.1.4 Multi-stage converter topologies

The following sections list a number of the potential grid-connected converter topologies. They can generally be divided into single and multi-stage converters. Some of these topologies use buck and some use boost DC converters, while the most flexible aim to combine the two [40]. Due to the many different needs of the operation, the power converters used to supply magnets at CERN are multi-stage.

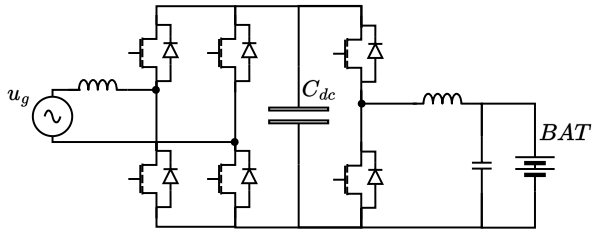

Figure 3.4: Topology of non-isolated on-board bidirectional charger composed of pulse width modulation (PWM) converter and bidirectional buck-boost DC-DC converter.

Figure 3.4 is a converter example used for a bidirectional connection. Such converters can be divided into isolated and non-isolated types, of which Figure 3.4 is the latter. It is composed of a single-phase Pulse Width Modulation (PWM) converter and a bidirectional buck-boost DC-DC converter. This topology uses fewer switches. However, without galvanic isolation, the safety of its operation is compromised.

Figure 3.5 depicts a topology composed of a single-phase PWM converter and cascaded buck-boost DC-DC converter. The cascaded buck-boost converter allows bidirectional energy flow and overlapping input and output voltage ranges. This topology is presented as a single stage, but the article [40] points to the fact that the

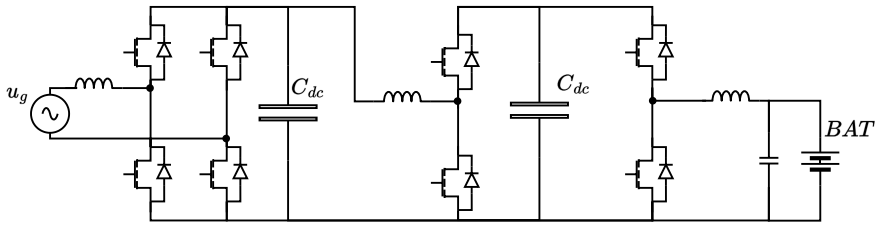

Figure 3.5: Topology of non-isolated on-board bidirectional charger composed of PWM converter and cascaded buck-boost DC-DC converter.

intermediate capacitor bank has made this into two stages, each one of which can act either as a buck or a boost converter. This enables the topology to have good voltage characteristics, that are useful in battery applications. However, the more complicated configuration leads to higher power losses compared to the topology shown in Figure 3.4.

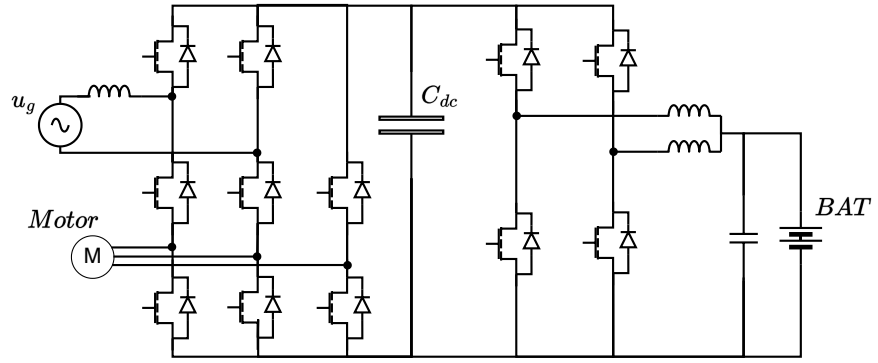

Figure 3.6: Topology of non-isolated integrated bidirectional charger composed of eight-switch inverter (ESI) and interleave DC-DC converter.

Figure 3.6 shows a much more complicated topology. In particular, this is an integrated bidirectional charger composed of an eight-switch inverter (ESI) and interleave DC-DC converter, integrating the DC-DC converter, on-board bidirectional charger, and DC-AC inverter together. This topology can act both as a three-phase DC-AC inverter or a single-phase PWM, making it a very flexible, but expensive solution, both in terms of cost and efficiency. This topology is also non-isolated and like the previous ones, a complex controller is required.

The most common method for obtaining galvanic isolation between the utility grid and the application, such as an energy storage device, is to use a transformer. Topologies as in Figure 3.4 can gain this functionality by introducing an insulating

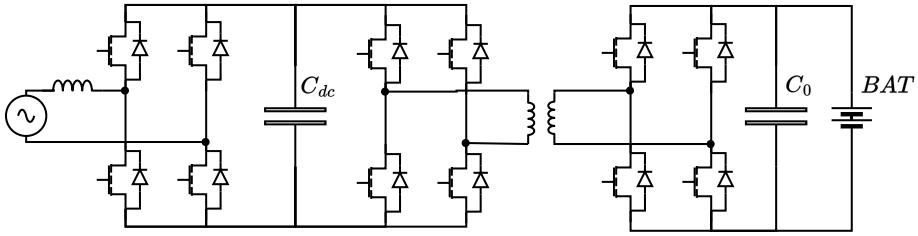

Figure 3.7: A two-stage topology composed of PWM converter and dual-active-bridge (DAB).

transformer, this will however increase volume, weight and noise significantly. By placing the transformer into the converter, it is possible to utilise a much higher transformer frequency by the use of PWM, enabling the galvanic isolation while keeping the transformer as small as possible. Figure 3.7 has taken a single-phase PWM AC-DC converter and connected it to a DAB high-frequency isolated DC-DC converter. The DAB converter has the insulating transformer placed in the middle, between the two H-bridges. The DC-DC part of this topology can be controlled by a phase shift control to achieve zero-voltage switching (ZVS), resulting in a resonant DAB. The lead and lag relationship between the two bridges, or the polarity of the phase shift angle, determines the direction of energy flow and the phase shift angle value controls the output power. Unfortunately, DAB converters have high input pulsating current, limited zero-voltage switching range under load variations, and high circulating current through devices and magnetics.

There are several other topologies are available [40], each new topology increases complexity and design requirements but makes important improvements, while there are always inherent trade-offs between adding functionality and keeping design and operations simple. A discussion of the converter topologies when used in the CERN framework is presented in Section 3.4.2.

3.2 Power semiconductors

The selection of power conductor technology has a profound impact on the performance of a power converter. Presently the IGBT and SiC MOSFET technologies are preferred for switch-mode power converters, due to their high-power handling capabilities, voltage controlled gate and high frequency spectrum. IGBTs are currently dominating in design of new power converters at CERN, due to the voltage blocking and current delivery capabilities being in line with the needs of the magnets.

As the SiC MOSFETs are maturing, and reaching similar voltage blocking and

current capabilities of the IGBTs, they also start to become a focus of interest for CERN, as they pose several significant advantages for CERN. This will be discussed in the following sections along with some critical considerations that have to be made when dimensioning a power converter for a high-energy physics pulsing converter.

3.2.1 IGBT - Insulated-Gate Bipolar Transistor

Insulated-Gate Bipolar Transistor (IGBT) is a well-established technology for switch-mode converters. IGBTs developed as a method to combine the low on-state losses of the Bipolar Junction Transistor (BJT) with the fast switching capability of the Metal–Oxide–Semiconductor Field-effect Transistor (MOSFET) [41].

They are built using a silicon wafer and are packaged into power modules, the specific methods used for the packaging have a great influence on the lifetime of the devices and are thus critical to consider when selecting a device. Silicon IGBT have well-known mechanical weaknesses [42] which are shown in Figure 3.8. The IGBT power modules offer advantages in high voltage and current ratings, combined with low on-state losses, making them interesting for many types of switch-mode converters. One important requirement that is decisive for the sizing of the power modules in a pulsed application is the ability to withstand power cycles. Power cycles cause heat generation in the silicon wafer during the on-phase, which results in temperature increase. While the temperatures drop down again during the off-phase. The temperature variation causes thermal expansion and contraction in the materials, which leads to mechanical stress that can result in failure. Increasing temperatures also leads to increased voltage drop across the collector-emitter of the device V_{CE}, as IGBTs has a positive temperature dependence [41]. Which in turn causes the power module to experience more losses and this results in higher V_{CE}. In applications where several IGBTs are connected in parallel, this leads to increased uneven distribution of the current between the modules. The module with the highest V_{CE} will also experience the highest losses, resulting in a higher delta temperature compared to the other modules and increasing the uneven stressing. Different materials have different coefficients of thermal expansion, and this adds stress to the interface between different materials. The relative forces and repeated contraction and expansion results in ageing of the device, eventually resulting in failure. The interfaces between the materials, in particular solder layers and bond-wires are the most exposed to these stresses. So lifting of bond wires and solder layer delamination are the predominant failure mechanisms in power cycling applications [42, 43], which has to be taken into account when designing for high-reliability requirements.

The details of the manufacturing process are often considered Intellectual Property

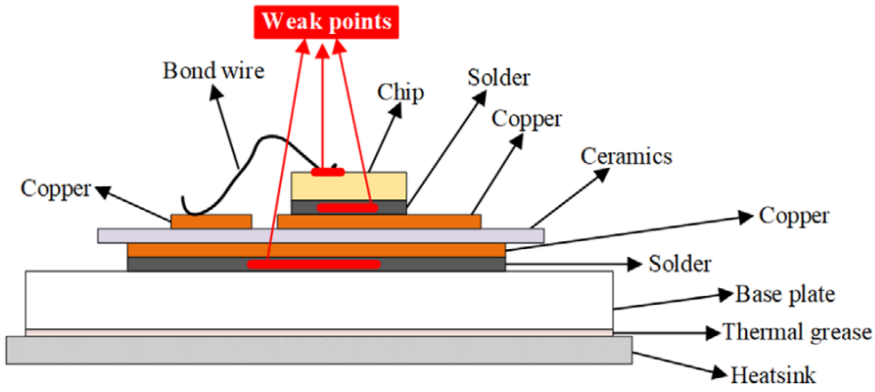

Figure 3.8: The weak point of a silicon IGBT, obtained from [42].

(IP) and are, therefore, not available to the customer, the manufacturers of IGBT often have well-documented datasheets that can be used to dimension the devices for their lifetime.

3.2.2 Silicon Carbide (SiC) Metal–Oxide–Semiconductor Field-effect Transistor (MOSFET)

The Silicon Carbide (SiC) Metal–Oxide–Semiconductor Field-effect Transistor (MOSFET) [41] exhibits several advantages over silicon based counterpart. The SiC material itself has inherently a higher electrical and thermal conductivity, as well as being a stronger and stiffer material compared to Silicon [44, 45]. These result in the SiC devices having lower on-state resistance in the wafer, even lower than that of the IGBT. Combined with the lower thermal resistance it can manage more dissipated heat and therefore manage higher current densities. The wider energy band-gap allows for the SiC to operate at higher temperature, while the the higher material stiffness makes the SiC more susceptible to cracking at these higher junction temperatures. The increased switching frequency capability of the SiC MOSFETs opens many opportunities in the design of high-power density converters [46].

It is expected that the SiC MOSFETs power modules will have similar weak points as silicon IGBT [47, 48] as shown in Figure 3.8. However, the package has different impacts on lifetime compared to that of Silicon [49] and so the lifetime models have to be updated to accurately predict the lifetime at lower temperature deltas ($< 40K$).

3.3 Energy storage

The electrical grid is always operated in a balance between the production and consumption of electric power. The grid itself does not have the ability to store energy. Traditionally the regulation of power balance has been achieved by taking advantage of the regulation capability of certain electricity production types, such as thermal electrical (coal, gas etc.) or dam-based hydro-power [50]. As the thermal electrical sources are to be phased out, and hydro-power generally has reached its full potential, the need for exploring other means of balancing production and consumption emerges. In recent decades significant efforts were made for the development of grid-scale energy storage systems for electric energy [51]. These technologies require normally power converters to interface them to the AC-grid, as they either have a variable frequency or are inherently DC devices [4].

Such converters and storage technologies are in the same power and energy range as the converters used to supply the electromagnets at CERN, and so they are relevant to such converters. In particular, the cycling of the magnets results in a very high peak power when the current is ramped [52]. The following sections give a brief overview of energy storage technologies that have been considered.

3.3.1 Capacitors

This thesis focuses on the use of capacitors to take advantage of their high-power capability and their ability to handle a large number of cycles ($\gg$ 1e6). Using capacitors introduces some challenges in the stored energy regulation since the energy is a function of the voltage. However, this also allows for relatively easy monitoring of the state of charge. The energy is stored in the electric field by accumulating charges on the electrodes, which is a very fast process, but the energy is limited by the field strength in the device.

Capacitors offer a very high peak power compared to stored energy [21]. And is therefore the type of energy storage primarily used at CERN for the magnets in the transfer lines and storage rings with warm magnets [52]. Typical applications considered in this thesis are ramping times of 200ms, and thus in order to take advantage of the installed energy, capacitors are beneficial.

3.3.2 Chemical storage - batteries

One of the most attractive means of storing electrical energy is to use batteries. In particular, Li-ion batteries in their various forms have been cited as one of the most critical components to enable the electrification of society and enable large amounts of intermittent power sources to be included in the grid [4].

Batteries are inherently a chemical process, where metals, such as Lithium are

oxidised to salt ions to release an electron producing the current from the battery during discharge. Since this is, in principle, a reversible process, then the same metals can be reduced back to their metal state during the charging process.

The optimal lifetime for a battery is currently in the range of 1C, where C is the charge rate required to charge the battery fully from empty in 1 hour. This sets a limit on the power capabilities of the batteries for any given amount of stored energy. For example a 1kWh battery can supply 1kW of peak power, assuming a discharge rate of 1C. While it is possible to operate batteries at 4C, this has negative impacts on lifetime and still limits the power ratio to 4, not the order of a power ratio of 10 the applications at CERN often require. Battery technology is under heavy development, and new solutions are sure to arrive that will improve batteries significantly in the coming years.

3.3.3 Mechanical storage - flywheels and pressure vessels

Mechanical storage has a higher power-to-storage ratio compared to batteries [4, 21], and can go as high as 10 or 100 for certain types of devices [22, 23].

Some technologies have emerged where the rotational speed of the flywheel is able to reach above 10 000RPM, giving the flywheels significantly increased specific energy density (kJ/kg) compared to previous versions of flywheels. Flywheels have also the ability to very rapidly deliver the stored energy and are generally limited by the interfacing power converter. A mechanical flywheel also has interesting safety advantages, and mechanical brakes can be used to completely remove any stored energy quickly and without the need for any electrical power of control in case of an emergency.

Another method considered mechanical energy, is to store energy using compressed air [4]. These systems have the same power limitations as flywheels, i.e. the size of the power converter running the compressor and the generator limits the power, not the technology itself. However, pressured air has very low volumetric power density, and is best suited if a large cavity already exists nearby, such as an abandoned mine or similar.

3.4 Technical considerations

3.4.1 System and production considerations

There are many points to the system requirements imposed on modern converter technologies [53]. The requirements in terms of low cost, high efficiency, high reliability, and tolerance over a wide range of input voltage variations have driven the converter development toward simpler topologies, lower component counts,

and tighter modular design.

The following list gives a summary of the main factors influencing development for modern PV inverters [53]:

- Component count. Fewer components give lower costs and higher operating efficiency, and often simpler components using hard switching which comes with the cost of harmonics which needs filtering.
- Input voltage range. To make topologies more flexible, the trend moves towards accepting a wide range of input and output voltages and the challenge is to keep the performance insensitive both to load and input variations.
- Higher switching frequency. The increasing switching frequency that reduces the size of energy storage elements and at the same time increases switching losses, is addressed by utilising resonant converters to achieve soft switching.
- Direct AC output, allowing for a wide range of DC-voltage levels, and connecting the converters directly to the grid, without the use of AC transformers.

All of these arguments are also applicable to grid-connected converters more generally and the converters operated at CERN. The various forms of potential energy storage, perhaps connected to the DC side, might result in a wide range of voltage and load profiles.

3.4.2 Topological variations

In the previous sections different topologies have been discussed. Utilising a multilevel converter topology enables the system to deliver a high output voltage while keeping the voltage level low on each sub-module. Such modularity would enable a single unit to be used across many applications, connecting more in parallel to increase the current capability and in series to increase the output voltage. However, strategies to deal with harmonics would have to be developed to avoid interference becoming too large for the system to handle. Presently, the converters at CERN aim to limit the number of switching devices used for each converter, as each switch represents a single point of failure. Any failure of a single device, whether it is an IGBT module, an inductor or a control card, could cause the complete CERN complex to stop and the beam will be dumped or inhibit a particular beam. While short term technical stops are tolerable, prolonged downtime due to maintenance is very costly for the organisation, and thus the goal is to move towards solutions where the number of failure points is kept as low as possible.

By having a number of relatively simple converters connected, perhaps as a combination of different types, the system also acquires the ability to include redundancy. If one of the components fails, by uncoupling the affected converter unit, the power could still be delivered, with a small reduction in capability compared to the initial mode. And such redundancy could easily compensate for the increased failure risk of a converter, yet this approach is not generally used for power converters at present.

This PhD thesis tries to move in the direction of simple topologies and uses a limited number of different types of devices and topologies. This standardisation will result in reduced utilisation of each component. However, this PhD thesis discusses a systematic approach to address the shortcomings of standardisation by taking advantage of the flexibility offered. By reducing the electrical rating of the devices, it is necessary to increase the number of identical devices, to maintain the overall power capability. The increased numbers of identical functioning devices can be operated slightly differently and at the same time respecting the total required output, and this flexibility gives some flexibility in control.

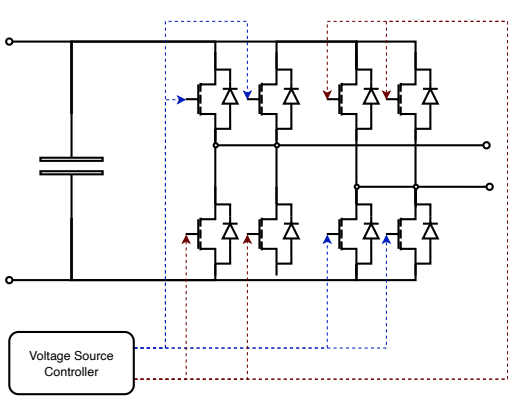

(a) Parallel connection of devices at switching position, requiring good signal synchronisation at higher switching frequencies.

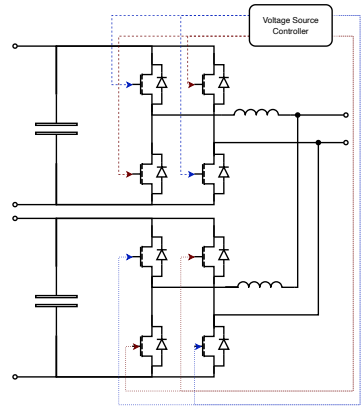

(b) Parallel connection of devices with bricks using a decoupling inductor.

Figure 3.9: Different approaches to increasing current capacity by parallel connecting devices.

Modularity often is considered to have many advantages, when multiple modules are parallel connected the challenge becomes to manage the simultaneous control of multiple devices. Rather than connecting devices in parallel at a single switching position, as shown in Figure 3.9(a), which can give challenges for the synchronisation of the gate drives at higher switching frequencies, this thesis fo-

cuses on an approach where the parallelisation is done at the brick level, such as in Figure 3.9(b). This allows the bricks to be controlled more independently by including a series inductance to disconnect the operation of the parallel connected devices. By parallel connecting at brick level it is possible to operate the brick with interleaving, which can be utilised to reduce the output ripple, while it can have some consequences for the circulation currents. Some approaches to deal with this are discussed more in Section 4.1.6.

3.5 Summary

The brief investigation of various power converter topologies for energy storage systems shows a large number of potential topologies with different strengths and weaknesses. From simple and reliable single-step converters to complex and flexible multi-stage converters, the possibilities for different combinations seem close to infinite. Selecting the right combination of topologies for a given set of constraints seems to be at the heart of the engineering challenge, and with such great flexibility, it is possible to optimise for different key metrics. By carefully selecting a good base, it is possible to construct a scalable converter where the complexity of maintenance is kept manageable and optimised for the lifetime cost of installation and operation.

Ultimately, the risk of failure associated with each component requires the design of power converters at CERN to go in the direction of proven reliable components and keep the total component number as low as possible. This results in a DAB being less desirable than a standard 3-phase 50Hz transformer despite many advantages for CERN. Therefore, the presented converter design is based on an H-bridge, similar to the present state-of-the-art, and a diode rectifier for AC-DC conversion with a grid-side transformer for galvanic isolation.

Bibliography

[1] I. Batarseh and K. Alluhaybi, “Emerging Opportunities in Distributed Power Electronics and Battery Integration: Setting the Stage for an Energy Storage Revolution,” *IEEE Power Electronics Magazine*, vol. 7, no. 2, pp. 22–32, 2020.

[2] M. Vasiladiotis and A. Rufer, “Analysis and control of modular multilevel converters with integrated battery energy storage,” *IEEE Transactions on Power Electronics*, vol. 30, no. 1, pp. 163–175, 2015. Publisher: IEEE.

[3] F. Errigo, L. Chedot, F. Morel, P. Venet, and A. Sari, “Modelling and Control of an MMC-HVDC Submodule with Energy Storage for Fast Frequency

Response," *2021 23rd European Conference on Power Electronics and Applications, EPE 2021 ECCE Europe*, 2021. ISBN: 9789075815375.

[4] J. M. Carrasco, L. G. Franquelo, J. T. Bialasiewicz, E. Galvan, R. C. Portillo Guisado, M. A. M. Prats, J. I. León, and N. Moreno-Alfonso, "Power-electronic systems for the grid integration of renewable energy sources: A survey," *IEEE Transactions on Industrial Electronics*, vol. 53, no. 4, pp. 1002–1016, 2006.

[5] P. Peng, Y. Li, Z. Li, Y. Shao, X. Luo, Y. Wang, and N. Zhang, "Analysis of Advantage of the Connection of Energy Storage System to Distribution Network and the Impact on the Voltage Quality," *2nd IEEE Conference on Energy Internet and Energy System Integration, EI2 2018 - Proceedings*, no. 1, pp. 2018–2021, 2018. Publisher: IEEE ISBN: 9781538685495.

[6] I. Stoppa, J. Lundin, N. Lima, and J. G. Oliveira, "Dual voltage/power system by battery/flywheel configuration," *2015 IEEE 13th Brazilian Power Electronics Conference and 1st Southern Power Electronics Conference, COBEP/SPEC 2016*, pp. 1–6, 2015. Publisher: IEEE ISBN: 9781479987795.

[7] A. Christopher, L. Fournié, M. Gabay, and H. de Sevin, "The role and need of flexibility in 2030: focus on energy storage," Tech. Rep. Study S07, European Commission, Directorate-General for Energy, Aug. 2016.

[8] I. Trintis, *Grid Converters for Stationary Battery Energy Storage Systems*. Department of Energy Technology, Aalborg University, 2011. Issue: September.

[9] S. Ould Amrouche, D. Rekioua, T. Rekioua, and S. Bacha, "Overview of energy storage in renewable energy systems," *International Journal of Hydrogen Energy*, vol. 41, no. 45, pp. 20914–20927, 2016. Publisher: IEEE ISBN: 9781467378949.

[10] T. M. Masaud, K. Lee, and P. K. Sen, "An overview of enrgy storage technologies in electric power systems: What is the future?," *North American Power Symposium 2010, NAPS 2010*, 2010. Publisher: IEEE ISBN: 9781424480463.

[11] S. A. Khan, M. R. Islam, Y. Guo, and J. Zhu, "A New Isolated Multi-Port Converter With Multi-Directional Power Flow Capabilities for Smart Electric Vehicle Charging Stations," *IEEE Transactions on Applied Superconductivity*, vol. 29, no. 2, pp. 1–4, 2019. Publisher: IEEE.

[12] Y. Yang, L. Dorn-Gomba, R. Rodriguez, C. Mak, and A. Emadi, "Automotive Power Module Packaging: Current Status and Future Trends," *IEEE Access*, vol. 8, pp. 160126–160144, 2020. Publisher: Institute of Electrical and Electronics Engineers Inc.

[13] S. Milovanovic, S. Strobl, P. Ladoux, and D. Dujic, "Hardware-in-the-Loop Modeling of an Actively Fed MVDC Railway Systems of the Future," *IEEE Access*, vol. 9, pp. 151493–151506, 2021.

[14] A. Lesnicar and R. Marquardt, "An innovative modular multilevel converter topology suitable for a wide power range," *2003 IEEE Bologna PowerTech - Conference Proceedings*, vol. 3, pp. 272–277, 2003. ISBN: 0780379675.

[15] G. J. Kish, "On the emerging class of non-isolated modular multilevel DC-DC converters for DC and hybrid AC-DC systems," *IEEE Transactions on Smart Grid*, vol. 10, no. 2, pp. 1762–1771, 2019. Publisher: IEEE.

[16] G. Kniegl, R. Weber, F. Bordry, and A. Dupaquier, "Four-quadrant converter [±600 A, ±12 V] prototype for LHC," in *Proceedings of the IEEE Particle Accelerator Conference*, vol. 5, pp. 3740–3742, IEEE, 1999.

[17] A. Dekka, B. Wu, R. L. Fuentes, M. Perez, and N. R. Zargari, "Evolution of Topologies, Modeling, Control Schemes, and Applications of Modular Multilevel Converters," *IEEE Journal of Emerging and Selected Topics in Power Electronics*, vol. 5, no. 4, pp. 1631–1656, 2017.

[18] M. N. Raju, J. Sreedevi, R. P. Mandi, and K. S. Meera, "Modular multilevel converters technology: A comprehensive study on its topologies, modelling, control and applications," *IET Power Electronics*, vol. 12, no. 2, pp. 149–169, 2019.

[19] M. Parchomiuk, R. Strzelecki, K. Zymmer, and A. Domino, "Modular power converter topologies for energy storage and electric power distribution systems," *2017 Progress in Applied Electrical Engineering, PAEE 2017*, 2017. ISBN: 9781538615287.

[20] M. Parchomiuk, R. Strzelecki, K. Zymmer, and T. Sak, "Modular high precision high current source for special applications-Simulation and verification," *Proceedings - 2016 10th International Conference on Compatibility, Power Electronics and Power Engineering, CPE-POWERENG 2016*, pp. 422–427, 2016. Publisher: IEEE ISBN: 9781467372930.

[21] G. Wang, G. Konstantinou, C. D. Townsend, J. Pou, S. Vazquez, G. D. Demetriades, and V. G. Agelidis, "A review of power electronics for grid connection of utility-scale battery energy storage systems," *IEEE Transactions on Sustainable Energy*, vol. 7, pp. 1778–1790, Oct. 2016.

[22] D. R. Brown and W. D. Chvala, "Flywheel energy storage: An alternative to batteries for ups systems," *Energy Engineering: Journal of the Association of Energy Engineering*, vol. 102, no. 5, pp. 7–26, 2005.

[23] R. Magdalena Stephan, R. de Andrade Jr., and G. Gonçalves Sotelo, "Third Generation Of Flywheels: A Promising Substitute To Batteries," *Eletrônica de Potência*, vol. 13, no. 3, pp. 171–176, 2008.

[24] T. Ise, M. Kita, and A. Taguchi, "A hybrid energy storage with a SMES and secondary battery," *IEEE Transactions on Applied Superconductivity*, vol. 15, no. 2 PART II, pp. 1915–1918, 2005.

[25] S. M. Goetz, A. V. Peterchev, and T. Weyh, "Modular multilevel converter with series and parallel module connectivity: Topology and control," *IEEE Transactions on Power Electronics*, vol. 30, pp. 203–215, Jan. 2015. Publisher: IEEE.

[26] J. Rodríguez, J. S. Lai, and F. Z. Peng, "Multilevel inverters: A survey of topologies, controls, and applications," *IEEE Transactions on Industrial Electronics*, vol. 49, pp. 724–738, Aug. 2002.

[27] M. Glinka and R. Marquardt, "A new AC/AC multilevel converter family," *IEEE Transactions on Industrial Electronics*, vol. 52, no. 3, pp. 662–669, 2005.

[28] P. Sun, Y. Tian, J. Pou, and G. Konstantinou, "Beyond the MMC: Extended Modular Multilevel Converter Topologies and Applications," *IEEE Open Journal of Power Electronics*, no. May, pp. 1–1, 2022.

[29] C. Wang, X. Li, H. Peng, L. He, and Y. Xue, "Segmented Energy Routing for a Modular AC/DC Hybrid System," *IEEE Journal of Emerging and Selected Topics in Power Electronics*, vol. 6777, no. c, pp. 1–1, 2021. Publisher: IEEE.

[30] S. M. Goetz, Z. Li, A. V. Peterchev, X. Liang, C. Zhang, and S. M. Lukic, "Sensorless scheduling of the modular multilevel series-parallel converter: Enabling a flexible, efficient, modular battery," *Conference Proceedings - IEEE Applied Power Electronics Conference and Exposition - APEC*, vol. 2016-May, pp. 2349–2354, 2016. Publisher: IEEE ISBN: 9781467383936.

[31] Z. Li, R. Lizana, A. V. Peterchev, and S. M. Goetz, "Distributed balancing control for modular multilevel series/parallel converter with capability of sensorless operation," *2017 IEEE Energy Conversion Congress and Exposition, ECCE 2017*, vol. 2017-Janua, no. 1608929, pp. 1787–1793, 2017. ISBN: 9781509029983.

[32] Z. Li, R. Lizana, A. V. Peterchev, and S. M. Goetz, "Predictive control of modular multilevel series/parallel converter for battery systems," *2017 IEEE Energy Conversion Congress and Exposition, ECCE 2017*, vol. 2017-Janua, pp. 5685–5691, 2017. ISBN: 9781509029983.

[33] B. J. Vermulst, J. L. Duarte, E. A. Lomonova, and K. G. Wijnands, "Scalable multi-port active-bridge converters: Modelling and optimised control," *IET Power Electronics*, vol. 10, no. 1, pp. 80–91, 2017.

[34] S. Galeshi, D. Frey, and Y. Lembeye, "Efficient and scalable power control in multi-port active-bridge converters," *2020 22nd European Conference on Power Electronics and Applications, EPE 2020 ECCE Europe*, pp. 2–10, 2020. ISBN: 9789075815368.

[35] F. Ma, X. Wang, L. Deng, Z. Zhu, Q. Xu, and N. Xie, "Multiport Railway Power Conditioner and Its Management Control Strategy with Renewable Energy Access," *IEEE Journal of Emerging and Selected Topics in Power Electronics*, vol. 8, no. 2, pp. 1405–1418, 2020. Publisher: IEEE.

[36] Z. Zhang, C. Jin, Y. Tang, C. Dong, P. Lin, Y. Mi, and P. Wang, "A Modulized Three-Port Interlinking Converter for Hybrid AC/DC/DS Microgrids Featured with a Decentralized Power Management Strategy," *IEEE Transactions on Industrial Electronics*, vol. 68, no. 12, pp. 12430–12440, 2021. Publisher: IEEE.

[37] S. Bandyopadhyay, P. Purgat, Z. Qin, and P. Bauer, "A Multiactive Bridge Converter with Inherently Decoupled Power Flows," *IEEE Transactions on Power Electronics*, vol. 36, no. 2, pp. 2231–2245, 2021.

[38] F. Ahmad, A. B. Jorgensen, S. M. Beczkowski, and S. Munk-Nielsen, "Daisy Chain PN Cell for Multilevel Converter using GaN for High Power Density," *2020 22nd European Conference on Power Electronics and Applications, EPE 2020 ECCE Europe*, pp. 1–9, 2020. ISBN: 9789075815368.

[39] Q. Chen, R. Li, and X. Cai, "Analysis and Fault Control of Hybrid Modular Multilevel Converter With Integrated Battery Energy Storage System," *IEEE Journal of Emerging and Selected Topics in Power Electronics*, vol. 5, pp. 64–78, Mar. 2017.

[40] J. Jiang, Y. Bao, and L. Y. Wang, "Topology of a bidirectional converter for energy interaction between electric vehicles and the grid," *Energies*, vol. 7, no. 8, pp. 4858–4894, 2014.

[41] T. M. U. Ned Mohan and W. P. Robbins, *Power Electronics, Converters, Applications and Design*. John Whiley and Sons, Inc, 2003.

[42] M. Hernes, S. D'Arco, A. Antonopoulos, and D. Peftitsis, "Failure analysis and lifetime assessment of IGBT power modules at low temperature stress cycles," *IET Power Electronics*, vol. 14, pp. 1271–1283, May 2021.

[43] M. Held, P. Jacob, G. Nicoletti, P. Scacco, and M.-H. Poech, "Fast power cycling test of IGBT modules in traction application," in *Proceedings of Second International Conference on Power Electronics and Drive Systems*, vol. 1, (Singapore), pp. 425–430, IEEE, 1997.

[44] J. Biela, M. Schweizer, S. Waffler, and J. W. Kolar, "SiC versus Si—Evaluation of Potentials for Performance Improvement of Inverter and DC–DC Converter Systems by SiC Power Semiconductors," *IEEE Transactions on Industrial Electronics*, vol. 58, pp. 2872–2882, July 2011.

[45] J. Rabkowski, D. Peftitsis, and H. Nee, "Silicon Carbide Power Transistors: A New Era in Power Electronics Is Initiated," *IEEE Industrial Electronics Magazine*, vol. 6, pp. 17–26, June 2012.

[46] K. N. Kumar, R. Miskiewicz, P. Trochimiuk, J. Rabkowski, and D. Peftitsis, "Performance Evaluation of SiC-based Isolated Bidirectional DC/DC Converters for Electric Vehicle Charging," *2022 24th European Conference on Power Electronics and Applications (EPE'22 ECCE Europe)*, p. 11, 2022.

[47] I. F. Kovacevic-Badstuebner, J. W. Kolar, and U. Schilling, "Modelling for the lifetime prediction of power semiconductor modules," in *Reliability of Power Electronic Converter Systems* (H. S.-h. Chung, H. Wang, F. Blaabjerg, and M. Pecht, eds.), pp. 103–140, Institution of Engineering and Technology, Dec. 2015.

[48] F. Hoffmann and N. Kaminski, "Power Cycling Capability and Lifetime Estimation of Discrete Silicon Carbide Power Devices," *Materials Science Forum*, vol. 1004, pp. 977–984, July 2020.

[49] F. Hoffmann and N. Kaminski, "Impact of the Chip Properties on the Power Cycling Performance of Silicon Carbide MOSFETs at Different Temperature Swings," in *2022 IEEE 34th International Symposium on Power Semi-*

conductor Devices and ICs (ISPSD), (Vancouver, BC, Canada), pp. 21–24, IEEE, May 2022.

[50] O. Schmidt, S. Melchior, A. Hawkes, and I. Staffell, "Projecting the Future Levelized Cost of Electricity Storage Technologies," *Joule*, vol. 3, no. 1, pp. 81–100, 2019. Publisher: Elsevier Inc.

[51] A. M. Abbas and P. W. Lehn, "A unified power delivery solution for integrating DER into distribution networks through VSC based DC system," in *2009 IEEE Power and Energy Society General Meeting, PES '09*, 2009.

[52] B. L. M. Lamaille, F. Dragoni, S. Evrard, F. J. Harden, E. Harrouch, M. Lazzaroni, R. Lopez, and K. D. Papastergiou, "Study of the Energy Savings Resulting From the East Area Renovation," *10th Int. Partile Accelerator Conferance*, pp. 4023–4025, 2019. ISBN: 9783954502080.

[53] S. Nema, R. K. Nema, and G. Agnihotri, "Inverter topologies and control structure in photovoltaic applications: A review," *Journal of Renewable and Sustainable Energy*, vol. 3, no. 1, 2011.

Chapter 4

Design and operation of scalable power converters

4.1 Designing a scalable converter

This section aims to find the electrical design parameters of the scalable modular converters, what benefits it can bring and how it can reduce the total cost of installation and operation. As discussed in Section 2.3, the electromagnets at CERN have a large range of resistance and inductance, which together with the required current determine the voltage and current requirement for the converters.

The fundamental building modules of the converter, here referred to as bricks, can either be connected to the grid or to separate energy-storage components. Energy recovery into the energy storage takes place by redistributing the current during inductive load ramp-down.

If a single conventional converter design is to supply all of these loads, in some cases the voltage capabilities will be underutilised, and for some, it will be the storage element which is underutilised. By dividing the large converter into smaller bricks, it is possible to find a combination of bricks which better matches the individual requirements, enabling both scalability and modularisation. The question is whether such a scalable modular converter can be cost-effective. The key finding is that the lifetime cost of the converter is highly dependent on the chosen power semiconductor technology (IGBT vs. SiC MOSFET) and the output voltage of the bricks. The latter creates a shallow U-shaped curve with the voltage on the x-axis and the optimal voltage range being in 300-600V for modules. When comparing different IGBT modules to each other, the difference is less obvious. Figure 4.1

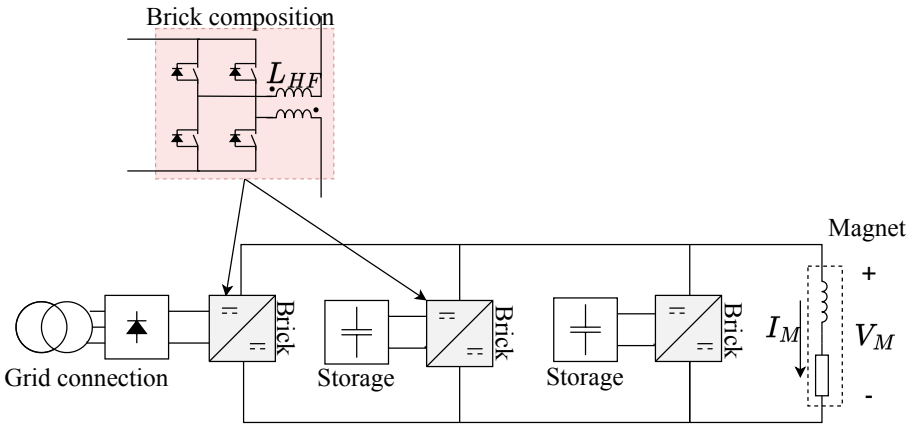

Figure 4.1: Proposed scalable converter, showed in a 1 grid brick 2 storage bricks configuration.

shows a possible configuration of the proposed converter.

Paper I aims to explore this question in a general way, in the following chapters some of the findings will be isolated and investigated in more detail. It attempt to answer the question for CERN and for the renovation project in the CERN North Area project.

In addition, the design raises two significant questions, which will be answered in later papers.

1. Given that some of the bricks do not have any grid connection, and thus no way of replenishing lost energy, how can the converter compensate for the energy loss in each cycle and does this enable other flexibility for the operation of the converter?

2. With a number of parallel connected bricks, what are the effects on output current ripple by using interleaving?

These questions were the starting point for the papers discussed in Section 4.2.1 and 4.1.6 respectively.

4.1.1 Assumptions

For Paper I the following assumptions were made, in addition to the assumptions listed in Paper I itself.

1. Constant voltage of 400V applied during ramping the current up. Ensuring

that the ramp time is kept inside the period of the pulses.

2. The same de-rating factors were used for all device types, obtained from existing converter design for these loads. 0.5 for current and 0.75 for voltage.

3. The bricks are either storage or grid bricks, meaning that the minimum possible brick count is 2.

4. The bricks can be connected in series and in parallel freely.

5. There is a margin of safety on the bus voltage with respect to the output voltage of 50V.

6. The output voltage level is set from $(V_{bus} - 50V)$ to $50V$ and each voltage level is used for the bricks to find assemble the converter for each magnet in the database of magnets.

4.1.2 Finding the optimal brick size

The following is a deeper discussion of the results from the work presented in Paper I. It is supplementary to the results in the paper, and they will make more sense if the paper is read first. The information shown below sheds more light on the results, to analyse the results further and investigate which parameters the results are most sensitive to.

Introduction to the plots

Using the algorithm presented in Paper I it is possible to perform a further analysis for this particular set of circumstances. In Figure 4.2 the relative cost line discussed in the paper is plotted for one of the devices, SiC MOSFET 600A (plotted in red). As in the paper the vertical line represent the sensitivity to price $(+/-10\%)$. In addition, the relative cost of the capital cost (cyan colour) and operational cost (yellow colour) are added. All are normalised to the same value of the total cost of the SIRIUS converter, such that the relative values of storage and capital adds up to the relative total cost and are referenced to the right y-axis. In this figure, the number of bricks is plotted in the blue colour and is referenced to the left y-axis.

For each voltage level in Figure 4.2 the blue dotted line represent the average number of bricks required at that voltage level across all the magnets, while the blue dot represents the 75% percentile at that voltage level, i.e. 75% of the converters have the number of bricks indicated or less. Since the average and 75% percentile is so close to each other, it is clear that the distribution of the number of bricks per voltage level is heavily skewed towards the lower numbers, and only a few reach

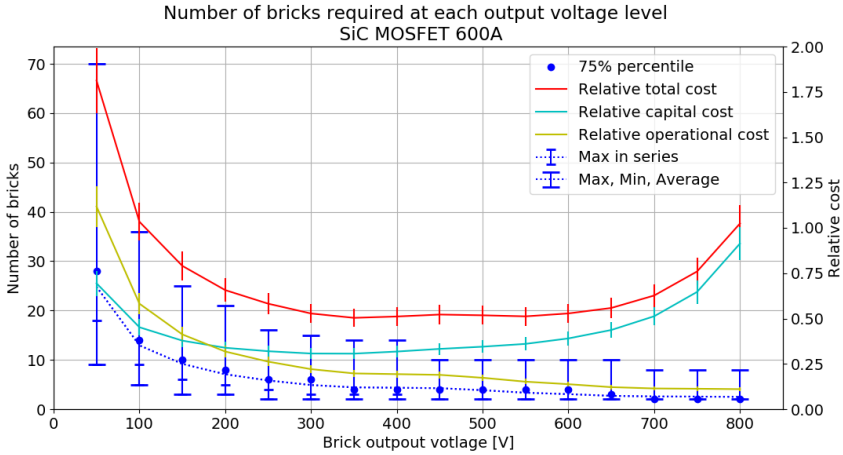

Figure 4.2: Bricks per voltage level for the SiC MOSFET, 600A. Coloured lines represent total costs (investment cost, operational cost and total referring to right vertical axis) for 350 power converters of the NA project. Whiskers (vertical blue lines associated with the left axis) represent min, max and average number of bricks per converter calculated across the 350 power converters.

the higher brick count. The horizontal bar lines show the minimum and maximum number of bricks at each voltage level.

As expected at low brick output voltage, a very large number of bricks is needed to provide the voltage to the load. Having a $50V$ brick output has the benefit of using almost 100% of the energy in the storage given the $900V$ bus voltage, but at the cost of requiring a huge amount of bricks, resulting in a high total cost and an impractical converter design.

As the brick output voltage is increased above 600V, the capital cost starts to increase again. This time is driven by the greatly increased cost of capacitors as the energy utilisation is poor, while the number of required bricks does not decrease much, as one brick has enough output voltage to ensure the required voltage is met.

Bricks and capacitors per voltage level

Using the same type of plot and considerations as for Figure 4.2, Figure 4.3 focuses on the most interesting voltage range, and includes this plot for 4 of the modules included in the paper. They follow the same trends as discussed above, except of course the TO-247 device which has a much lower bus voltage, and so the optimal range is shifted down towards 200V. The 3 other plots have a more or less flat cost

curve between 300V and 600V, and the number of bricks are stepping in the same places, which will be discussed in the next section.

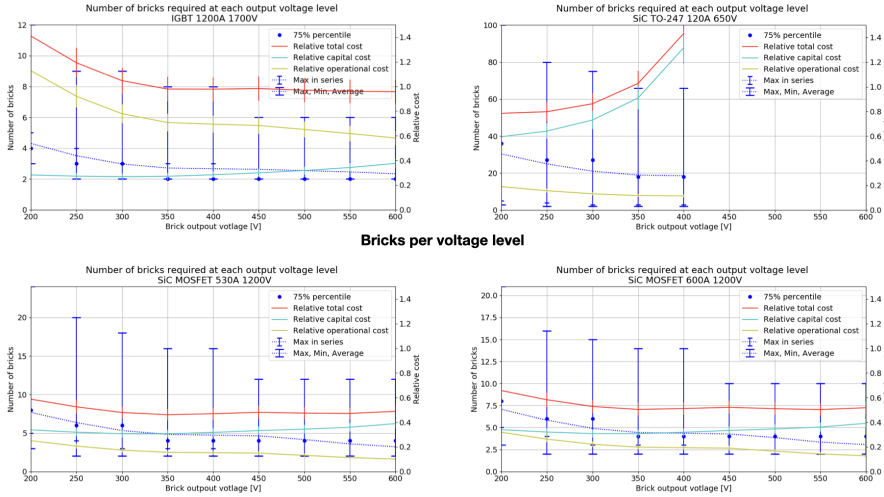

Figure 4.3: Bricks per voltage level.

Looking at the number of capacitor stacks, where one stack is the number of series connected capacitors required to achieve the bus voltage, Figure 4.4 shows how the number of capacitors stacks are inversely correlated with the number of bricks. While the maximum number of bricks is steadily rising through the range, the average and the 75% percentile are almost the same and rising only slightly. They are more representative of the total cost of storage, as they represent the majority of the bricks. Even so, a typical brick will need somewhere in the range of 20-30 capacitors. This will not be so different from the current solutions as the energy stored is determined by the magnet current and inductance. Yet, a low brick output voltage will increase the utilisation significantly and reduce the amount of storage. It is also worth mentioning that the number of storage capacitors per converter is more like 3-8, which seems reasonable.

The distribution of the bricks for 4 different brick output levels is also included. The plots are selected for only one device, the SiC MOSFET 600A, as the different devices have very similar distributions. From these plots in Figure 4.5 the same observations as in Figure 4.3 can be made, they show the number of bricks connected in series, parallel and total for each converter on the x-axis and the number of times each of these appear in each converter on the y-axis. For example, at 200V output voltage, upper left plot in Figure 4.5, there are almost 290 converters out of the 350 converters with 4 bricks in series and approx 60 with 5 in series and

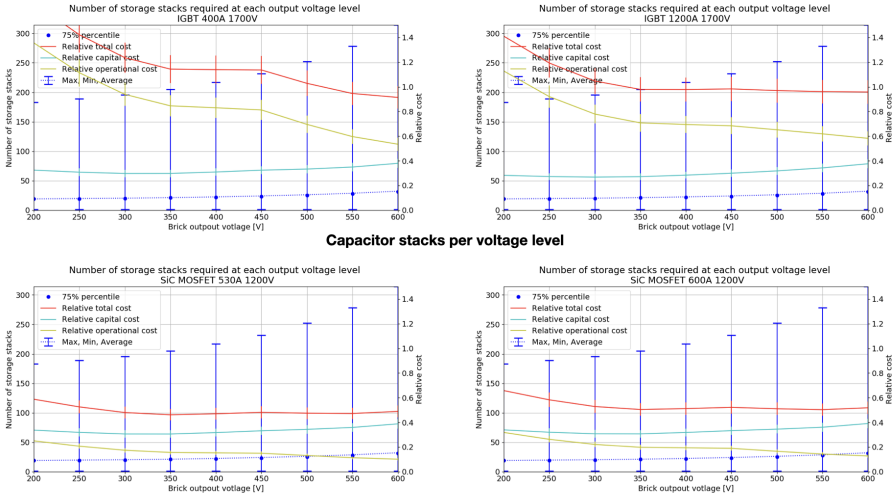

Figure 4.4: Capacitor stacks per voltage level. Coloured lines represent total costs (investment cost, operational cost and total referring to right vertical axis) for 350 power converters of the NA project. Whiskers (vertical blue lines associated with the left axis) represent min, max and average number of bricks per converter calculated across the 350 power converters.

only a few having more, whereas approx 150 converters have 2 strains of bricks in parallel. Note that each of the 3 colours of the plots add up to the total of 350, so the plots show how prevalent each configuration is. By multiplying the number of series connected bricks with the number of parallel strains, the results is the total number of bricks for each converter. For the upper left plot the converter with the largest number of bricks has 21 bricks, made of 3 bricks in series and 7 strains in parallel.

The distributions are heavily skewed towards the lower number of bricks, with only a few outliers. The output brick voltage is very important for determining the distribution of a series of connected bricks, which is dominated by one or two possibilities. While the parallel connected bricks are not affected by the brick output voltage, the necessary multiplication of series and parallel connections is what in turn gives the very high extremes in terms of the total number of bricks. The plots show how the series and parallel connected bricks are combined together to create the total numbers. If the desire is to reduce the number of bricks and maintain the low output voltage, increasing the current capability of each brick by using power modules with larger current ratings could be an interesting approach. It is also possible to connect devices parallel on each switching position, to increase the current

capability of each module. However, if the cost of the modules are approximately proportional, then increasing the current in terms of more modules also gives the other benefits of the increased number of modules as discussed before.

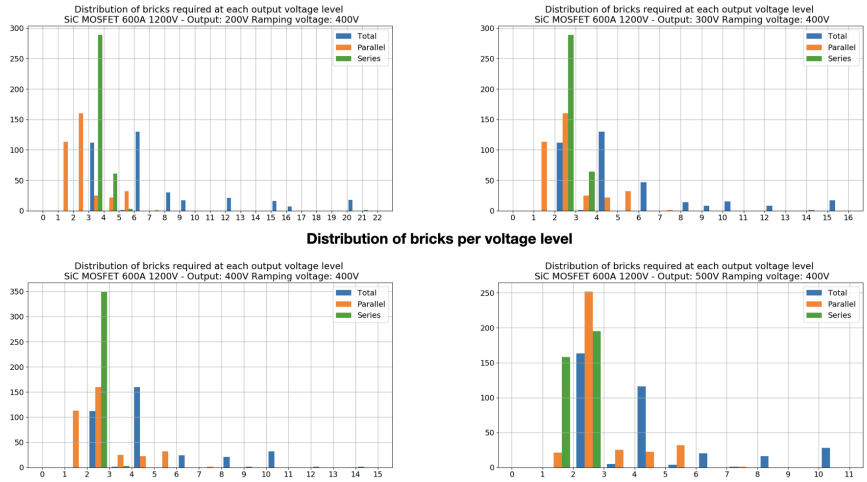

Figure 4.5: Distribution of bricks per voltage level. Coloured lines represent total costs (investment cost, operational cost and total referring to right vertical axis) for 350 power converters of the NA project. Whiskers (vertical blue lines associated with the left axis) represent min, max and average number of bricks per converter calculated across the 350 power converters.

Effect of magnet current ramping rate (di/dt)

Figure 4.6 shows the effect of the magnet current ramping rate (di/dt) requirement on the number of bricks and thus the total cost, and how this optimum cost point discussed above moves with the value of the magnet ramping rate value significantly. This is one of the single parameters with the biggest impact on the overall cost consideration.

As mentioned in the assumptions in the previous section, there is a requirement for ramping voltage present. Since most of the magnets have internal resistance and current requirement such that $50V$ is sufficient to maintain the current, the sum of this flat-top voltage and the ramping voltage ($V_{crit} = 450V$ in this case), becomes a critical value. For bricks with output voltage above this value, one brick in series is enough in most cases, and for bricks below this value, the bricks have to be connected in series until they achieve V_{crit}. From the plots it is possible to observe when the maximum number of bricks required for any of the converters increases from 2, his point is marked by the orange circle in the plots in Figure 4.6.

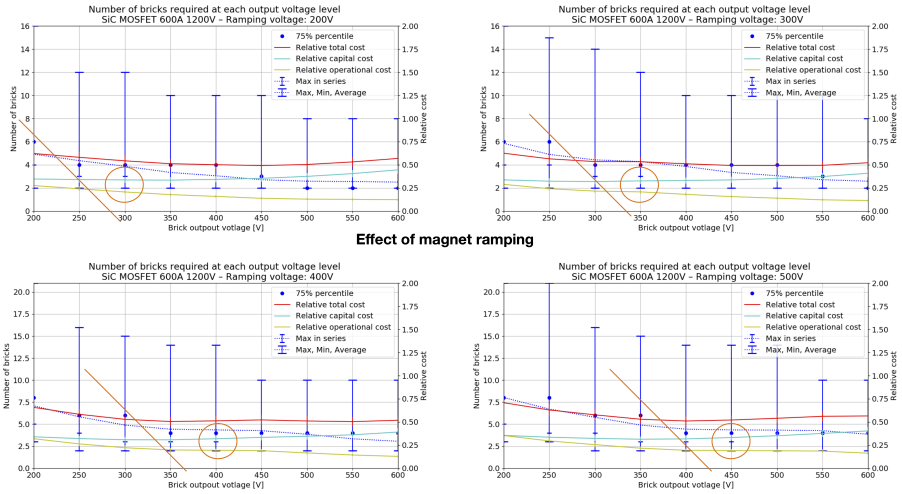

Figure 4.6: Effect of magnet current ramping rate (di/dt) on the distribution of bricks per voltage level. Coloured lines represent total costs (investment cost, operational cost and total referring to right vertical axis) for 350 power converters of the NA project. Whiskers (vertical blue lines associated with the left axis) represent min, max and average number of bricks per converter calculated across the 350 power converters.

This point indicates the start of the transition, where for lower voltages the series connection of bricks starts to increase significantly. It shows how for brick output voltages above the ramping voltage, a minimum of two bricks is possible, given that at least one magnet requires $1000V$ in total. Whereas for the brick output voltages below the ramping voltage, a minimum of 3 bricks in series are required. Since the total number of bricks are a multiplication of the series connected bricks and the number of parallel strains, the number of bricks starts to quickly increase.

Focusing on the $400V$ case first, when dropping the brick output voltage below 100V of the ramping voltage, the 3 bricks in series becomes the most common solution across the range, and the 75% percentile moves up to 6 bricks because of this (marked by the orange line in Figure 4.6). The same is true for the other voltage levels, but shifting the ramping voltage requirement down by $100V$ only moves the two points by half the value ($50V$), the same is true both for stepping up and down.

As can be seen from the results in the previous paragraphs the voltage requirement is important when considering the complexity of the converters used to supply these loads. In Figure 4.6 the influence of the ramping voltage, which has a particular influence on the number of series connected bricks, is further analysed. The

optimal output voltage of the design is determined by the ramping voltage requirement, and relaxing this requirement somewhat can allow for better storage utilisation. AS reducing the peak-voltage requirement moves the optimal output voltage in the calculation to a lower output voltage. On the other hand, it can reduce the overall costs at the optimum output voltage point. However, as these variables are not so sensitive in this analysis, the trade-off between desired complexity, redundancy and ramping voltage is more important. The cost of complexity and benefit of redundancy is highly dependent on the scalable converter configuration and application and is not further investigated here.

4.1.3 Distribution of the number of bricks in the optimal range

The results in the previous section focus purely on the overall cost of the system, but the developed algorithm also reveals a lot of information on the presumed complexity of such systems. In particular, the number of required bricks is a key parameter to understand the operational challenges and availability of redundancy. By considering the SiC MOSFET 600A-rated power module (green line) from Figure 7 in Paper I, and selecting only the voltages that lie in the optimal range (output of 200-600V), Figure 4.7 shows the number of bricks required at each voltage level.

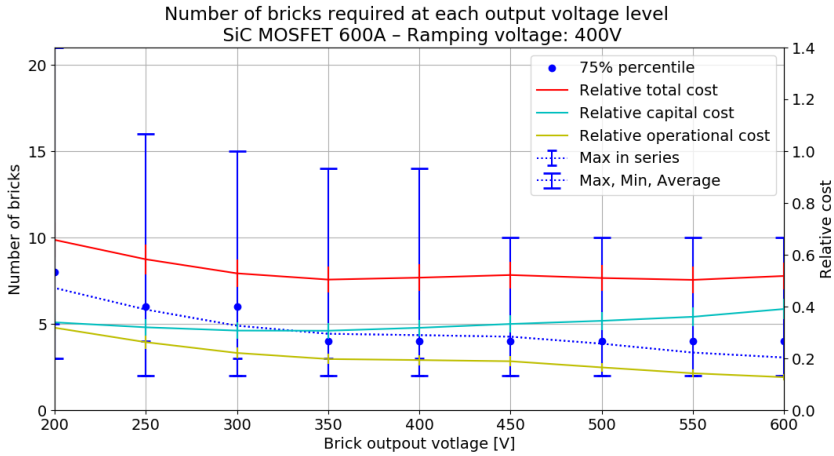

Figure 4.7: The number of bricks required at each voltage level for a SiC MOSFET module at 600A 1200V. Coloured lines represent total costs (investment cost, operational cost and total referring to right vertical axis) for 350 power converters of the NA project. Whiskers (vertical blue lines associated with the left axis) represent min, max and average number of bricks per converter calculated across the 350 power converters.

In Figure 4.7, the red line is the same as the green line in Figure 7 in the paper, and

it also includes the relative capital and operational costs, the sum of these two adds up to the red line. The blue lines show the number of bricks required at each output voltage level, it shows the sum of parallel and series connected bricks if both are required. First, the dotted blue line shows the average number of bricks required for each magnet across the 350 magnet data set. At 600V the average number of bricks is relatively low, at only 3 bricks. As the output voltage decreases, the number of bricks gradually increases, plateauing at 350-450V before gradually increasing again. This effect has been studied more closely in section 4.1.2 (i.e., Figure 4.6).

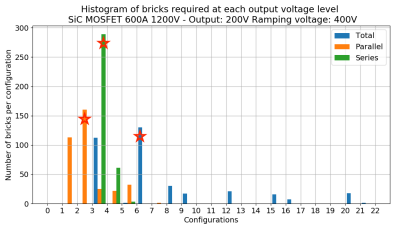

(a) Histogram at 200V output voltage.

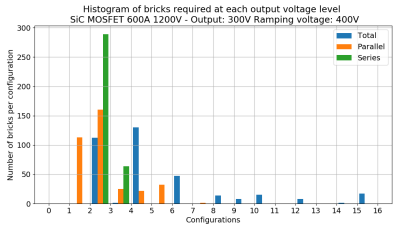

(b) Histogram at 300V output voltage.

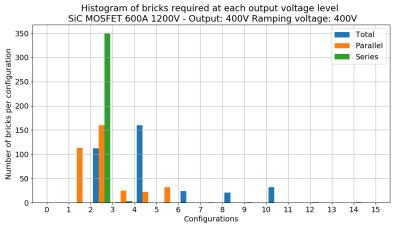

(c) Histogram at 400V output voltage.

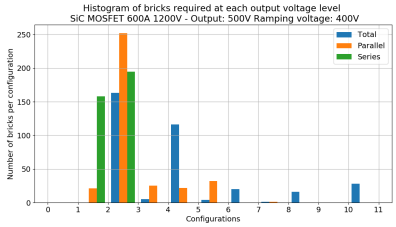

(d) Histogram at 500V output voltage.

Figure 4.8: Histogram in the number of bricks required at output voltages of 200V, 300V, 400V and 500V.

The blue dot in Figure 4.7 represents the 75% percentile. This value is in fact very close to the average, which indicates that the distribution is skewed towards lower numbers of bricks, and only a few outlier cases have a high number of bricks. This distribution is shown in Figure 4.8, where the distributions are broken down to show series and parallel connected bricks as well. Finally, the small horizontal line shows the maximum number of series connected bricks and the two wider blue horizontal lines show the maximum and minimum number of bricks required. At 450-600V output voltage, the small blue line disappears as the minimum number of series-connected bricks is the same as the minimum number of total bricks. It is worth noting that these min and max values might only be referring to the converter supplying a single magnet, due to the dataset having some quite large outliers for current and voltage. In Figure 4.9 an example configuration is shown, which is the

most common configuration for the 200V output voltage marked by the red star in Figure 4.8(a).

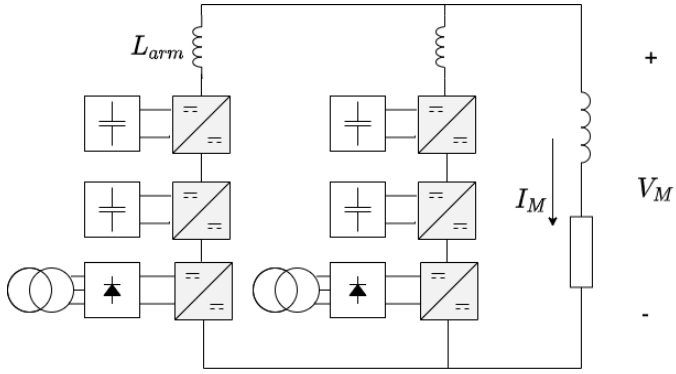

Figure 4.9: Example of the most common configuration for 200V output voltage, corresponding to the red star in Figure 4.8(a).

Looking closer at the distribution in Figure 4.8 it is clear that the series and parallel connection of the bricks is never exceeding 6 parallel connections and 5 series connected bricks. However, as the total number of bricks required depends on the product of the series and parallel connected bricks for each converter, the total number can quickly become quite large. Yet the maximum number of bricks is 20, so no load requires both the maximum series and the maximum parallel connected bricks at the same time. This is a way the scalability comes into practice, meaning that a large storage, voltage and current capability is rarely required, so only a few converters actually have it. Even though reducing the output voltage from 500V to 400V results in a significant increase in the series connecting of bricks. At 500V both 2 and 3 series connected bricks are common, while at 400V most loads only need 2 series connected bricks in order to supply the required output voltage for the loads. Despite the reduction in the number of series connected bricks, there is no increase in the overall cost, the increased cost of the bricks, is off-set by the increased utilisation of the storage. Even going from 400V to 300V output voltage the costs do not really increase significantly. With such insights early in the planning stage, prioritising utilisation of storage, grid-connected power capacity needed, practical limits for complexity and cost-efficient re-use and integration of existing infrastructure is easier to quantify. Trading of the converter output voltage and type of technology and type of power module is made possible when the relationships between these parameters are made clear.

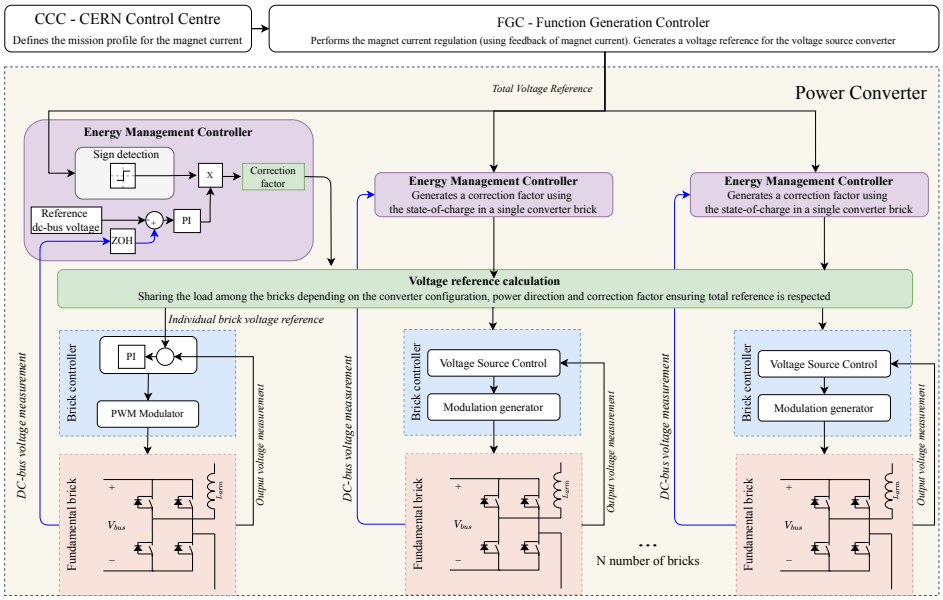

Figure 4.10: The structure of the control algorithm used in the experimental validation and the simulations.

4.1.4 Controlling power flow of the scalable converter

The following chapter describes the proposed scalable DC/DC converter topology with modularised energy storage as presented in Paper II. The work demonstrates the operation of such a converter with a lab specimen load and a full-scale converter prototype.

The lab experiment is based on the theoretical work from the paper presented in Section 4.1.2, and it shows an experimental verification of the scalable converter, where the different bricks of the converter can be independently controlled. The control strategy overview is presented in Figure 4.10. In Figure 4.11 the experimental verification of one of the the converter configurations is shown. In this figure a cycle-agnostic control strategy is shown, where the converter uses the energy stored in the magnet to replenish the energy storage fully after each cycle. Due to the complicated process of planning and operating the converters, it's desirable to have a converter where each pulse can be planned completely independently of each other. Therefore the storage and output stage should be able to deliver any sequence of pulses as long as each individual pulse is within the capabilities of the converter. In Paper II two potential configurations for the scalable converter have been demonstrated. Option I is referring to a configuration with 3 grid bricks

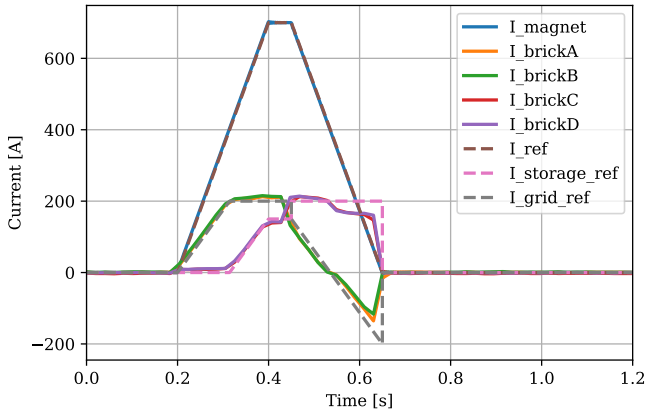

(a) Measured brick and output currents.

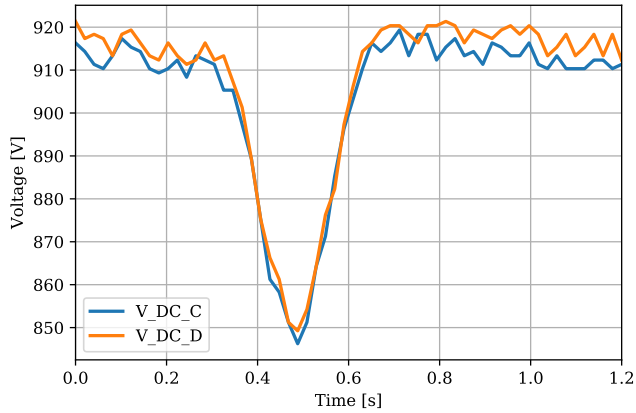

(b) Measured bus voltage for the storage bricks C (V_{DC_C}) and D (V_{DC_D}).

Figure 4.11: Option II - Experimental results of a current pulse at 700A with 2 grid and 2 storage bricks. I_{magnet} is the total current supplied to the magnet, I_{brick} is the current from each of the bricks A-D. Bricks A and B are grid-connected, while bricks C and D are energy-storing. I_{ref} is the total current reference, $I_{storage\_ref}$ and I_{grid} are the references for the storage and grid bricks respectively.

and a single storage brick connected in parallel. This configuration minimises the cost of the installed storage. Whereas Option II, using 2 grid bricks and 2 storage bricks, makes sure that the full energy of the magnet is recycled and minimises the installed grid capacity. In Figure 4.11 the results of Option II is shown.

The key finding is to demonstrate that the storage bricks can indeed be operated without a direct grid connection, by taking advantage of the energy stored in the electromagnets. It also demonstrates that there is flexibility in the combination of storage and grid bricks since multiple configurations are able to supply the magnet. This flexibility in hardware allows the scalable converter to be optimised on a facility level, finding the most cost-effective solution for hundreds of converters. The cost-effectiveness has already been discussed in Section 4.1.2.

4.1.5 Experimental verification

For the experimental validation, an existing 800kW power converter in the CERN laboratory was utilised. The converter is a CERN-developed DC-DC converter employing four full-bridge circuits with energy recovery connected in parallel. A photograph of this test setup is illustrated in Figures 4.12 and 4.13, with the schematics of the topologies shown in Figure 4.14, a more detailed circuit diagram can be found in Figure 2.1. The energy recovery is conducted via a large capacitor bank on the DC bus of the converter and the load and system losses are supplied from the electrical grid via a transformer, diode rectifier and a DC/DC boost converter stage. By increasing the voltage of the DC bus, more energy is stored in the capacitors, and conversely, by reducing the voltage the stored energy is reduced. The usable energy is described by Equation 4.1.

$$E_{cap} = \frac{1}{2} C \cdot V_{bus}^2 \tag{4.1}$$

Table 4.1: Converter IGBT parameters.

CM1200DC-34N	Voltage	Current
Rated value	1700V	1200A
Max designed	450V	450A

The controller is a Texas Instrument DSP integrated with a CERN-developed current measurement system, and LEM sensors for voltage measurements (LV 25-P/SP5 both on the output and the bus). The current measurement system has the ability to measure current with significant accuracy in the ppm range. The parameters of the IGBT used are listed in Table 4.1. The devices are significantly

de-rated in their designed operation due to lifetime requirements and the thermal nature of pulsed loads.

Figure 4.12: Photograph of the laboratory set-up.

As shown in Figure 4.14, the four bricks have a grid connection via a transformer each, a diode rectifier, a boost, a DC-bus and an IGBT-based full-bridge circuit on the output. The design parameters of the converter in the test setup are summarised in Table 4.2. The two types of bricks used in this paper were obtained by modifying the existing converter. The storage bricks are made by disabling the boost stage. This reduced the storage brick to a large capacitor bank with a full-bridge circuit connecting it to the output. As such the losses occurring in the storage and full-bridge have to be supplied via the energy recovered from the load at the end of each pulse. The grid brick is made by removing the energy storage and disabling the boost stage from the existing system. This simplifies the grid bricks to a grid-connected diode rectifier with a full-bridge circuit on the output. By separating the grid connection and storage, it is possible to have a simple building block (i.e. brick) at the cost of increased system complexity.

The load is a lab specimen of an electromagnet, designed to have similar parameters and properties as the electromagnets used in the CERN accelerator facilities. The magnet parameters are listed in Table 4.3.

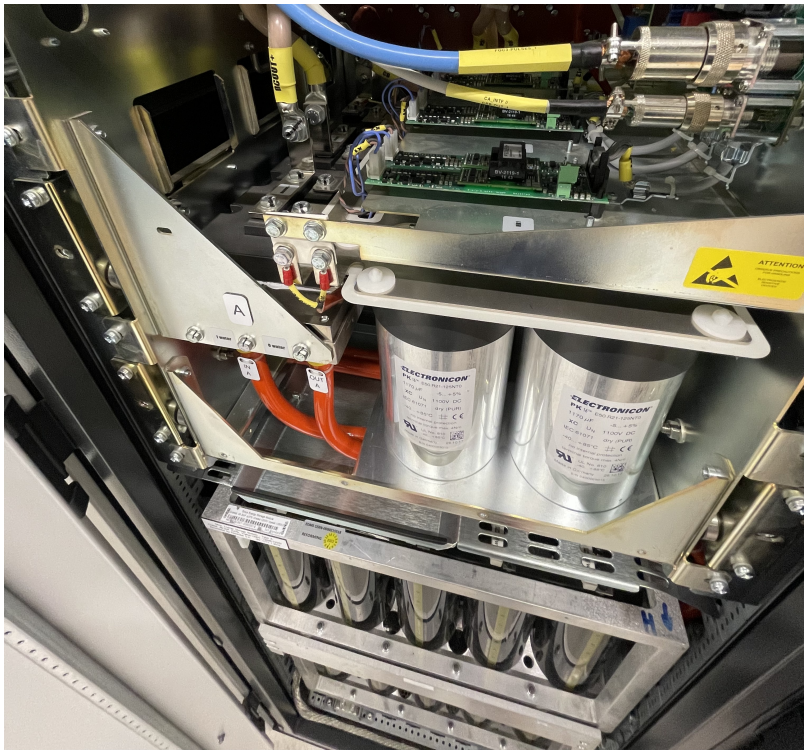

Figure 4.13: Photograph of the laboratory set-up, showing the power stack, gate drivers and DC-bus filter capacitors integrated into the cabinet. The storage capacitors can be seen in the bottom.

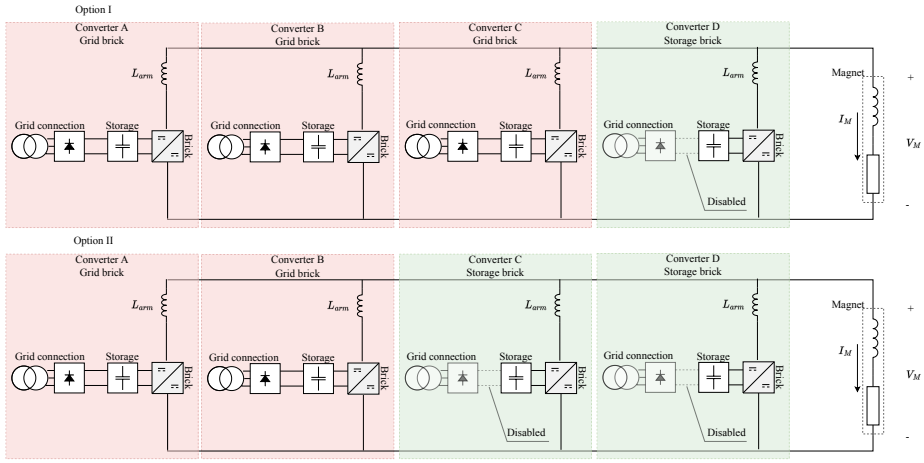

Figure 4.14: System topology used in the lab setup, showing the two configurations used. On top, Option I with 3 grid bricks and 1 storage bricks, and on the bottom Option II with 2 grid and 2 storage bricks.

Table 4.2: Converter parameters

	Grid Connected Brick	**Energy Storage Brick**
Max Voltage	200V	200V
Max Current	200A	200A
Energy Available	N/A	9.4kJ @900V

4.1.6 Achieving high precision for accelerator magnets

The lower conduction power losses and the positive temperature coefficient that favours parallel connections, make Silicon Carbide (SiC) MOSFETs to be an excellent replacement for existing Silicon IGBT technology. These characteristics combined with high switching frequency operation, enable the design of high-accuracy DC-DC converters with minimised filtering requirements. This section of the thesis compares two design approaches for a converter with high-accuracy current (0.9ppm) supplying a 0.05H electromagnetic load; one design with the topology and filter for a typical IGBT-based full-bridge and a second one with a SiC MOSFET-based topology without a filter. This investigation demonstrates a good approximation for the peak-to-peak ripple as a function of a number of interleaved outputs and switching frequencies. The findings have been published in Paper III.

Table 4.3: Case load

Load parameter	Value
Inductance	55mH
Resistance	75mΩ
Max current	960A
Pulse current flat-top	700A
Peak stored energy at @700A	13.5kJ
RMS power	8kW
Peak power	140kW

Interleaving of parallel bricks

The following sections will provide the background on the results presented in the Paper III, and explain a bit further how the results in the paper were obtained. Figure 4.15 shows the basic principle of the simulated topology, with the arm inductance and parallel connected bricks.

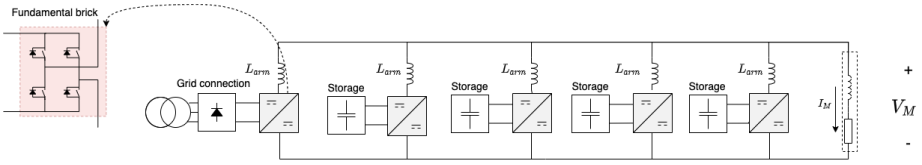

Figure 4.15: A possible configuration of interleaved bricks.

If a system has storage and/or grid bricks connected in parallel, another benefit is to introduce interleaving in order to reduce the current ripple. For some applications the requirement for a very accurate current results in significant filter costs reduction if interleaving is used. This can perhaps be better achieved by interleaving parallel-connected bricks.

Figure 4.16 shows simulation results, where the 4 different combinations of bricks are operated interleaved at 1 kHz of switching frequency. Similar to the topology presented in Figure 4.1, but with different number of parallel connected bricks. These simulation results were obtained considering 1, 2, 4 and 8 bricks in parallel respectively and using a full-bridge with no filtering, as well as an arm inductance of 1 mH connected to a $100m\Omega$ and $50mH$ load. The voltage shown in Figure 4.16 gives an idealised view of the voltage across and the currents circulating in the arm-inductors.

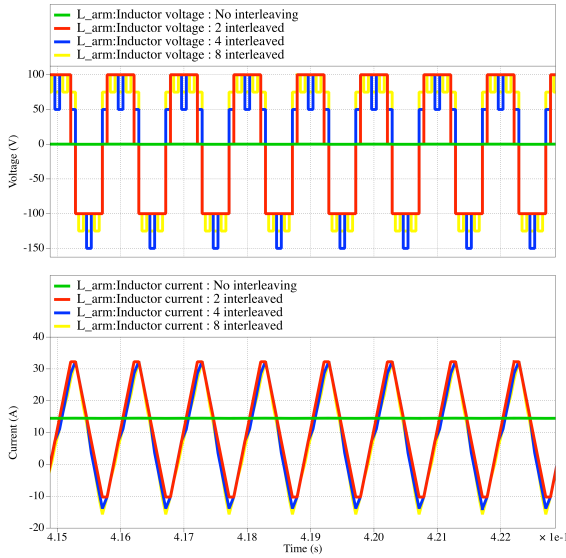

Figure 4.16: Simulations showing ripple current from the converters arm inductors, taken during the flat-top of the current pulse.

Figure 4.17 show the resulting output voltage and the current ripple. The effect of interleaving on the magnet current ripple is approximately inversely proportional to the square of the number of bricks. The arm current ripple is regulated primarily by the arm inductance and the switching frequency, and it is not influenced by the number of interleaving bricks.

Switching frequency

The peak-peak current ripple in the magnet scales linearly with the inverse of the switching frequency, as determined by the fundamental relation of the equation for an inductance. If the assumption is that the magnet inductive component is supplied with a voltage V_M, the current in the magnet i_M is given by Equation 4.2.

$$\begin{aligned} V_M =& L_M \frac{di_M}{dt} \\ \Longrightarrow& \Delta I_{arm} \approx \frac{V_{bus} - V_M}{2 f_{sw} L} \end{aligned} \tag{4.2}$$

The voltage over the arm inductance is given by the bus voltage in the brick and the voltage over the magnet, either $V_{inductor} = V_{bus} - V_M$ or $V_{inductor} = -V_{bus} - V_M$. Since the duty cycle is close to 50% most of the time, the delta time for the increasing current is $\approx \frac{1}{2f}$, and the change in current is as described in Equation

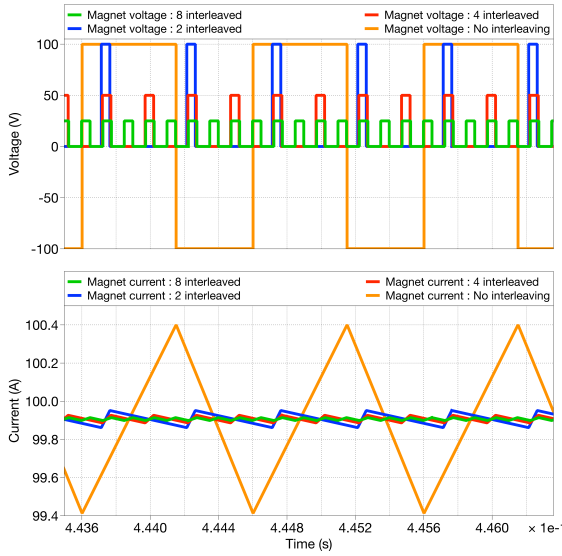

Figure 4.17: Simulations showing the current ripple in the magnet, taken during the flat-top of the current pulse.

4.2 on the right for a single arm inductor. In the example shown in Figure 4.17, the estimated current ripple is 0.043A, while the simulated is 0.05A.

Considering the ripple in the magnet itself, the interleaving makes the current ripple calculation a bit more complicated. The effect of interleaving reduces the current ripple approximately proportional to the number of sources since for each addition of interleaved source the apparent frequency is increased proportionally. This comes as a result of each new parallel connected brick having the same switching frequency and modulation, but are shifted in time.

This results in a modification of the voltage seen by the magnet, shown in Figure 4.17. The average voltage over a switching period, as seen by the magnet, is determined by the average voltage over the resistor, consisting of a square pulse of $\frac{V_{bus}}{N_{arms}/2}$ followed by zero voltage. The ripple is increasing during the time when the voltage is applied and decreases when the net voltage is zero.

For the interleaved voltages the rise-time is a very short part of the switching period, as can be observed from the voltage in Figure 4.17. From this the assumption is made that the rise time can be neglected and the fall time is equal to the switching period. During the phase when the net voltage from the interleaved bricks is zero, the negative voltage over the inductor part of the magnet is approximately equivalent to the average of the voltage over one period. Since the resistive

part of the magnet carrying the same current, the voltage drop across this component remains the same. This enables the current ripple to be described as a function of the output voltage, rather than the bus-voltage for interleaved bricks, when the average output voltage is much lower than the bus-voltage, which is the case for the application discussed in this PhD thesis.

Since $V_{bus}m = \hat{V}_M$, where $\hat{V}_M$ is the average voltage over a pulse cycle and m is the modulation ratio for the PWM function, this enables the equation to be expressed without considering the bus voltages and modulation ratio.

The absolute current ripple for the interleaved case is described in Equation 4.3. The relative current ripple then becomes as described by the result on the second line in Equation 4.3. Given that the output ripple is inversely proportional to the switching frequency there is a benefit of utilising high switching frequency to reduce the output ripple, such as SiC MOSFET modules. Currently switching is done at 6.5kHz, while SiC MOSFETs could bring this up to 60kHz and beyond. Resulting in an accuracy improvement by an order of magnitude. The higher switching frequency also results in a higher frequency on the ripple, reducing sizing requirements of the filters and reactors used, reducing the anticipated cost and losses of filters.

$$\begin{aligned} \Delta I_{ripple} \approx & \frac{\hat{V}_M}{f_{sw} L_M N_{arms}} = \frac{I_{flat} R_M}{L_M f_{sw} N_{arms}} \\ \Longrightarrow & \Delta I_{ppm} \approx \frac{R_M}{L_M f_{sw} N_{arms}} \end{aligned} \tag{4.3}$$

4.2 Optimised operation and control of the scalable converter

Assuming that a modular power converter is an attractive proposition as demonstrated in the previous section, it is necessary to have a method for controlling the internal power flow of the individual bricks. Even if all the bricks have the same types of components and parameter values, the natural variation in the components will result in a small imbalance between the bricks, for example due to manufacturing tolerances in magnetics. Even a small imbalance between the bricks can result in the energy in the storage either increasing or decreasing over time. Since in this case, the storage bricks do not have a grid connection and no ability to charge themselves, there needs to be a way to bring the stored energy back to the nominal value.

Paper IV shows a control structure using the bus voltage to approximate the state-of-charge and modify the individual references to ensure a stable operation even when the storage is significantly different from each other. It is also possible for such a modular converter to incorporate redundancy, and using simulations the controller is demonstrated to be able to manage the open-loop failure of a module without interruption. Paper IV also demonstrates that the flexibility of the modular converter can be used to optimise the references for different targets, and 4 different strategies were proposed and simulated. In Paper V the findings were demonstrated experimental for a full-scale prototype on a real load from the accelerator complex.

4.2.1 Energy flow control in a modular DC-DC converter with energy recovery

The controller developed in Paper IV formed the basis for the lab work that is proposed in Paper V and the results are presented in the papers introduced in this section and 4.2.2. The controller takes the bus voltage from each of the bricks as the state-of-charge information pertaining to the storage capacitors. Using Equation 4.4 it is possible to calculate how much of the energy in the bricks has been used at any given time, and thereby how much energy needs to be re-injected into the storage to maintain the energy level at the end of the cycle. The energy from the storage is used to increase the current in the load but also contributes to losses due to the operation of the converter, whereas the energy recovered primarily comes from the stored energy in the load.

$$E_{brick} = \frac{1}{2} C_{str} (V_{bus}^2 - V_{out}^2) \tag{4.4}$$

By knowing the amount of energy stored in each brick at any given time, and also knowing the remaining cycle, the energy management controller can calculate the current references for each brick individually using a correction factor, the total current and the shape of the current as given by the strategy. Combined with the voltage reference calculations, each brick is given a reference which both ensures the correct current supplied to the load and a power flow resulting in the energy storage recovering to its target at the end of the cycle. The correction factor is found using a PI-controller updated once per power cycle, which allows the controller to run on the DSP without too much calculation time and reduces interference between the power flow controller and the existing current and voltage controllers. The control strategy overview is presented in Figure 4.18. The findings were published in Paper IV.

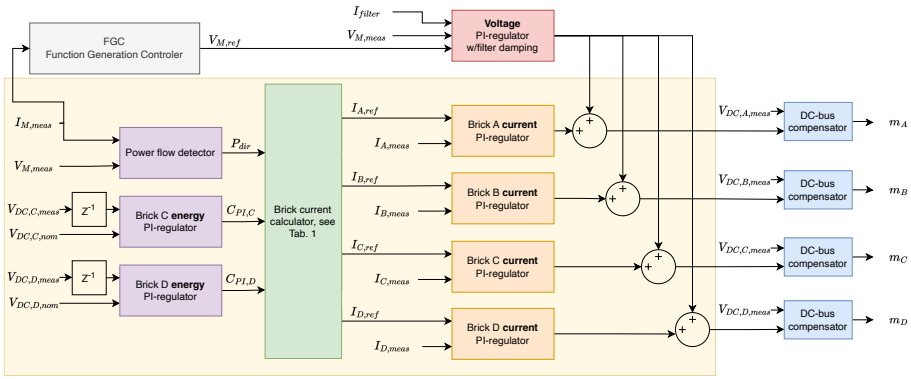

Figure 4.18: Control signal block diagram used in the experimental validation and the simulations.

Given the nature of the cycle, there will usually be some headroom in terms of voltage and current capability in the cycles during the different phases. This gives some flexibility in how the converter can be operated and these strategies have been investigated in Paper IV. Showing that the strategies allow the converter's performance to be optimised for different key metrics, such as optimised utilisation of storage, thermal loading of bricks or load on the grid.

Power flow control strategies

The list below enumerates the 5 strategies tested and verified in this thesis. The first is enumerated as strategy zero, as it is considered the default behaviour of the converter and presented in Paper II. This also keeps the strategy number for 1-4 consistent between Paper IV, Paper V and the thesis. Presently the converters at CERN separate between the current control in the Function Generation Controller

(FGC) and the voltage source control done by the DSP in each converter. There is a limited possibility for these two systems to communicate their states and references and only a voltage reference is sent from the FGC to the DSP in addition to some state bits and state machine status. However, as described in Section 2.4, the trend is towards merging these functions in the future, which allows for greater transparency and enables more varied strategies taking into account the immediate future. Therefore, the following strategies have been devised and tested, to overcome the limitations of the current system, for the implementation of those strategies some custom code was developed for the DSP.

0. *Cycle agnostic:* This strategy can be considered the default and describes how the scalable converter in this thesis will behave when no information on the evolution of the cycle is provided. It was presented in Paper II. Figure 4.11 shows the experimental verification of the agnostic cycle. The grid bricks supply the current until their capabilities are met, and then the storage bricks kick in. During the ramp-down phase, the storage bricks calculate how much energy they need to recover, and ensure that they have sufficient current to recover what they need.

1. *Sharing current stress:* This approach tries to evenly share the current stress between the grid and storage bricks while ensuring the recovery of the energy in the storage bricks by supplying a negative current from the grid bricks during ramp-down. The principle of this strategy is shown with the grid brick current reference as the red line in Figure 4.19.

2. *Sharing current stress - Short:* At the end of the flat-top, the previous strategy has a large and abrupt change in current for the grid brick. Strategy 2 aims to mitigate this, by letting the storage bricks fully recover the current during the ramp-down and thus absorb all the energy in the magnet. This limits the usage of storage, as no energy can be supplied directly from the grid brick. This is shown with the grid brick current reference as the blue line in Figure 4.19.

3. *Minimal grid current RMS:* The grid brick current reference is shown as the pink line in Figure 4.19, it shows a strategy where the absolute value of the current from the grid bricks is kept constant, minimising the RMS current of the grid brick. Note that the voltage is not constant during the pulse as shown in Figure 2.5, thus the power of the grid brick is not constant.

4. *Minimal peak grid power:* The final strategy tries to keep the grid brick power constant, and thus the power supplied from the grid constant. This is

done by mirroring the voltage of the magnet as shown in Figure 2.5 which gives a current as shown by the grid brick current reference with the green line in Figure 4.19.

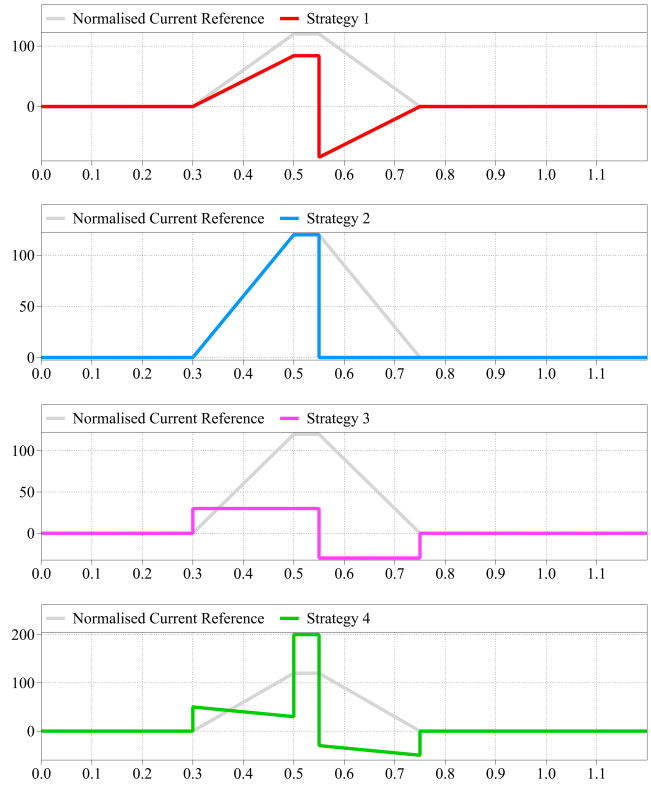

Figure 4.19: Possible grid brick reference shapes for the grid brick to implement the different energy management strategies.

Redundancy

In addition to the different key target optimisation, there is also a possibility for the scalable converter to operate in redundancy mode. Figure 4.20 shows how the controller allows for the continuing operation of the converter in the event of a single storage brick failure. Naturally assuming that the brick fails in an open circuit mode, and does not cause a short-circuit. This might either be because the switches fail in an open circuit, or because the failure is detected and the failed brick is disconnected. In the case of a short-circuit some kind of switch would be needed to isolate the fault from the rest of the circuit. Since the current sharing

between the types of bricks is done dynamically, there is no need for the controllers to be reconfigured, so they can run without interruption assuming sufficient redundancy is included. Figure 4.21 shows the topology used for the simulation. Storage brick 1 is assumed to fail and disconnected between pulses 3 and 4.

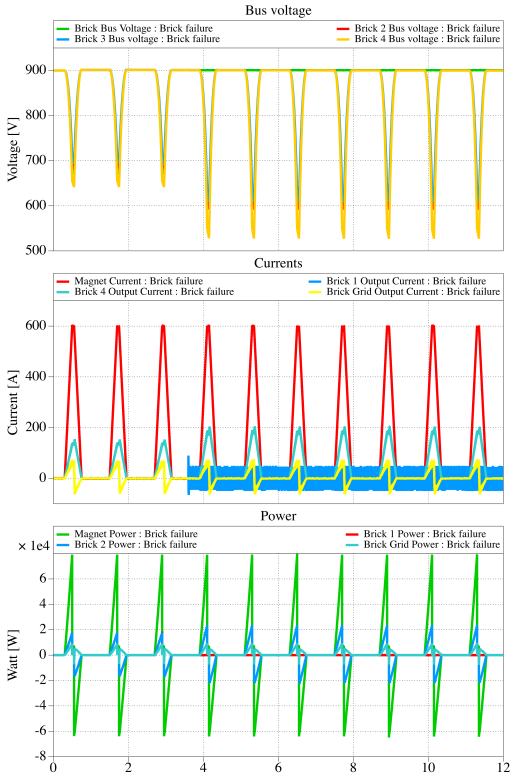

Figure 4.20: Simulation showing the controller compensating for a brick failure and redistributing the power flow.

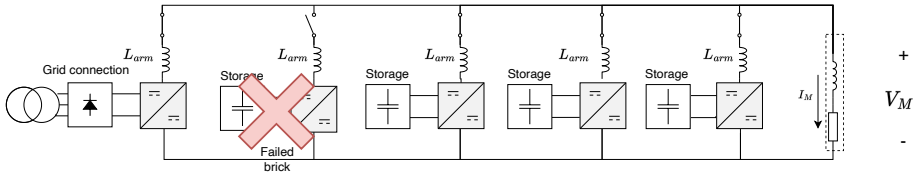

Figure 4.21: The topology used for the simulation, with 1 grid brick and 4 storage bricks.

4.2.2 Experimental verification

The lab experiment is based on the theoretical work from the paper presented in Section 4.2.1, which shows an experimental verification of the scalable converter, where 4 different strategies were implemented to optimise for different key metrics. Such metrics can be the grid side current, component thermal stress or storage utilisation. Each strategy ensures that the storage is fully replenished at the end of each cycle. The complete experimental verification is included in Paper V.

Laboratory configuration

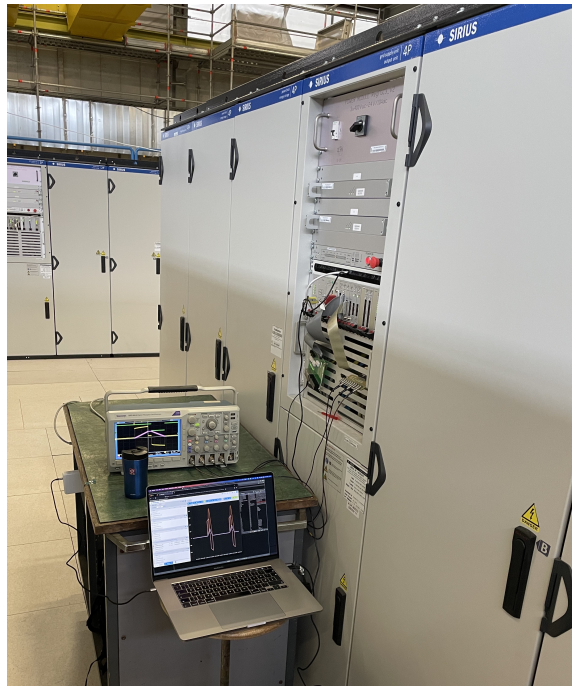

Figure 4.22: Photograph of the laboratory set-up.

For the experimental validation, an existing 800kW power converter in the CERN

Table 4.4: Converter IGBT parameters

CM1200DC-34N	Voltage	Current
Rated value	1700V	1200A
Max designed	450V	450A

East Area was utilised. The location of East Area in the CERN accelerator complex can be seen in Figure 1.1. The converter is a CERN-developed DC-DC converter employing four full-bridge circuits with energy recovery connected in parallel. A photograph of this test setup is illustrated in Figures 4.22 and 4.23, with the schematics of the topologies shown in Figure 4.14. (A more detailed circuit diagram can be found in Figure 2.1.) The energy recovery is conducted via a large capacitor bank on the DC-bus of the converter and the load and system losses are supplied from the electrical grid via a transformer, diode rectifier and a DC/DC boost converter stage. By increasing the voltage of the DC-bus, more energy is stored in the capacitors, and conversely, by reducing the voltage the stored energy is reduced. The usable energy is described by Equation 4.1.

Figure 4.23: Photograph of the laboratory set-up, showing the power stack, gate drivers and DC-bus filter capacitors integrated into the cabinet. The storage capacitors can be seen at the bottom.

The controller is the same Texas Instrument DSP integrated with a CERN-developed current measurement system as described in Section 4.1.5.

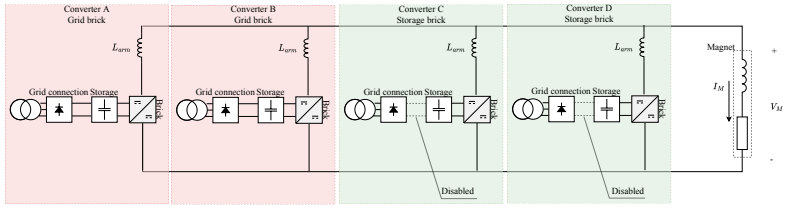

Figure 4.24: System topology used in the lab setup, showing the two configurations used.

Table 4.5: Converter parameters

	Grid Connected Brick	**Energy Storage Brick**
Max Voltage	200V	200V
Max Current	400A	400A
Energy Available	N/A	9.4kJ @900V

As shown in Figure 4.24, the four bricks have a grid connection via a transformer each, a diode rectifier, a boost, a DC-bus and an IGBT-based full-bridge circuit on the output. The design parameters of the converter in the test setup are summarised in Table 4.5. The two types of bricks used in this paper were obtained by modifying the existing converter in the same ways as described in Section 4.1.5.

Table 4.6: Case load

Load parameter	**Value**
Inductance	55mH
Resistance	75mΩ
Max current	960A
Pulse current flat-top	700A
Peak stored energy at @700A	13.5kJ
RMS power	8kW
Peak power	140kW

The load is an operational specimen of an electromagnet. The magnet parameters are listed in Table 4.6. In this set-up, 2 storage bricks are required to have enough storage capacity to recover the energy stored in the magnet and 4 total bricks was required to have the current capacity to test the strategies. The output voltage was also limited to 200V to protect the magnet in case of instabilities in the converters.

This is a load used in the accelerator complex, and risking any damage to the magnet was not acceptable.

Summary of main findings

The four strategies used in this experimental validation have been enumerated in Section 4.2.1, and some of the main findings are given below. The full description and findings are presented in Paper V. In these plots the grid bricks are Brick A and B, while the storage bricks are Brick C and D.

In Figure 4.25 a plot from the experimental validation of Strategy 1 is illustrated. This plot shows the bricks delivering different currents based on whether they are grid bricks or storage bricks. In these plots, the grid bricks supply a current with a shape equal to that of the total reference, while the storage bricks use their stored energy to ensure the load supplied to the magnet is correct. At 3 seconds into the cycle in Figure 4.25, the current supplied by the grid bricks is reversed and goes to negative values. At the same moment, the voltage also reverses, as the current is ramped down, thus the *grid bricks* need to reverse the current in order to supply a positive power into the load since they do not have any ability to store energy in the scalable converter. This strategy allows for the grid and storage bricks to have relatively similar RMS currents, optimising for similar lifetimes between the two types of bricks. The RMS of the grid and storage bricks found in the experimental validation was 45.1A and 115A respectively.

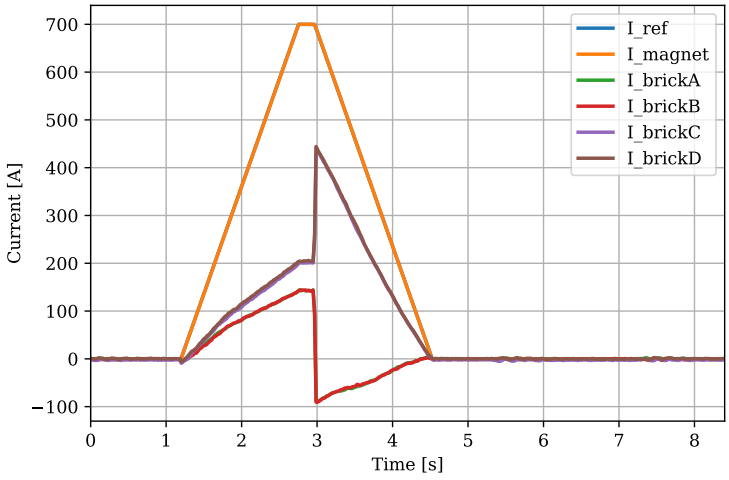

Figure 4.25: Results from the experimental validation showing the currents from the bricks using one of the strategies (Strategy 1).

Figure 4.26 show the experimental verification of Strategy 2, which is similar to

Strategy 1, except the grid bricks do nothing during the ramp-down. This limits the energy that the storage bricks can recover, and thus, the amount of energy they can supply in the other phases. In Strategy 1 the grid brick can inject energy into the storage bricks during the ramp-down phase, but in Strategy 2 this is not used and so the total re-usable energy is the energy stored in the magnet minus the losses in the storage bricks. The advantage is the absence of negative currents for the grid bricks, which limits the peak current of the storage bricks and improves the stability of the converter during the transition phase.

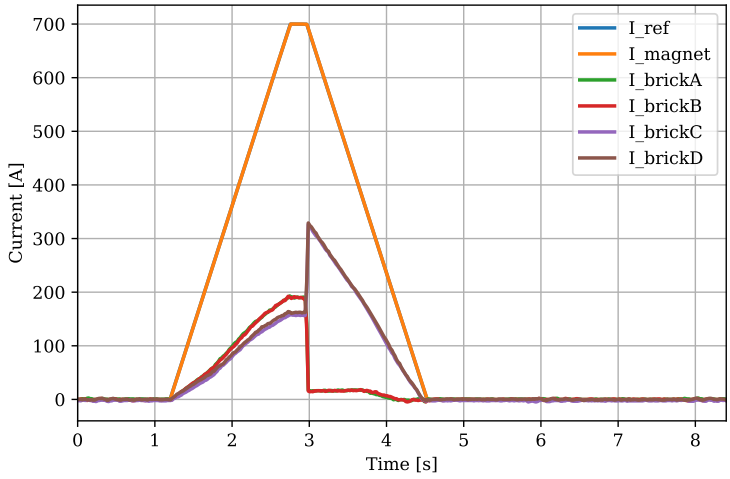

Figure 4.26: Results from the experimental validation showing the currents from the bricks using one of the strategies (Strategy 2).

Strategy 3 and 4 are strategies optimising for the grid load and trying to use the converter to provide peak-shaving of the peak power to the operation of the converter. Strategy 3 tries to supply a constant grid brick current, as shown in Figure 4.27. It has a constant supplied current, but due to the non-constant voltage, the power is not constant. This strategy uses the storage better than Strategies 1 and 2, at the cost of higher storage brick peak and RMS currents.

The final strategy (Strategy 4) tries to supply constant power from the grid brick. Since the bricks are parallel connected, and the output voltage is constrained by the global current reference and thus the global voltage reference, the current is calculated by dividing the constant power target by the measured output voltage. This gives the result in Figure 4.28, where the current from the grid bricks is very sensitive to the output voltage, and there needs to be a filter or delay to ensure that voltage oscillations do not propagate into the current reference. This strategy is the most challenging to control but perhaps has the clearest advantage as it creates

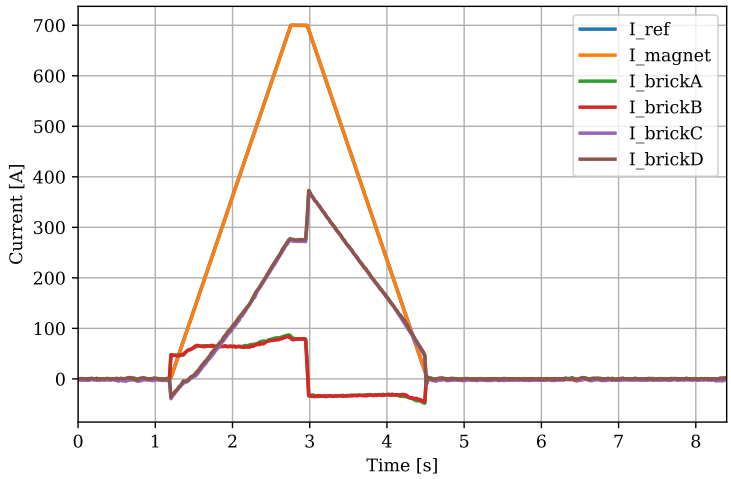

Figure 4.27: Results from the experimental validation showing the currents from the bricks using one of the strategies (Strategy 3).

very predictable and constant power drawn from the grid. It also utilises the storage quite well compared to the other strategies, since the storage bricks are very active; yet, the peak currents are quite high and there are several transitions which could impact the accuracy of the output.

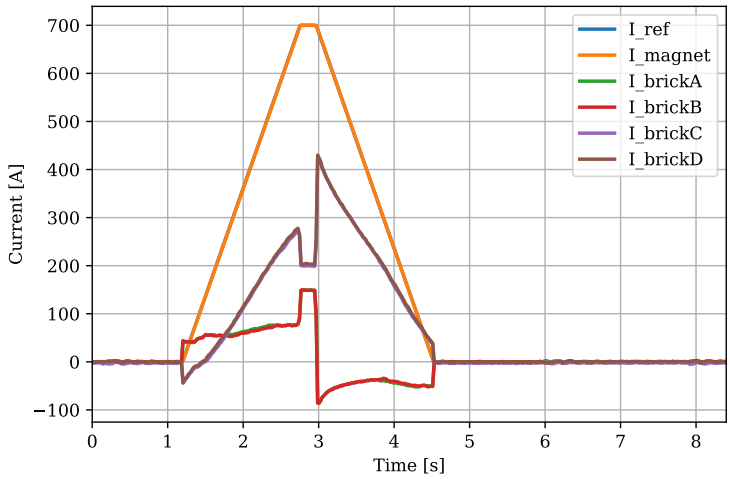

Figure 4.28: Results from the experimental validation showing the currents from the bricks using one of the strategies (Strategy 4).

4.3 Summary and scientific contributions

Modular power converters are built using identical power bricks that are controlled in the same way to multiply the current or the voltage capability, often resulting in less efficient use of the hardware such as energy storage or semiconductor capability. While scalable modular power converters yield the additional benefit of better component utilisation buy a care full selection of the fundamental hardware block size with an additional layer of control software.

There seems to be a very interesting range of output voltages for the design of the scalable brick between 300V and 600V, where the cost of storage is balanced by the cost of semiconductors. Choosing the higher voltage from the range may be interesting from a minimising the complexity perspective while choosing the minimum brick voltage is interesting for enhanced scalability, redundancy and utilisation of storage. It is also noticed that the scalable brick does not require the boost stage to the DC-bus used by the converters as described in item 2 in the list in Section 2.1. This makes the converter hardware more scalable and allows it to more closely be adapted to the need of the individual magnet.

The flexibility offered by the separation of storage and grid allows for internal algorithms to be implemented. They can enhance the performance of the converter in many different ways to optimise for different key parameters, while four planned strategies have been demonstrated in addition to one agnostic strategy.

The four planned strategies allow the converter to optimise for lifetime (Strategy 1) or peak-shaving and storage utilisation (Strategy 4). There are also two more stable versions of this optimising for lifetime (Strategy 2) and peak-shaving and storage utilisation (Strategy 3). This allows the converters to be optimised in different ways by utilising the same hardware and only re-configuring the software.

Therefore the results demonstrate a scalable approach both in hardware and in software. Based on the work presented in this thesis, the main scientific contribution of the thesis are repeated here and linked to the papers where the results were published.

1. A scalable power converter for supplying high-precision current to the accelerator magnets and recovering the energy. The converter allows for safe and stable operation on par or exceeding existing solutions.

   Paper I found the optimal technology and a voltage range of 300-600V for the scalable converter and, it showed a cost advantage employing SiC MOSFETs when considering the lifetime costs by including the cost of the electrical losses.

   Paper II demonstrates that the scalable converter can be designed and operate with separated storage and can perform on par with the existing converter solution. It also shows that when compared directly with the existing solution the hardware costs can be reduced by 30%.

   Paper III investigates the impact of switching frequency and interleaved parallel connections on the output current ripple. It shows that increasing the number of interleaved bricks can reduce the peak-to-peak current ripple from 12ppm for 2 bricks to less than 2ppm for 16 bricks, when the bricks are all switching at 40kHz.

2. A method to find the most cost-effective switching technology and electrical characteristics of the proposed converter design, including lifetime cost and other external targets. It has been published in Paper I, showing a cost saving of 50% for SiC MOSFET compared to silicon IGBT, when considering the lifetime cost of the device.

3. Energy flow control scheme to allow for adapted operation of the scalable converter, increasing the utilisation of the hardware.

   The analytical investigations were published in Paper VI and the full-scale hardware verification in Paper V.

Chapter 5

Conclusion and Further Work

5.1 Conclusion

After investigating several topologies and the performance with regard to the CERN requirements for their power converters, the simplest form of a more scalable converter has been suggested.

The main results of this PhD project are to propose the design principle for this scalable converter and demonstrate its feasibility, both in theory and in practice. The primary difference between this scalable converter and the current state-of-the-art is the ability of the proposed concept to separate the storage into discrete units. This enables the converter to scale for the resistive and inductive power independently. In particular the number of grid bricks is determined by R_{mag} and the supply of storage bricks by L_{mag}, while a check to ensure the bricks can manage the total current I_{flat} should also be done. If more bricks are needed to supply the total current, the designer has a choice and can optimise for that particular case. Compared to the existing solution, a cost saving of 30% can be obtained when using the same components.

Since the modular scalable converter enables a greater number of modules, revisiting the current and voltage targets for the converters seems to provide a great opportunity. When considering silicon IGBTs the optimal output voltage range is 300V-500V, which is close to the current design, which is using 450V on the output. However, when SiC MOSFETs are considered a significant cost saving can be achieved, and the optimal current and voltage parameters shift towards lower values and higher numbers of bricks. For SiC MOSFETs based bricks the optimal output voltage is between 300V and 600V. The increased number of bricks in-

creases the utilisation of the components, as the total voltage and current rating of the combined bricks are more likely to be close to the load requirements. This also increases safety, as less energy is stored in each unit, while it also makes redundancy a more feasible option. This is definitely an altogether promising direction for the power converters at CERN.

The separated storage and grid supply impose a need to control the internal power flow of the converter since the storage has no direct way of being replenished. This is achieved by utilising the headroom afforded by the trapezoidal nature of the current pulse and by recovering the energy stored in the magnet. In total five different strategies to control the power flow have been investigated and verified. The default strategy is agnostic, and so does not require any information on the duration or peak current of the cycle, which is compatible with the current way the converters are operated at CERN.

The other four strategies assume that the full cycle is known to the converter and allows it to plan the power flow based on this. Of the four strategies demonstrated the first focuses on lifetime, by sharing the current stress among the bricks as equally as possible. The second strategy also shares the current stress, but it improves stability by reducing large transitions. This strategy has the highest stability of the four. The final two strategies aim to peak-shave the peak power load on the grid and grid bricks as much as possible. In particular, the third strategy does peak-shaving by supplying a constant current from the grid bricks during the pulse. However, since the voltage on the output is not constant, the power is also not constant. So the last strategy tries to find a constant power by using the measured voltage on the output to derive the current reference based on a constant power target. The latter strategy utilises the storage the most, at the cost of very sensitive current control, while the third strategy might offer an interesting compromise while still utilising the storage well. So the different strategies allow the converter to be optimised based on lifetime, peak grid power required or utilisation of storage.

5.2 Future work

If the direction of lower ratings and thus a higher number of bricks per converter is chosen, many different advantages for dynamic and selective control of the power converters can be utilised. By having the ability to selectively disconnect or bypass individual bricks, the peak-shaving methods discussed here can be deployed further and the load can be shared across the full operation of the converter and not just the pulse phase.

The nature of the scalable solution is based on power bricks, and the SiC MOS-

FETs have a beneficial positive thermal coefficient to increase current, making them suitable for parallelisation. This offers benefits for the segmentation of storage and more cost-effective redundancy, where the extra hardware needed for redundancy can be relatively inexpensive. The lifetime of the SiC MOSFET is determined primarily by the thermal cycling of the device but is also related to the absolute temperature for a cycling application like this. The initial assumption is that the temperature should be kept as constant as possible and below 100°C. Finding a thermal design that can enable SiC MOSFETs seems to have a large potential. Currently, the lifetime under thermal cycling is the primary limitation for using SiC MOSFETs in cycling applications such as those discussed in this thesis.

A lot of possible topics proposed for further developing this scalable converter concept is as follows:

- Individual bricks are disconnected or bypassed when not needed for specific load types.
- Redundancy to enable the power converters to continue to operate after failures of a module.
- Lifetime of SiC MOSFETs in high power cycle applications, where not enough is known at present to accurately predict the lifetime for 100 million cycles and above.
- Using DAB to replace the galvanic isolation of the input transformer with a more compact and energy-efficient solution.

If a more compact, flexible and efficient converter is desired, then combing a resonant DAB to the DC-bus with a full-bridge between the bus and magnet offers a very interesting solution, both for the grid brick and the existing solutions. As the attitudes currently stand, this is the end of the road for this concept. The utility has been demonstrated.

Article I

K. L. Haugen, K. Papastergiou, P. Asimakopoulos, and D. Peftitsis

On dimensioning the fundamental brick for a scalable DC-DC converter with energy recovery

Submitted to European Conference on Power Electronics and Applications (EPE'21 ECCE Europe), September 2021.

On dimensioning the fundamental brick for a scalable DC-DC converter with energy recovery

Krister Leonart Haugen
DEPARTMENT OF ELECTRIC POWER ENGINEERING
NTNU, Trondheim, Norway
Email: krister.l.haugen@ntnu.no

Konstantinos Papastergiou
MEDIUM POWER CONVERTERS SECTION
CERN, Geneva, Switzerland
Email: k.papastergiou@cern.ch

Panagiotis Asimakopoulos
MEDIUM POWER CONVERTERS SECTION
CERN, Geneva, Switzerland
Email: panagiotis.asimakopoulos@cern.ch

Dimosthenis Peftitsis
DEPARTMENT OF ELECTRIC POWER ENGINEERING
NTNU, Trondheim, Norway
Email: dimosthenis.peftitsis@ntnu.no

Abstract

For the design of a power converter with energy recovery operation, a trade-off is related to the choice of the output and dc-link voltages, which, in turn, determines the choice of the blocking voltage capability of the semiconductor switches. This work investigates the possibility to optimise the capital and operation costs and the performance (ripple) globally for a farm of 350 converters by considering the voltage rating and device type of a fundamental brick used in these modular converters. It is shown how considering the purchasing and operating costs separately can yield in different conclusions. It also highlights the effect of high precision requirements on the converter scalability and final cost. This paper investigates the design of the fundamental brick and optimisation possibilities for such converters in terms of cost, efficiency, reliability and precision. Another important design and operating requirement for a converter is to deliver the required current in a large range of loads, such as electromagnets. In order to keep the maintenance cost low and components availability high, it is desirable to have only one solution for a given converter design. The optimal converter size from the perspective of a large converter farm, could be different from the design of an individual converter, or indeed if the optimisation focuses on cost, efficiency, reliability or precision.

≪Power Supply≫, ≪DC-DC power converter≫, ≪Modular Converter≫, ≪Energy Storage≫

Introduction

Large electromagnets are used to control the beam of particles in large physics experiments at CERN. The ultimate technology for powering these magnets is a power electronic converter [1]. Different operating constraints for such facilities necessitate the design of electromagnets having a wide range of sizes and current levels. In particle transfer lines at CERN, the electromagnets are used in circular accelerators facilities, the electromagnets are operated in cycling mode implying a significant amount of energy flow to and from the electromagnet in every cycle [2]. An example of such a pulse train is shown in Fig. 1a. As shown in this example, electromagnets receive a current pulse, typically trapezoidal, ramping from

zero to a certain flat-top value, before ramping down again to zero and remaining at zero until the next pulse is requested [3]. This process requires a high power for a short time, in particular as the current ramps up, to supply both the power losses, as well as changing the magnetic field.

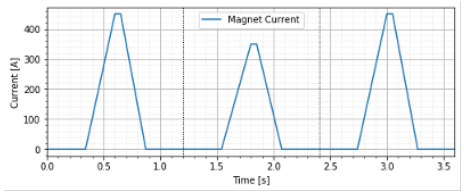

(a) Typical current cycle sequence, dotted lines indicate division between cycles.

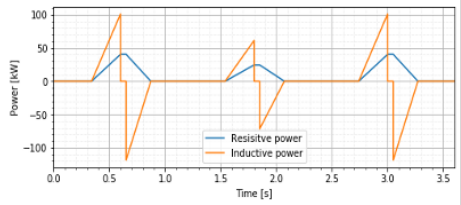

(b) Typical power requirement for the cycles.

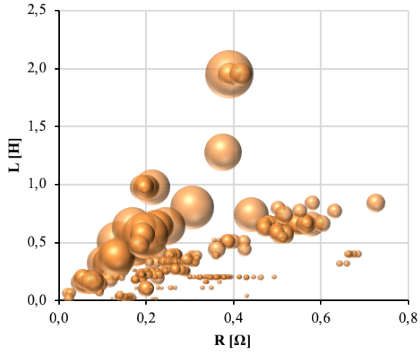

(c) Resistance and inductance plot of 350 electromagnets for CERN's North Area project, the blob size represents the total stored energy.

Fig. 1: Examples of load which the DC-DC converters have to be designed for.

If the ramping of the current is done over a minimal time, the power losses over a cycle duration are reduced. However, this requires higher power during the ramp-up and vice-versa. The curve shapes for the typical power requirements for such an application are shown in Fig. 1b. For a single such electromagnet, it is possible to find the optimum balance between the cost of installed power converter and the cost of power losses in the electromagnet. Therefore, for all identical magnets the same circuit can be deployed. However, these electromagnets are of many different sizes and require different current levels. To keep maintenance and part availability efficient, the ultimate desire is to have a scalable converter topology, whose design is based on a fundamental building brick to serve all these loads. Some similar approaches have been described before [4], but these do not include the energy recovery.

When these electromagnets operate at maximum current, they have a certain energy stored in the magnetic field, which is expressed as in Eq. 1, where L_{magnet} is the inductance of a particular electromagnet, I_{magnet} is the current through the magnet at any given time and E_{magnet} then becomes the energy stored in the magnet. Since the current is ramping from zero, the energy delta is the same as the energy stored in the magnet at the maximum current value.

$$E_{magnet} = \frac{1}{2} L_{magnet} I_{magnet}^2 \tag{1}$$

When the current of the electromagnet is ramped down, this energy can be recovered and reused in the next ramping up phase. This requires the presence of a storage system that is sufficient to handle this amount of energy, and with the power capability to deliver this energy in the relatively short time ($<$1s) of the ramp up and down process.

For all of the electromagnets the maximum operating current has been considered as the highest value for the flat-top. The inductance of the electromagnets is in the range from 4 mH to 2.9 H and the resistance is between 0.02-1.7 Ohm. It is worth to mention that the highest inductance, L, and resistance, R, of 2.9 H and 1.7 Ohm correspond to a single magnet (not shown), while the rest are shown in Fig. 1c. The R to L

ratio for these magnets is between 0.2 and 25, and the total energy stored in the magnet's magnetic field is between 10 kJ and 670 kJ with a median energy of approximately 20 kJ. This paper presents a scalable converter concept designed using a standardised fundamental brick. The circuit design and sizing of the fundamental brick is defined, and a system-level perspective is applied in order to obtain the brick output voltage and the size of the brick's storage component.

Fundamental brick concept

Each of these electromagnets can be modelled as a series connection of a resistor and an inductor. The resistive component models the power losses caused by the current, and the inductive component models the the recoverable energy stored in the form of magnetic field. By keeping this in mind, it becomes possible to separate the power requirements of the electromagnets into two types. From the power plot in Fig. 1b, showing the power for the inductive and resistive components separated, the power supplied by the two types of bricks can be considered. The inductive power; alternating positive and negative power flow and in principle without losses hereby called the *storage brick*. On the other hand, the resistive power is supplied by the so-called *grid brick*.

If the converter consists of two types of bricks, it is possible to scale the power to the inductive and resistive requirements independently. Thus, by choosing the minimal feasible brick output voltage for each type of brick, the converter can be scaled to each magnet in an optimal way. What is considered optimal depends on the requirements and can be cost, losses and cooling requirements, precision in the value of the supplied current, storage requirement and utilisation etc.

The application has very stringent requirements for the accuracy of the supplied current, and the energy recovery for the storage bricks requires a converter with a 4-quadrant operating capability to handle the bidirectional power flow. These types of converters are currently based on a H-bridge circuit [5, 6, 7], which is also considered here. The fundamental brick is shown in Fig. 2a in the red box. The full-bridge converter will be used for both storage and grid bricks to keep the system complexity to a minimum. While topics of control [8, 9, 5] and power flow [10] of DC-DC converters have been discussed elsewhere, this paper focuses on the challenge to find the most cost-effective size of these two bricks.

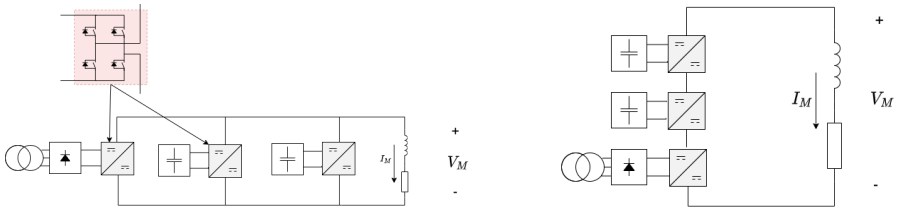

(a) Parallel connection of the bricks.

(b) Series connection of the bricks

Fig. 2: Schematic diagrams showing the parallel and series connection. The fundamental brick topology is shown in the red shaded area.

Storage brick

The storage bricks will use the H-bridge circuit presented in Fig.2a and connected on the left side to a storage component. The storage component can be any type of electrical energy storage, such as batteries, capacitors, mechanical flywheel [11, 12] or super-capacitors, depending on the amount of stored energy required, delivered power and storage time [13]. Given the short operating time of the current ramping, it seems that only capacitors are appropriate as storage elements [14]. This causes the voltage on the storage bus to be dependent on the state of charge of the capacitor. The amount of energy in the storage capacitor determines the total amount of storage in the brick. Using an H-bridge to control the voltage generated from the brick, only stepping down the dc-link voltage is possible. This sets constraints on

the lowest voltage on the storage bus during usage, since there always have to be sufficient charge left in the capacitors in order to keep this minimum voltage. The minimum requirement for the voltage on the capacitors reduces the amount of usable energy in the capacitors. Eq. 2 expresses the usable energy in the storage brick.

$$E_{brick} = \frac{1}{2}C(V_{bus}^2 - V_{out}^2) \tag{2}$$

Here the fundamental trade-off for the storage brick emerges. For a given capacitance in the storage brick, if the output voltage is set very low, a significant amount of energy can be used and thus, the cost of the storage is reduced. This, however, can result in a larger number of bricks in series in order to reach the voltage level required for the electromagnet, which eventually increases the cost of the semiconductors switches, since the bus voltage is kept at the same level in this scenario. This balance is one of the components used to arrive at the optimal brick size. It also allows for different blocking voltages on the switches to be considered, as the nominal bus voltage can be chosen, and it is determined by the device blocking voltage. The number of storage bricks required can then be calculated from the energy in the electromagnet in Eq. 1 divided by the energy in each brick calculated in 2. Modularising the energy storage in the fundamental brick, as opposed to having it central in the topology, is also related to safety. Managing smaller amount of energy tends to be easier and less costly, for example for building protection systems.

A modular design allows the investigation of different voltage levels for the bricks, the brick switches with different blocking voltages and current capabilities, and finally permits the segmentation of the storage into smaller units. By optimising for different targets, a brick-based design can be scalable in different ways.

Grid brick

The grid brick exhibits a simpler scalability design procedure. This is due to the fact that it needs to supply the power losses in the resistive part of the magnet, and also to compensate for the losses in the total system. To keep the idea of the modular system completely, the grid brick will use the same bus voltage and output voltage as the storage brick. However, the grid brick will be supplied by a diode rectifier connected to a three-phase AC grid. As there is not foreseen to have power flowing back to the grid, and the bus voltage is kept constant, the need for an active connection (e.g., active-front-end rectifier) to the grid to enable reverse power flow to the grid is eliminated. To allow the grid bricks and storage bricks to be connected in series and parallel freely, the total voltage required for all the grid bricks is also used for the total voltage on the storage bricks. This applies a constraint on the storage brick voltage in the calculations. Combining these assumptions and constraints, it is now possible to calculate the brick input voltages, but in order to select the optimal switches the current also has to be considered, and in order to figure this out the bricks first have to be combined into a system.

System configuration

The number of converter bricks is calculated based on the magnet properties and the fundamental brick ratings. Series connection of all the bricks forces the switches to carry the same current, requiring either parallel connection of several power semiconductor devices at switching positions or parallel connection of two identical arms if the required current is higher than a single switch can carry, in this paper we only consider the latter. The advantage is a large voltage capability allowing for low brick voltage or low ramping times of the current in the electromagnet, similar to the performance of a modular multilevel converter (MMC) [5]. This configuration is shown in Fig. 2b.

Parallel connecting all the bricks maximises current sharing between the switches, and thus reducing losses. It also allows the different bricks to be interleaved increasing accuracy on the current to the electromagnet. The energy now has to be transferred between the bricks by circulating the currents during the current pulse to the electromagnet, since the assumption is that no magnetic field can be allowed in the magnet outside the requested pulse. This configuration is shown in Fig. 2a.

The third principle is to combine series and parallel connection of bricks. More specifically one grid brick and one storage brick are always placed in series in a single arm, and the combined bricks are then parallel connected. This allows the energy to be corrected by the grid brick in each arm during the current pulse, enabling a good current sharing and utilising interleaving. The storage bricks can also be used for peak-shaving, by supplying the power required by the magnet for the power losses during the flat-top of the pulse. If the storage bricks are only used during current ramping, a bypass switch can be connected to soften the stresses on the storage switches and reduce the losses.

Optimum brick design and characteristics

Using the system described above, the various combinations were simulated in order to investigate their electrical performance. The critical parameters used in the optimisation algorithm are discussed and defined in the following sections.

Series connection of bricks

The inherent advantage of series connection is the ability to share the voltage supplied to the load. However, the basic principle is that the storage bricks are concerned with the inductive component, i.e. the recoverable energy of the magnet. While the the grid bricks are concerned with the restive part, i.e. the joule losses, is always central to the dimensioning of each type of brick. It also allows the storage to be distributed.

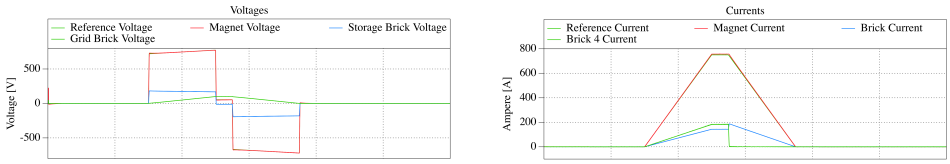

(a) The voltage in series connected bricks

(b) The current in parallel connected bricks

Fig. 3: Simulation results showing the series and parallel connection of bricks.

Figure 3a shows the voltage of the 4 series connected bricks, while all bricks conduct the same current since they are series-connected. By examining the voltages it is possible to see how the storage bricks, in this case 4, have a different voltage compared to the grid bricks. While the storage bricks work both to supply power and recover power, the grid brick works to supply power during the complete cycle to compensate for the joule losses.

Parallel connection of bricks

By sharing the current between parallel arms, the obvious advantage is to reduce the current stress on each brick, but it also allows the distribution of storage. For short pulses the total current stress can be shared between storage and grid bricks, and the grid brick current is significantly reduced. On the other hand, for pulses with longer flat-top, the storage bricks can have zero current and in principle they stop switching.

Figure 3b shows an example where there are 4 storage bricks and 1 grid brick, all connected in parallel. Therefore, they have to share the voltage, whereas they can deliver different currents. In this example, the green line in the current plot shows the current supplied from the grid, where it is observed that this current is zero during the recovery phase. If the grid brick should deliver power during the recovery phase, this current should be negative, since the voltage is negative, which would increase the peak current stress for the storage bricks.

Interleaving of parallel bricks

If a system has either storage or grid bricks connected in parallel, another benefit is to introduce interleaving in order to reduce the current ripple. For some applications the requirement for a very accurate

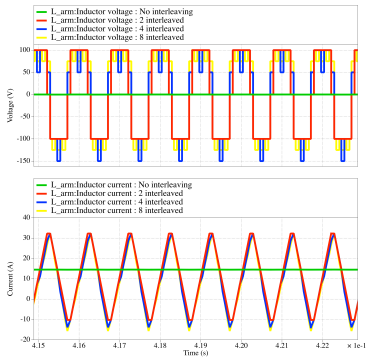

(a) Ripple current from the converters arm inductors.

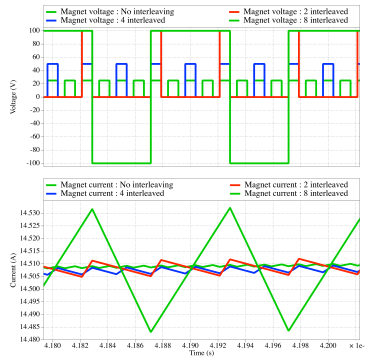

(b) Current ripple in the magnet.

Fig. 4: Simulation results showing the current ripple and effect of interleaving on the arm inductance and the magnet.

current results in significant filter costs reduction if interleaving is used. This can perhaps be better achieved by interleaving of parallel connected bricks.

Figure 4a shows simulation results, where the 4 different combinations of bricks are operated interleaved at 1 kHz of switching frequency. These simulation results were obtained considering 1, 2, 4 and 8 bricks respectively and using H-bridges with no filtering, as well as an arm inductance of 1 mH. The effect of interleaving on the magnet current ripple is approximately inversely proportional to the square of number of bricks. The arm current ripple is regulated primarily by the arm inductance and the switching frequency, and it is not influenced by the number of interleaving bricks.

Switching frequency

The peak-peak current ripple scales linearly with the inverse of switching frequency, as determined by the fundamental relation of the equation for an inductance. If the assumption is that the magnet inductive component is supplied with a voltage V_M, the current in the magnet i_M is given by Eq. 3.

$$V_M = L_M \frac{di_M}{dt} \Longrightarrow \Delta I_{arm} \approx \frac{V_{bus} - V_M}{2 f_{sw} L} \tag{3}$$

The voltage over the arm inductance is given by the bus voltage in the brick and the voltage over the magnet, either $V_{inductor} = V_{bus} - V_M$ or $V_{inductor} = -V_{bus} - V_M$. Since the duty cycle is close to 50% for most of the time, the delta time for the increasing current is $\approx \frac{1}{2f}$, the change in current is as described in Eq. 3 on the right for a single arm inductor. In the example shown in Fig. 4b, the estimated current ripple is 0.043A, while the measured is 0.05A.

Considering the ripple in the magnet itself, the interleaving makes the current ripple calculation a bit more complicated. The effect of interleaving reduces the current ripple approximately proportional to the number of sources since for each addition of interleaved source the apparent frequency is increased proportionally, which gives a modification of the voltage seen by the magnet. The average voltage over a switching period, as seen by the magnet, is determined by the average voltage over the resistor, consisting of a square pulse of 900V followed by zero voltage. The ripple is increasing during the time when the voltage is V_{bus} and decreasing when the net voltage is zero. The former is a very short part of the total time and so an assumption can be made, that the rise time can be neglected and the fall time is equal to the switching period. During the phase when the net voltage from the interleaved bricks are zero, the negative voltage over the inductor is equivalent to the average of the voltage over one period. The current change is very small, and the net voltage from the sources is zero. So the assumption $V_{bus} m = \hat{V}_M$, where

$\hat{V}_M$ is the average voltage over a pulse cycle and m is the modulation ratio for the PWM function, enables the equation to be expressed without considering the bus voltages and modulation ratio. The absolute current ripple for the interleaved case is described in Eq. 4. The relative current ripple then becomes as described by the result on the right in Eq. 4.

$$\Delta I_{ripple} \approx \frac{\hat{V}_M}{f_{sw} L_M N_{arms}} = \frac{I_{flat} R_M}{L_M f_{sw} N_{arms}} \Longrightarrow \Delta I_{ppm} \approx \frac{R_M}{L_M f_{sw} N_{arms}} \tag{4}$$

Optimisation algorithm

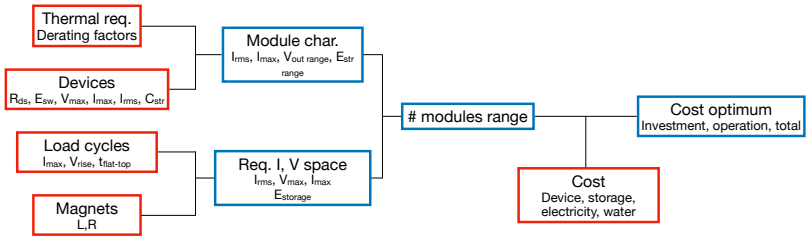

Fig. 5: Flow chart showing the steps of the algorithm.

Combining the assumptions in the above sections, it is possible to develop a flow chart for the optimisation procedure as shown in Fig. 5. The algorithm can be used to optimise the bricks' designs considering different design criteria and different constraints can be set to enforce a particular requirement. The result is a calculation optimising for the total cost for all converters given certain constraints. A Python script is used to handle the large number and range of the potential inputs, allowing different types of switches to be considered as well. The algorithm can take into account any type of restriction which can be expressed as an equation or if-test. It does not currently consider the costs of installation, cabling and other ancillary devices; such as inductors and gate drivers.

Table I: Algorithm input parameters

Type	Label	Range
Magnet resistance	R_M	0.01-1 Ω
Max magnet current	I_{max}	0.01-1 H
Voltage used for current ramping	V_{rise}	100-500 V
Time spent at max current	$t_{flat-top}$	5-20 ms
Device conduction resistance	R_{ds}	0.01-0.1Ω
Device switching energy	E_{sw}	1-100 mJ
Device max voltage	V_{max}	650-1700 V
Device peak current	I_{max}	50 - 1200 A
Device RMS current	I_{RMS}	25 - 600 A
Storage capacitance	C_{str}	1-100 mF
Thermal de-rating factor	$K_{thermal}$	0.1-1
Device cost, relative to reference design	C_{dev}	0.1-10
Storage cost, relative to reference design	$C_{storage}$	0.1-10
Electricity cost	$C_{electricity}$	0.01-0.1 EUR/kWh
Cooling cost, instalment, relative to reference design	$C_{cooling,install}$	0.1-10
Cooling cost, operation, relative to reference design	$C_{cooling,operation}$	0.1-10

The algorithm, shown in Fig. 5, works by considering the magnets parameters, resistance and induc-

tance, and combining it with the specific load cycle for each magnet, listed in Table. I. This results in a set of I_{RMS}, I_{max}, V_{max} and $E_{storage}$. Then the list of possible devices is collected from a data set generated from data sheets, these devices can be of any type and size. And in the results below both IGBT modules, MOSFET modules and TO-247 discrete SiC device are considered. For each type of device the thermal environment is considered and a module is compiled. Each module has a range of possible output voltages, and a corresponding available energy storage. The required current and voltage for each magnet is then achieved by every module in the range, and the losses and other costs are calculated for each of the possible bricks. The losses are calculated per device from the I_{RMS}, device conduction resistance and switching energy for hard switching. Only the device losses are considered, not the other system losses or the losses in the magnet, as they are assumed to be similar for all the cases and don't contribute to the optimal selection. Finally the costs are added together for each of the brick output voltages and plotted. From the curves it is then possible to find the value of the brick output voltage corresponding to the lowest cost. To generate the results below, a total of 126 727 cases has been considered for the 353 magnets and the costs are scaled relative to the cost of the existing solution. The vertical lines represents an uncertainty in the cost of +/- 10%, showing the sensitivity of the solutions to the costs considered.

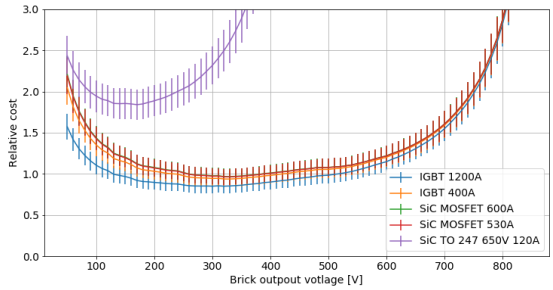

Fig. 6: Example of a brick output voltage optimised for total switch and storage installation cost.

In Fig. 6 the result of one such optimisation is shown. In this example only the capital cost of the H-bridge and storage is considered, where the optimum voltage is found to be in the range of 300 V to 500 V. Considering only the investment cost, there is perhaps no surprise that the traditional IGBT design with the largest current capability is also the most cost efficient, because it implies less series and parallel connected bricks in each converter.

By introducing parameters for lifetime cost of the converters, the optimum brick design changes. Here the cost of water-cooling is added, both the initial capital cost and the operation costs during the a project lifecycle of 20 years for the cooling, along with the cost of electricity lost in the converter. Figure 7 shows the total costs when the operational costs are included, and SiC MOSFETs emerge as a more interesting solution.

Another possibility is to optimise for current accuracy, a threshold value for a required accuracy delivered by the combined DC-DC converters without using filters. When this requirement is introduced, the number of parallel connected arms generally increases, thus increasing the costs. However, the TO247 type device already requires a large number of parallel connections due to the low current rating and thus the cost of the solution based on these devices does not increase significantly. It's also worth pointing out that the switching frequency is always kept constant in these results. However for the SiC devices the possibility to increase switching frequency is a large benefit to increase the accuracy. Considering the set accuracy requirement the results are plotted in Fig. 8. The costs have generally increased as a new important constraint has been applied, in particular the costs of the IGBTs have increased by 50% or more. Using interleaving to achieve an accuracy target does not seem interesting for the IGBT based solutions, but it is very compelling when smaller SiC devices are considered.

In summary a brick voltage in the range of 500 V for SiC based MOSFETs and 200 V for TO-247 seem

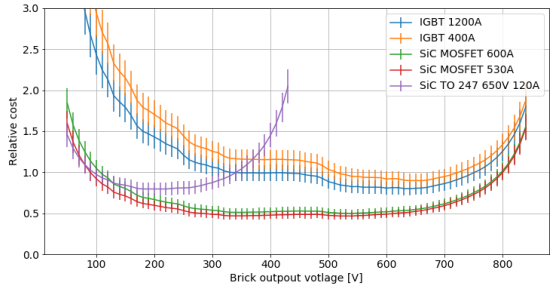

Fig. 7: Example of a brick output voltage optimised for total installation and operation costs.

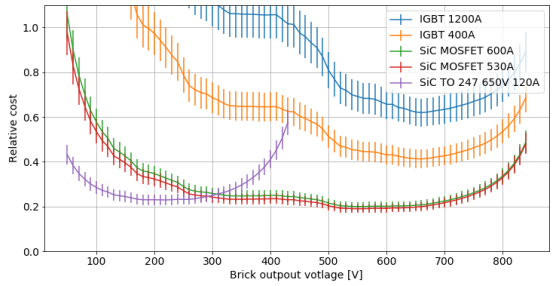

Fig. 8: Example of a brick output voltage optimised for total installation and operation cost with a strong requirement on the accuracy of the output current.

very interesting when considering the total cost of the system for a large range of loads. It also shows the benefits of considering smaller devices or SiC MOSFET emerge when operational costs and filtering are introduced. It also shows how lifetime costs can be the dominating driver of the lifetime costs of a system solution and it is fundamental to consider if a true low cost solution is to be selected.

Conclusion

This paper shows how a modular power converter can be assembled from a number of smaller DC-DC converters, and for certain applications provide benefits, and demonstrates how the fundamental brick ratings affect the a large-scale converter facility. An optimisation tool that includes the storage design and cost, as well as the semiconductor switches has been developed. This tool can be used to find the optimal brick size for an application given targets such as the converter output ripple, target semiconductor ratings, losses etc. It is shown that when the target is to minimise capital and operation costs of the project over a 20-year period, a fundamental brick voltage rating of 500V is optimal with power modules and 200V is optimal when evaluating discrete devices only. When considering the IGBT based bricks, the optimum voltage is relatively high by comparison to the SiC based bricks and this reflects the higher conduction losses of the devices and the need to keep the number of modules to a minimum. A step down in the relative project cost can be noticed at around 500V of brick rating; this is a reflection the fact that for most of the magnets the total voltage required is 500V or less. As this level is reached, most of the magnets are supplied by a solution with only one brick of each type. While the SiC based devices have the same step, this step is less pronounced, indicating that the SiC devices are more suited to parallelisation. If the lifetime costs of the system is considered, the SiC based technologies emerge as competitive.

References

[1] Sebastian Maestri et al. “Figures of merit for the evaluation of regenerative power converters”. In: *2016 18th European Conference on Power Electronics and Applications, EPE 2016 ECCE Europe* (2016), pp. 1–9. DOI: 10.1109/EPE.2016.7695462.

[2] B L M Lamaille et al. “Study of the Energy Savings Resulting From the East Area Renovation”. In: *10th Int. Partile Accelerator Conferance* (2019), pp. 4023–4025. DOI: 10.18429/JACoW-IPAC2019-THPRB087.

[3] Panagiotis Asimakopoulos et al. “On Vce Method: In Situ Temperature Estimation and Aging Detection of High-Current IGBT Modules Used in Magnet Power Supplies for Particle Accelerators”. In: *IEEE Transactions on Industrial Electronics* 66.1 (2019), pp. 551–560. ISSN: 02780046. DOI: 10.1109/TIE.2018.2823689.

[4] Marcin Parchomiuk et al. “Modular high precision high current source for special applications-Simulation and verification”. In: *Proceedings - 2016 10th International Conference on Compatibility, Power Electronics and Power Engineering, CPE-POWERENG 2016* (2016), pp. 422–427. DOI: 10.1109/CPE.2016.7544225.

[5] A. Lesnicar and R. Marquardt. “An innovative modular multilevel converter topology suitable for a wide power range”. In: *2003 IEEE Bologna PowerTech - Conference Proceedings* 3 (2003), pp. 272–277. DOI: 10.1109/PTC.2003.1304403.

[6] Gregory J. Kish. “On the emerging class of non-isolated modular multilevel DC-DC converters for DC and hybrid AC-DC systems”. In: *IEEE Transactions on Smart Grid* 10.2 (2019), pp. 1762–1771. ISSN: 19493053. DOI: 10.1109/TSG.2017.2777473.

[7] Stefan M. Goetz, Angel V. Peterchev, and Thomas Weyh. “Modular multilevel converter with series and parallel module connectivity: Topology and control”. In: *IEEE Transactions on Power Electronics* 30.1 (Jan. 2015), pp. 203–215. ISSN: 08858993. DOI: 10.1109/TPEL.2014.2310225.

[8] Bas J.D. Vermulst et al. “Scalable multi-port active-bridge converters: Modelling and optimised control”. In: *IET Power Electronics* 10.1 (2017), pp. 80–91. ISSN: 17554543. DOI: 10.1049/iet-pel.2016.0191.

[9] Soleiman Galeshi, David Frey, and Yves Lembeye. “Efficient and scalable power control in multi-port active-bridge converters”. In: *2020 22nd European Conference on Power Electronics and Applications, EPE 2020 ECCE Europe* (2020), pp. 2–10. DOI: 10.23919/EPE20ECCEEurope43536.2020.9215905.

[10] Krister Leonart Haugen et al. “Energy flow control in a modular DC-DC converter with energy recovery”. In: *PEDG*. 2021. ISBN: 9780738142.

[11] Daryl R. Brown and William D. Chvala. “Flywheel energy storage: An alternative to batteries for ups systems”. In: *Energy Engineering: Journal of the Association of Energy Engineering* 102.5 (2005), pp. 7–26. ISSN: 15460118. DOI: 10.1080/01998590509509440.

[12] Richard Magdalena Stephan, Rubens de Andrade Jr., and Guilherme Gonçalves Sotelo. “Third Generation Of Flywheels: A Promising Substitute To Batteries”. In: *Eletrônica de Potência* 13.3 (2008), pp. 171–176. ISSN: 14148862. DOI: 10.18618/rep.2008.3.171176.

[13] Guishi Wang et al. “A review of power electronics for grid connection of utility-scale battery energy storage systems”. In: *IEEE Transactions on Sustainable Energy* 7.4 (Oct. 2016), pp. 1778–1790. ISSN: 19493029. DOI: 10.1109/TSTE.2016.2586941. URL: http://ieeexplore.ieee.org/document/7506096/.

[14] Tarek M. Masaud, Keun Lee, and P. K. Sen. “An overview of enrgy storage technologies in electric power systems: What is the future?” In: *North American Power Symposium 2010, NAPS 2010* (2010). DOI: 10.1109/NAPS.2010.5619595.

Article II

K. L. Haugen, K. Papastergiou, and D. Peftitsis

A scalable DC/DC converter topology with modularised energy storage for high energy physics applications

Published in IEEE Journal on Emerging and Selected Topics in Power Electronics, Mai 2023.

This article has been accepted for publication in IEEE Journal of Emerging and Selected Topics in Power Electronics. This is the author's version which has not been fully edited and content may change prior to final publication. Citation information: DOI 10.1109/JESTPE.2023.3268420

A scalable DC/DC converter topology with modularised energy storage for high energy physics applications

Krister Leonart Haugen, *Member, IEEE,* Konstantinos Papastergiou, *Member, IEEE,* and Dimosthenis Peftitsis, *Senior Member, IEEE,*

***Abstract*—This paper presents the design and control of a high-power modular DC-DC converter for electromagnets used in high energy physics applications. The fundamental building modules, herein called bricks, can either be connected to the grid or to separate energy-storage components. The proposed modular converter enables independent power flow control among the bricks under control that is agnostic to mission profiles. In particular, the proposed converter design and control allow for independent control of currents delivered from each brick, while respecting the total voltage constraints, and losses optimisation of the converter without compromising the desired electrical performance. In addition, the cost potential of the converter is briefly analysed. The performance of the proposed modular converter is validated experimentally on a full-scale lab prototype rated at 800 kW. The proposed converter demonstrates how separating the total storage into a number of storage bricks can be beneficial to adapt the design of a modular converter to a large range of profiles and operating constraints. It is shown that up to 30% cost savings can be achieved by eliminating converter components in the storage and grid connection, while the converter performance on the load is maintained and the same amount of energy is recycled.**

I. Introduction

THE European Organisation for Nuclear Research (CERN) is a large complex, where a large range of physics experiments are conducted. In order to supply these experiments with the high energy particles, large electromagnets are used. They have to cover many different functions, but fundamentally they supply a bending (Lorenz) force to the charged particle beams. The size and accuracy of such a force is essential to ensure stable and reproducible high energy physics experiments, and thus the currents supplied are critical [1], [2].

A state-of-the-art power electronics topology for supplying these electromagnets with high precision currents is the full-bridge DC-DC converter [3]–[6]. The four quadrant operation of such converter also enables the possibility to recover energy stored in the magnetic field, when this field is no longer required by the load. For the majority of the electromagnets in the transfer lines between accelerator or to experimental areas at CERN, the particle beams pass through in short time intervals (i.e., in the range of milliseconds) at a regular cadence (e.g., 1.2 s is a typical cadence used at CERN). By turning the electromagnets off between each beam passing, significant energy savings have been achieved [7]. Thus, it follows that future power converters should have the ability to recover and recycle the magnet energy. The current profile and the highly inductive loads result in a very high peak power requirement, yet the losses of the magnet can be relatively low. The energy need supplied from the grid as the losses can be equivalent to 10% of the total energy injected into the magnet [8]. This poses a challenge for the design of the converter.

The current trend in power converter design at CERN is towards standardisation. As the CERN complex is growing the need to have fewer types of converters is important to ensure effective operation and maintenance. This naturally leads the way to using modular converters. Such converters have been proposed for high energy physics before [9]; however, those designs do not include the energy recovery capability. While at CERN this approach have been implemented using a floating voltage design [10]. In principle such a power converter can be compared to a Modular Multilevel Monverter (MMC) [4], where extensive research has been done to optimise the topologies for AC applications [11]–[14]. On the other hand, the loads considered at CERN mainly require a cycled direct current.

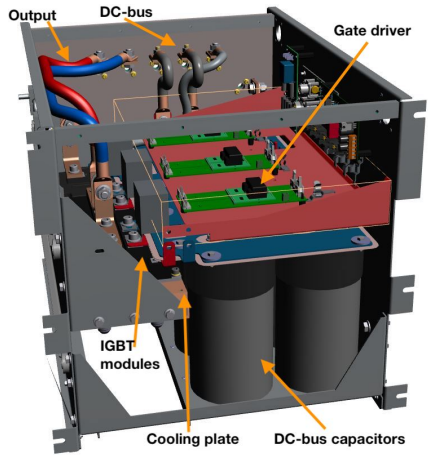

Fig. 1. The scalable converter fundamental brick.

By constructing a converter from several smaller fundamental bricks, with independent energy sources, the possibility for optimally controlling the internal power flow becomes feasible [15]. Such power converters with Distributed Energy

Manuscript received December, 2022; revised February, 2023.

Resources (DER), exhibit a distinct advantage in achieving a large degree of modularisation [16], and deliver more scalable systems. It is possible to imagine this converter to be re-configurable, and offer the flexibility sought in Electric Vehicle (EV) charger applications [17].

In a previous work [18], it has also been shown that a modular design with a larger number of bricks, can be cost effective when considering a larger range of electromagnet loads. In that paper, it has been shown that the selection of the electrical ratings and thus, the number of converter bricks is a cost-to-performance consideration. In particular, this becomes important in case of supplying loads with a large spread in their inductive and resistive characteristics. The design parameters for the converter presented in this paper have been derived by following the optimization procedure shown in [18]. However such converters present some complexity in the power flow management [19].

This paper presents a converter concept that extends the scalability of the existing conventional CERN design, to allow two different brick implementations; one with energy storage and for grid connection, all based on a single fundamental brick shown in Fig. 1. The proposed converter design incorporates a control strategy to regulate the power flow independently from the storage and the grid bricks. This makes them different to other full-bridge [17] and cascaded MMC converters [20], as the proposed converter are operated with different modulation indexes for each of the bricks allowing for very different power flows.

The objective is to demonstrate that it is possible to select appropriate number of storage and grid connected bricks for a given electromagnet, hence further reducing the overall converter cost in comparison with the conventional design.

The paper is organised as follows. Section II briefly presents the fundamental constrains and load requirements of the application. Section III describes the fundamental brick design with the 2 types of proposed bricks. The concept of the modular converter and its characteristics, as well as the analysis of a selected case scenario are presented in Section IV. Section V introduces the control system and how the references are distributed to the bricks. The design of the full-scale 800 kW laboratory prototype is demonstrated in Section VI where the 2 bricks are working together in a system. While Section VII presents and analyses the experimental results and some calculations to show how the energy is flowing in the converter. Finally, the conclusions of this work are presented in Section VIII.

II. Operating Constraints and Load Requirements

The converters discussed here operate in cycling mode with periods between 1 and 25 s. A typical current cycle supplied to the electromagnets is illustrated in Fig. 2. The typical current ramp duration is in the order of 100 ms to 1 s and the flat-top duration can last for several seconds [21]. This process requires a high power for a short time, in particular during current ramps.

When these electromagnets operate at peak current, they have a certain energy stored in the magnetic field,

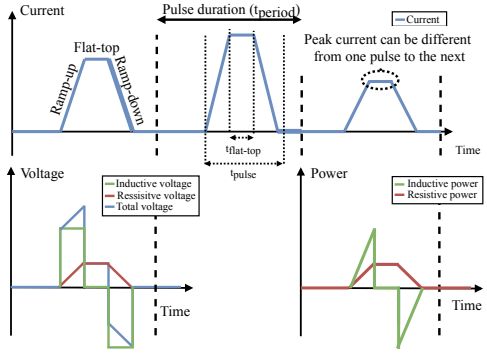

Fig. 2. Typical current cycle sequence, dotted lines indicate division between cycles. t_{period} is typically 1.2s, $t_{flat-top}$ is typically 50ms and t_{pulse} can vary from 300ms-800ms depending on the load and flat-top current.

$E_{magnet,peak}$, which is expressed as in Eq. 1, where L_{magnet} is the inductance and I_{magnet} is the current through the magnet at any given time.

$$E_{magnet} = \frac{1}{2} L_{magnet} I^2_{magnet} \tag{1}$$

During the current ramp down, this energy is recovered in the energy storage units and reused during the next cycle.

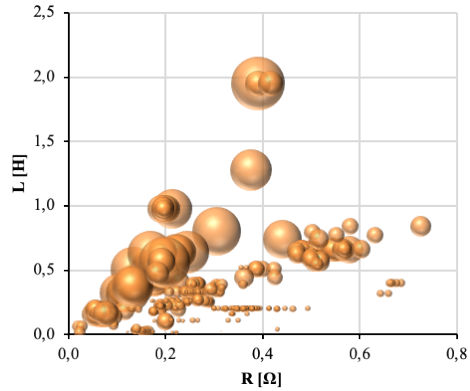

Fig. 3. Resistance and inductance plot of 350 electromagnets for CERN's North Area project, the blob size represents the total stored energy.

Previous work [18] discussed the powering requirements for the North Area project at CERN. The diversity of converter loads (illustrated in Fig. 3), highlights the spread of resistance and inductance, with an R to L ratio varying between 0.2 and 25, and the total energy stored in the magnet between 10 kJ and 670 kJ with a median energy of approximately 20 kJ.

These electromagnets are designed to deliver a strong magnetic field, and hence some loads have an inductance of more than 500 mH, see Fig. 3. Due to the high inductance of these electromagnets, a high voltage is required in order to ramp up the current, compared to the voltage required to maintain the

flat-top current. To keep the RMS current for each cycle low, the ramping up and ramping down phases should be kept as short as possible; however, this requires the highest possible voltage. As the voltage and the dI/dt the magnets can receive are limited, this constraint is often described by a ramping voltage for the projects at CERN. Such a voltage is shown in Fig. 2 (denoted as inductive voltage), and it is a design input that has to be considered when designing a power converter.

III. Fundamental brick concept

The existing or *conventional* design, is a modular design with each module capable of delivering a maximum of 450V and 200A. It employs a front-end comprising a passive diode rectifier and a boost regulator that adjusts the voltage of the DC bus that acts as energy storage.The output stage is an H-bridge topology with a low pass filter.

The proposed scalable converter design allows to decouple and independently use the grid-connected front-end from the energy-storing capability of the conventional converter. Two new brick variants, namely the *grid brick* and the *energy storage brick*, are employed to supply the inductive and resistive components of the electromagnet's power (plotted at the bottom graph of Fig. 2)

If the converter consists of two types of bricks, it is possible to scale the power to the inductive and resistive requirements independently, the *storage brick* scales for the inductive energy and the *grid brick* for the resistive losses in the magnet. Thus, by choosing the minimal feasible brick output voltage for each type of brick, the converter can be scaled to each magnet and have fewer oversized components. The current capability of the brick is limited by the specific current ratings of the power semiconductor switches and the de-rating factor required to respect the lifetime of the semiconductors. The cooling system and the maximum allowed junction temperature are also critical design aspects determining the brick's current capability.

The particle accelerator applications have stringent requirements with regards to accuracy of the supplied current. Additionally, energy recovery from the magnet to the storage bricks requires a converter with a 4-quadrant operating capability to handle the bidirectional power flow. The topology considered in this work is a full-bridge circuit. The schematic of the fundamental brick is shown in Fig. 4a in the brick composition (red) box. The same full-bridge converter is used in both storage and grid bricks and each brick contains a brick inductance L_{HF} which allows the voltages of each brick to be independently controlled.

A. Energy storage brick design considerations

The energy storage brick comprises a full-bridge circuit presented in Fig. 4a and an energy storage component connected directly to the DC-bus of the full-bridge. The energy storage can be implemented with batteries, capacitors, mechanical flywheel [22], [23] or super-capacitors, depending on the amount of stored energy required, delivered power and storage time [24]. Given the short operating time of the current ramping, capacitors are appropriate as storage elements [25] in this case. This causes the voltage on the storage bus to

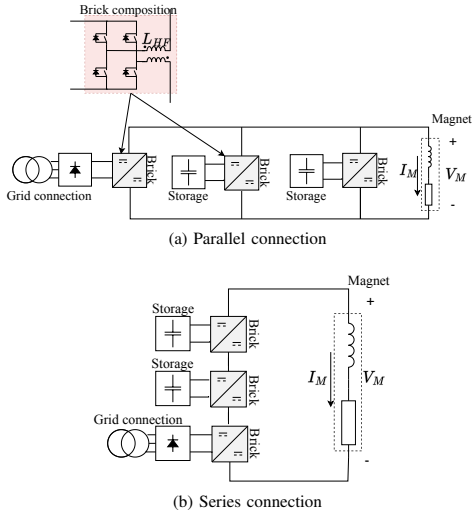

(a) Parallel connection

(b) Series connection

Fig. 4. Schematic diagrams showing the series and parallel connection of bricks. The fundamental brick topology is shown in the red shaded area.

be dependent on the state of charge of the capacitor as for any storage system. The DC-bus voltage is always selected to be the highest blocking voltage that the power semiconductor devices can safely withstand under hard-switching conditions.

The amount of energy in the storage capacitor determines the total amount of storage in the brick. Using a full-bridge to control the voltage generated from the brick, only stepping down the dc-link voltage is possible. This sets constraints on the lowest voltage on the storage bus during usage, since there always have to be sufficient charge left in the capacitors in order to keep this minimum voltage. Equation 2 expresses the usable energy in the storage brick, E_{brick}. C_{str} is the capacitance of the storage brick, V_{bus} is the nominal DC-bus voltage and V_{out} is the lowest allowable voltage on the bus, in order to deliver the required voltage to the output selected for the brick.

$$E_{brick} = \frac{1}{2} C_{str} (V_{bus}^2 - V_{out}^2) \tag{2}$$

However, the usage of other storage solutions is possible for applications with different timescales and storage needs. When using batteries with an accompanying battery management system (BMS), or mechanical flywheel with an inverter or similar, the DC-bus voltage can be considered constant and therefore, the control and operation of the scalable converter would be simpler. This does also open the possibility to reduce the DC-bus voltage which will allow to use bricks designed with power semiconductors with a lower voltage rating. Given the application's design requirement for rapid cycling, if batteries were considered, the need for increasing device voltage ratings would also be imposed, resulting in higher losses.

B. Grid brick design considerations

The grid-connected brick exhibits a simpler scalability design procedure. This is due to the fact that it needs to supply the power losses in the resistive part of the magnet, and also to compensate for the losses in the total system (such as the switching and conduction losses of the grid and storage bricks). To keep the idea of the modular system, the grid brick uses the same bus voltage and output voltage as the storage brick. However, the grid brick is supplied by a diode rectifier connected to a three-phase AC grid. Since the energy recovery function is entirely handled by the storage brick, it is not foreseen to have power flowing back to the grid, and the bus voltage is kept constant, hence a grid supply through a passive (diode) rectifier is adequate.

The following section describes the series and parallel connection of bricks to form a converter system that can both supply the required resistive and inductive power to the load.

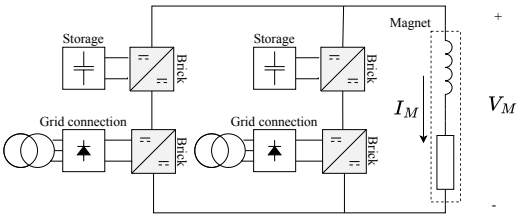

Fig. 5. Schematic diagram showing the combined series and parallel connection of the bricks including the brick inductance used to control the current sharing.

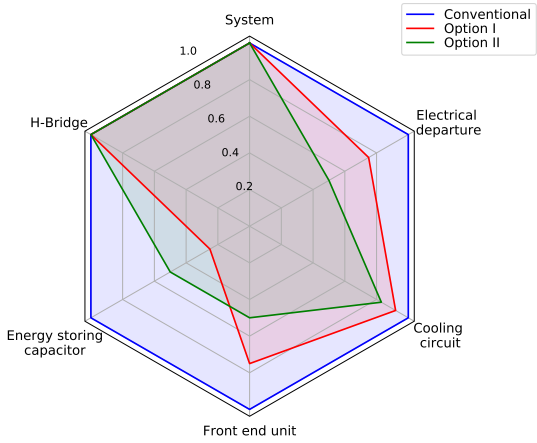

Fig. 6. Relative cost of the converter options

IV. System configuration

The number of grid and storage bricks is calculated based on the magnet's electrical characteristics and the fundamental brick ratings. The configurations that are possible are:

TABLE I
Relative cost of the converter options

Components	Cost weight	Conventional (Fig. 7a)	Scalable converter Option 1 (Fig. 7b)	Scalable converter Option II (Fig. 7c)
System - control card - sensors - cabling and install	16.3%	1	1	1
H-bridge	17.3%	1	1	1
Energy storing capacitor	26.8%	1	0.25	0.50
Front end unit - insl. transformer - diode rectifier - boost regulator	15.7%	1	0.75	0.50
Cooling circuit - cooling plates - piping accessories	16.0%	1	0.92	0.83
Electrical departure - 3ph 400V, 125A - incl. protections	7.9%	1	0.75	0.50
Overall	**100%**	**1**	**0.73**	**0.72**

A. Series connection

This configuration (Fig. 4b) allows for achieving higher voltage on the load but forces the switches in each branch to carry the same current.

B. Parallel connection

This configuration (Fig. 4a) results in lower output voltage, but scales the converter up in current capability by current sharing among the switches; hence reducing conduction losses for a given current. It also allows the different bricks to be interleaved, enabling significantly lower current ripple and, thus, increasing accuracy on the current to the electromagnet.

In this arrangement, the energy has to be transferred among bricks and rebalanced by the end of each cycle. This is done by properly distributing the currents during the current pulse into the electromagnet.

C. Series-Parallel connection

Another option is to combine series and parallel connections of bricks as shown in Fig. 5. In this arrangement the grid bricks inject adequate voltage in order for the resulting grid-supplied power to cover the system losses. This topology enables current sharing and utilises output current interleaving to reduce output current ripple. The storage bricks can also be used for peak-shaving, by supplying the power required by the magnet for the power losses during the flat-top of the pulse. If the storage bricks are only used during current ramping, a bypass switch can be connected across the storage brick to soften the stresses on the switches and reduce the losses.

D. Scalable system cost

In this paper the benefits of the scalable converter are demonstrated by conducting experiments on a full-scale laboratory prototype supplying an electromagnet as load. The

This article has been accepted for publication in IEEE Journal of Emerging and Selected Topics in Power Electronics. This is the author's version which has not been fully edited and content may change prior to final publication. Citation information: DOI 10.1109/JESTPE.2023.3268420

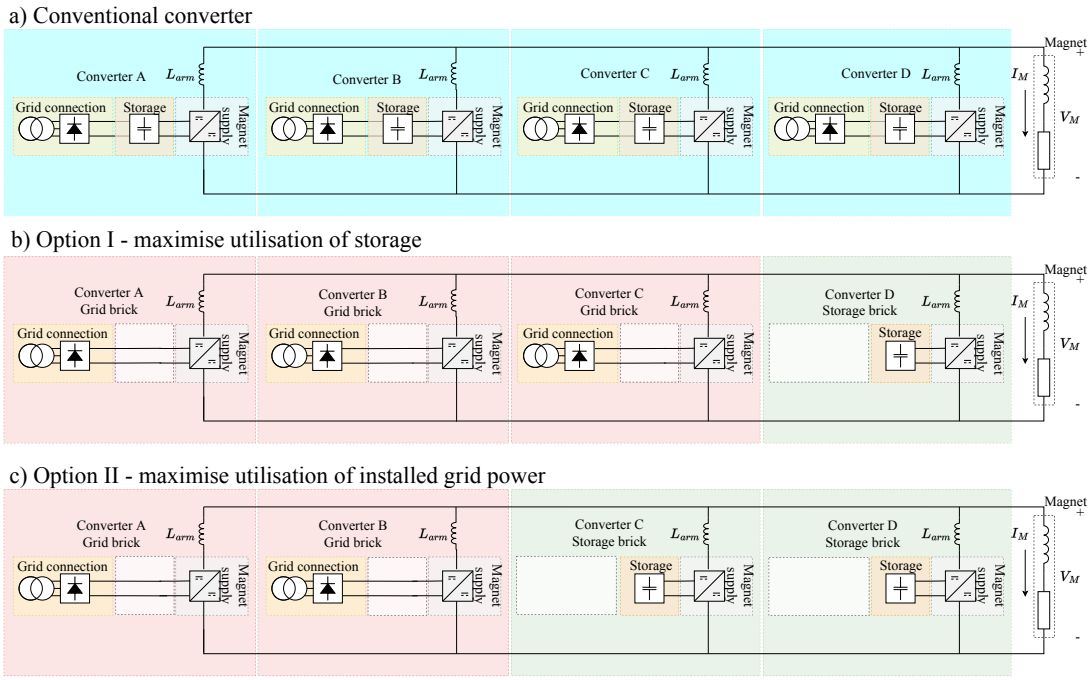

Fig. 7. The benefit of the scalable converter; the number of storage bricks and grid-connected bricks reflects the load inductive and resistive components respectively. From top to bottom: (a) conventional modular converter with four bricks operating with identical control, (b) scalable converter option with three grid connected and one storage brick and (c) a scalable converter option with two grid connected and two storage bricks.

load has a nominal inductance of 0.055H and a resistance that equals 0.075Ω and is designed to be representative of the operational load.

Assuming the maximum brick output of 200A and 200V, such a load would require 4 parallel-connected bricks in order to supply a current up to 800A. Three system configurations are examined and compared:

- The state-of-the-art system configuration (labelled conventional converter) comprises four identical bricks (Fig. 7a), all comprising grid-connection and energy storage.
- Scalable option I - comprising three grid bricks and one energy storage brick (Fig.7b) to maximise the capacitor depth of discharge.
- Scalable option II - comprising two grid bricks and two energy storage bricks (Fig.7c) to minimise the ratings/cost of the electrical departure.

In this paper the calculated cost estimations of the alternative system configurations are made using the known conventional converter costs from recent projects (in Fig. 7a). The cost can be considered to be approximately 1.5 EUR per peak installed Watt.

Table I and Fig. 6 indicates the various converter components, such as the IGBT H-bridge, the storage capacitors etc. along with their weighting towards the cost of a conventional converter. The columns on the right in Table I indicate the relative costs of the scalable options (normalised to the original conventional converter cost). Fig. 6 shows a radar plot of the converter components, the blue surface for the Conventional converter gives the baseline, where every cost is normalised to 1, and then the relative normalised costs of Option I and II are overlaid. It visualises the importance of the costs of the energy storing capacitors and front-end unit, which serves as the motivation for separating these functions.

As expected, option I results in cost savings mainly thanks to the minimisation of energy storage, while option II saves most on the electrical departure. It is noted that the installed electrical departure rating in Tab. I and Fig. 6 are linked to the number of grid bricks of the power converter. An alternative approach (with little relative impact to the overall cost) would be to specify the electrical departures based on the actual RMS power consumed by the magnet load.

In summary, the total investment cost is reduced to 73% for Option I and to 72% for Option II, compared with the existing conventional modular converter. This benefit comes at the cost of implementing an extra layer of energy management in the controller software, described in the following paragraph.

V. System Control Implementation

The purpose of an energy controller is to distribute the energy flow among the grid-connected and the energy storage bricks of a converter to fulfil an objective such as to limit the grid-current, to control the capacitor voltage fluctuation, and

This article has been accepted for publication in IEEE Journal of Emerging and Selected Topics in Power Electronics. This is the author's version which has not been fully edited and content may change prior to final publication. Citation information: DOI 10.1109/JESTPE.2023.3268420

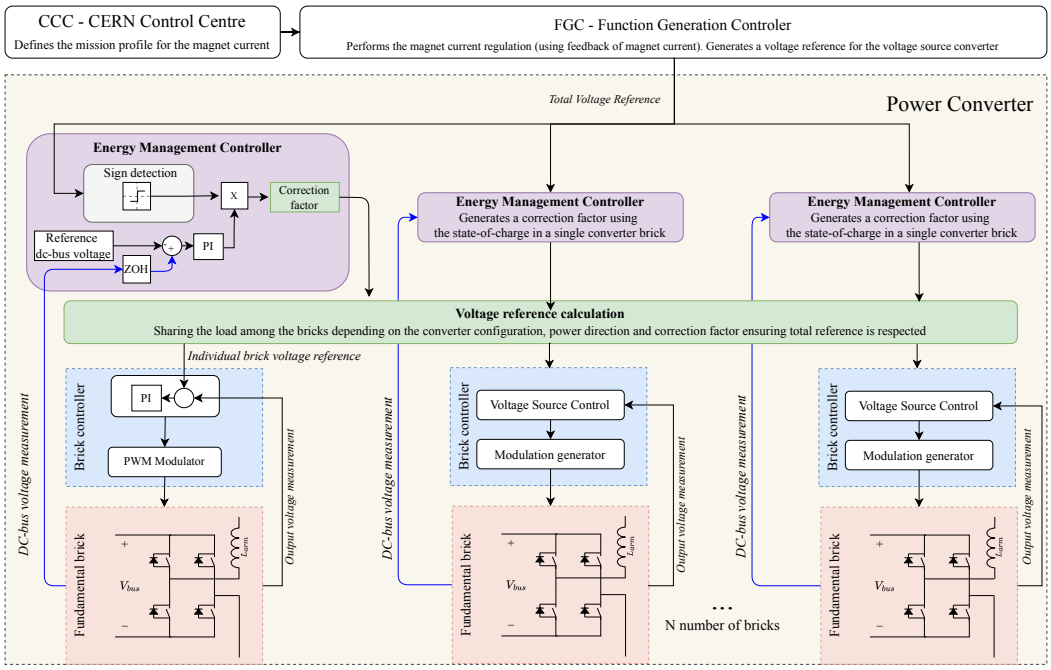

Fig. 8. High level controller of the converters at CERN showing where the energy controller is inserted into the control chain.

to achieve a certain regulation precision in the output. As a result such a controller impacts the peak and RMS loading of each brick. Additionally, the power flow among different bricks may be optimised for smaller temperature variations of the semiconductors and thus, improving the expected lifetime of power modules.

To fulfil these requirements four levels of control have been implemented; a global current controller responsible for regulating the total current and current accuracy, a voltage controller on each series connected brick, an arm-level current controller for the current control in different arms and a system level energy-controller. Significant work has been done on MMC to control and manage the energy stored in the cells [14], [26]–[28]. However, this concerns MMCs having bricks with identical energy sources used for AC/DC applications and not a modular DC/DC converter scheme combining grid and storage bricks, such as [10]. The controller hierarchy discussed in this paper is shown in Fig. 8. The controller uses the energy storage state-of-charge information, and relies on the use of circulating currents to balance the energy in the bricks.

The controller configuration shown in Fig. 8 applies when the current is shared among parallel bricks. A similar approach can be used for the series connected bricks. In this case, a simpler control structure is required. At the highest level, a system controller used in CERN applications, namely the function generation controller (FGC) performs the current control at the load level. The energy controller can also control the voltage on the storage bus and modifies the references accordingly in order to keep the correct energy stored in the bricks. It is interjected between the references given by the CERN operators and before being passed to the individual converter bricks and is also responsible for deriving the total current and voltage references into the individual references for each brick. For a series-connected system this correction will be added to the voltage reference for the bricks and subtracted from the corresponding grid brick voltage reference. For a parallel connected system the correction will be added to the *current* reference, and subtracted from the grid reference. Subtracting from the grid reference ensures that the total current reference is always respected. In a system with both parallel and series bricks, while it is possible to do it both ways, it is probably best to manage the energy within a single arm first, before redistributing across several arms. However, this is out of scope of this paper. Through controlling the functioning of each brick, it can also control the power flow between the bricks. The converter bricks are in essence managed as separate converters, with independent power flow control and independent voltage loops. If the mission profile can be assumed to be known, then more flexibility in the control strategies can be proposed. The theoretical background for this implementation strategy and the details of its response have been presented in [29].

In this paper the splitting of the currents between the bricks will be based on an agnostic approach, wherein the mission profile (current reference) is not known in advance and hence the controller shall allocate the load to bricks in

This article has been accepted for publication in IEEE Journal of Emerging and Selected Topics in Power Electronics. This is the author's version which has not been fully edited and content may change prior to final publication. Citation information: DOI 10.1109/JESTPE.2023.3268420

TABLE II
CONVERTER IGBT PARAMETERS

CM1200DC-34N	Voltage	Current
Rated value	1700V	1200A
Design value	450V	450A

a predetermined fashion; the grid bricks will first share the current evenly until they have reached their maximum current. Then the storage bricks will start and supply the remaining current to reach the required flat-top current. Then during the ramp-down phase, the storage bricks will calculate how much energy they have delivered and ask for a current during the ramp-down which ensure that their total energy is fully recovered. Hence, the control configuration between the two options are identical, and the choice is made based on flat-top duration and magnet energy. In this approach the energy used in the storage brick depends on the length of the flat-top and the value of the current. In the lab experiments, the longest possible flat-top duration was found, serving as an operational constraint on the RMS current supplied by this converter.

VI. DESCRIPTION OF LABORATORY DESIGN

The experimental validation was performed on a 800kW prototype at the CERN laboratory. The converter was designed internally implementing the topology of a conventional converter shown in Fig. 7a. Photographs of the prototype is illustrated in Figs. 9 and 10. The converter allows energy recovery into the DC-bus storage capacitors. Increasing the voltage of the DC-bus, allows more usable energy to be stored in the capacitors, and conversely by reducing the voltage the energy is reduced. The usable energy is described by Eq. 2. The capacitors used in this setup are Hitachi HCGW2G293BF236W2VC electrolytic capacitors connected directly to the DC-bus. Three of these capacitors are connected in series and four capacitor arms are connected in parallel, resulting in a total of 12 capacitors at 41.7mF per brick.

The controller is a Texas Instrument DSP TMS320C6727 and are regulating at a switching frequency of 6.5kHz. The LEM sensors for voltage measurements are LV 25-P/SP5 both on the output and the bus. The current measurement system has the ability to measure current with a significant accuracy in the part-per-million range. The parameters of the IGBT used are listed in Tab. II. The devices are de-rated to achieve lifetime requirements of more than 250 million full cycles.

As shown in Fig. 7(a), in the conventional converter, each of the four bricks have a grid connection via an isolating transformer, a diode rectifier, a boost connecting the diode rectifier to the DC-bus, a DC-bus and an IGBT-based full-bridge circuit on the output. The design parameters of the converter in the test setup are summarised in Tab. III. The two types of bricks used in this paper were obtained by modifying the existing converter (see Fig. 7(b) and (c)). The storage bricks have been made by disconnection of the boost stage from the DC-bus. Disconnecting a brick from the grid implies that its power losses (switching and conduction) have to be supplied by recovering adequate energy from the magnet load.

Fig. 9. Photograph of the laboratory set-up.

Fig. 10. Photograph of the laboratory set-up, showing the power-stack, gate drivers and DC-bus filter capacitors integrated into the cabinet. The storage capacitors can be seen in the bottom.

TABLE III
CONVERTER PARAMETERS

	Grid Connected Brick	Energy Storage Brick
Max Voltage	200V	200V
Max Current	200A	200A
Energy Available	N/A	9.4kJ at 900V

The grid brick is made by removing the energy storing capacitors from the output of the boost stage. The boost stage is not necessary for the operation of the converter in this configuration, but it was kept in order to avoid reconfiguration of critical protection and control systems. By separating the grid connection and the energy storing functions of the conventional brick, it is possible to have a simple brick building block at the cost of an increased system complexity.

The load is a water cooled electromagnet with a solid magnetic core and a large air-gap such as the ones used in the accelerator facilities. The magnet parameters are listed in Tab. IV.

TABLE IV
CASE LOAD

Load parameter	Value
Inductance	55mH
Resistance	75mΩ
Max current	960A
Pulse current flat-top	700A
Peak stored energy at 700A	13.5kJ
RMS power	8kW
Peak power	140kW

VII. EXPERIMENTAL RESULTS

A. Scalable option I: 3 grid-connected and 1 energy storage bricks in parallel

The first set of experiments were conducted on a system configuration comprising 3 grid bricks and 1 storage brick. In this case, the reference currents are shown as dashed lines in Fig. 11a. All grid bricks receive the same reference and hence perform the same function.

The control principle employed in this control scheme is that the minimum possible amount of energy storage shall be used for a given load. To achieve this, the grid-connected bricks shall supply current to the maximum of their capability before the storage brick is absolutely required to release its stored energy. Conversely, during the energy recovery phase (ramp-down of the current), the storage brick takes priority in recovering energy, using its maximum current capability $I_{storage\_ref}$ to replenish the capacitor bank.

To achieve this result, the storage brick local controller predicts in real time the remaining energy in the magnet. During the first part of the ramp-down phase, the calculated reference current value is higher than the brick maximum current, and is therefore caped at the maximum current. Then after 100ms of ramp-down the current starts to decrease as the storage brick has recovered sufficient energy. In this 3:1 ratio of brick to storage brick sizing it can be seen that the energy storage volume is rather small for the magnet stored energy; hence, the grid bricks are commanded to recover energy while this is not their role.

As shown in Fig. 11b the ramp-up phase takes 200ms and the peak voltage approximately equals 200V. On the contrary, the ramp-down phase takes 200ms and the peak voltage is measured to be -160V. Since the ramp-rate of the current was kept the same, the voltage drop across the resistive component of the magnet results in the lower voltage during ramp-down phase. The trapezoidal current has been chosen to ramp as quickly as possible in order to minimise the resistive losses in the magnet, while respecting the dI/dt limit of the magnet. It is noted that the voltage takes 40ms to reverse, due to the resistive voltage drop in the magnet. This results in the existence of a short phase at the beginning of the ramp-down process when energy recovery is not possible. In fact the storage brick will continue to supply energy to the magnet in this phase. The amount of energy exchanged in this phase is relatively small, since the RMS voltage is low and the time is very short. A summary of electrical performance parameters

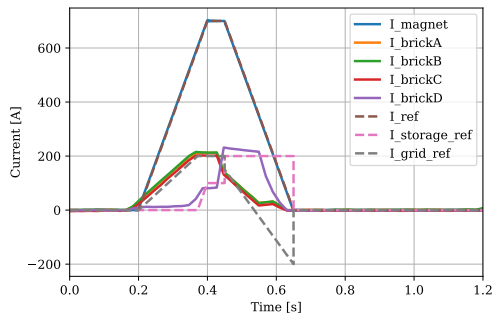

(a) Brick and output currents. I_{magnet} is the total current supplied to the magnet, I_{brick} is the current from each of the bricks A-D. I_{ref} (dashed brown line) is the total current reference, $I_{storage\_ref}$ (dashed pink line) and I_{grid} (dashed black line) are the references for the storage and grid bricks respectively.

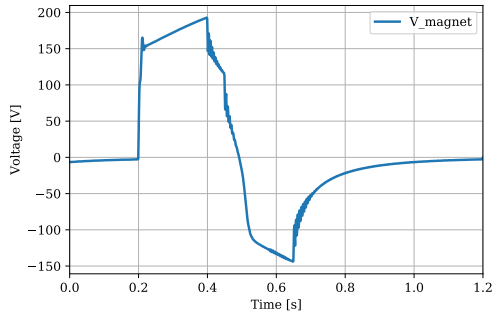

(b) Output Voltage, V_{magnet} is the total voltage across the magnet load.

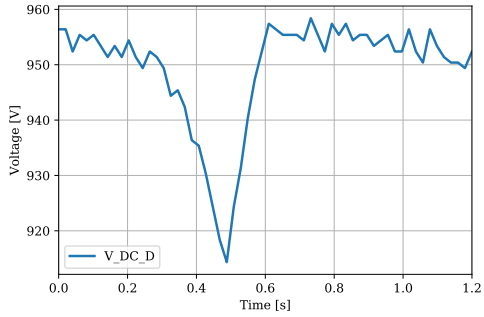

(c) Bus voltage for the storage brick V_{DC_D}

Fig. 11. Option I - Experimental results of a current pulse at 700A with 3 grid and 1 storage bricks.

of the bricks are given in Tab. V. Fig. 11b shows the ramping voltage, and it is approximately 150V, and then the voltage increases with the increasing current, to compensate for the resistive voltage drop. During the flat-top, the voltage should drop down to a value equal to $V_{flat-top} = I_{flat-top}R_{mag}$, as this is a DC-current. However, the voltage takes some time to ramp-down, and never reaches the expected flat-top value, as the magnets in the lab exhibit a non-linear behaviour at higher currents (due to saturation and excessive eddy currents in the core). The non-linearity (saturation) of the magnet also results in a lower inductive value.

In theory the magnet stores at peak current 13.5kJ, using Eq. 1. However, estimating the inductance after saturation based on the voltage values and current derivatives, a value of 36mH is calculated, thus the available energy in the magnet is 8.9kJ. Using the voltage presented in Fig. 11c and Eq. 2, the energy returned to the storage has been calculated to be 1.64kJ. This is due to the storage brick being current limited and the RMS voltage being governed by the load. The estimated energy consumed by each brick is presented in Tab. V. In this case almost 50% of the energy recovered from the magnet is consumed in power losses, before it is recovered to the storage.

In this first experiment, it was shown that the controller converges to balanced energy transfer between the magnet and the energy storage, despite the latter being rather limited for the magnet stored energy. This demonstrates that the objective of operating with minimal amount of energy storage can be achieved.

B. Scalable option II: 2 grid-connected and 2 energy storage bricks in parallel

Fig. 12 demonstrates the experimental results when the converter operates in the 2-grid and 2-storage bricks configuration. The resulting load voltage and currents are very similar to that of Option I shown in Fig. 11, while the brick current distribution is different.

Fig. 12a shows the total and the individual currents from the bricks. The same principle as before is applied; the two grid bricks supply the maximum possible current, while the storage bricks only contribute with their stored energy when the output current exceeds 400A (the combined capability of two grid bricks).

During the energy recovery phase, however, the four bricks are now able to follow the references much better since enough energy storage is available for recovering the energy of the magnet. The grid bricks on the other hand reverse their current which indicates that they continue to supply positive power helping the storage bricks to replenish their energy while compensating also for the power converter losses. A summary of electrical performance parameters of the bricks are given in Tab. V.

The total voltage in Fig. 12b is identical to the voltage in Fig. 11b, along with identical currents. Therefore, the two different options have no impact on the total performance of the converter.

Using the voltages in Fig. 12c the total energy recovered is approximately 8.64kJ of energy is recovered from the magnet

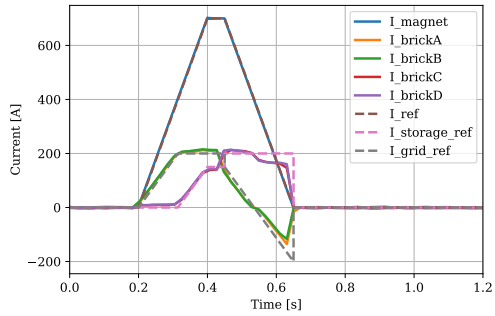

(a) Measured brick and output currents. I_{magnet} is the total current supplied to the magnet, I_{brick} is the current from each of the bricks A-D. Bricks A and B are grid-connected while bricks C and D are energy storing. I_{ref} is the total current reference, $I_{storage\_ref}$ and I_{grid} are the references for the storage and grid bricks respectively.

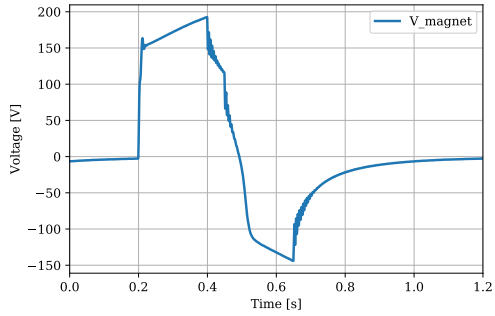

(b) Measured output Voltage, V_{magnet} is the total voltage across the magnet load.

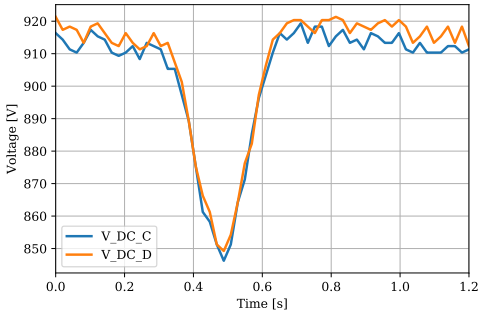

(c) Measured bus voltage for the storage bricks C (V_{DC_C}) and D (V_{DC_D})

Fig. 12. Option II - Experimental results of a current pulse at 700A with 2 grid and 2 storage bricks.

(4.32kJ per brick), out of a theoretical 13.5kJ. Given the inductive saturation, an actual available energy of 8.9kJ is more likely. The energy recovered into the bricks are summarised in Tab. V. From this table and using the bus voltages in Fig. 12c, it is observed that an energy of 0.62kJ is dissipated to the 2 sets of discharge resistors on the capacitor banks in the 2 storage bricks and 3.48kJ in the two full-bridges circuits. This energy loss, leaves 5.16kJ of energy to be returned to the storage for use in the next cycle. Thus, this case absorbs twice the energy from the magnet.

$$E_{recovery\_max} = V_{ramp-down\_RMS} \cdot I_{brick\_max} \cdot t_{ramp-down} \tag{3}$$

C. Discussion

The experimental setup was used to validate the hypothesis that parallel connected converter bricks could indeed operate independently; the energy controller is able to recycle power between the load and the power converter, adjusting the contributions of storage and grid-connected bricks in real-time using cycle agnostic control.

Using cycle-agnostic control is needed in accelerator applications due to the varied particle beam energy that results in a constantly varying mission profile of the magnet current waveform. The 2:2 grid-connected to storage-brick configuration allowed energy recovery with ease and despite the significant switching and conduction power losses in each of the bricks. Even the single storage-brick prototype performed the function illustrating that the control objective of minimising the volume of the required energy storage was achieved.

The 200V and 200A fundamental brick was used for both the grid and storage connected bricks. The parallel connection of four bricks allowed operation up to 800A (700A was demonstrated in this work). The claimed scalability can be achieved in many different ways to cover for a wide range of load resistance and inductance values. Loads with greater resistance value can be supplied using more grid-bricks in parallel, whereas loads with greater inductance value require series-connected bricks reaching 400V or more.

Additionally, this configuration of converter allows for better energy storage utilisation with greater discharge depth of capacitors, by series connecting storage bricks to achieve a higher output voltage to the load.

The conventional converters at CERN operate in an agnostic way, which means that the voltage loop and bus voltage controllers are real-time controllers with no information on the future current profile or the pulse duration. This means that the current from each of the bricks follows the same approach for both scalable options (Option I and II), the grid bricks ramps to full current first, and only then the storage bricks enter in order to deliver the peak current to the load. During the ramp-down phase, the storage bricks recover the energy they need to replenish the storage, and the grid bricks cover the rest. Thus, the range of control for the for the two options is very limited. However, if it is assumed that the controller has full knowledge of the cycle, then far more options for control emerge. The theoretical background for such control has been discussed in [29] including some failure scenarios. In that paper, four control strategies optimising for minimised thermal stress, minimum power supply from the grid or optimal storage utilisation have been proposed and evaluated in a scalable converter comprising one grid-connected and four storage bricks. Given the modular design of the converter, it has been shown that the storage can be reduced by 12% just by selecting the proper control strategy, while another strategy maintain the thermal stress among the bricks equal in order to have the same expected lifetime, or the grid RMS current can be reduced by 59% by keeping the grid current constant. While in the this paper the scalability has been shown in hardware configuration, this further enhances the flexibility of the scalable converter, by optimising for different parameters in software.

Figs. 11b and 12b show the voltage across the load, following a typical curve for the voltage shape. This voltage is identical for the 3 different converters shown in Fig. 7, and confirms that the individual correction of the bricks done by the controller does not influence the performance of the converter. Using Option II, results in a higher utilisation of storage. As shown in Fig. 12b, the delta voltage is lower compared to Option I, but since two bricks are used, the total energy recovered as presented in Tab. V is higher. With 3 grid bricks, Option I has a lower RMS load current for each of the grid bricks, but since the total energy recovered is reduced, it is clear that the total energy consumed in a pulse is higher in this case.

TABLE V
CONVERTER ELECTRICAL PERFORMANCE SUMMARY PER BRICK

Configuration	**Option I** **1 storage brick**	**Option II** **2 storage bricks**
Energy recovered from magnet	3.20kJ	4.32kJ
Energy recovered to storage	1.64kJ	2.58kJ
Magnet supply losses (est.)	1.56kJ	1.74kJ
Losses between pulses	0.32kJ	0.31kJ
Energy used in next cycle	1.32kJ	2.23kJ
Grid brick current RMS	81.3A	89.0A
Grid brick current peak	210.6A	215.0A
Storage brick current RMS	81.5A	90.4A
Storage brick current peak	229.6A	215.0A

The inherent flexibility of the scalable converter has been demonstrated by considering a load case allowing two possible converter configurations. The storage bricks are limited by the energy available during ramp-down as described in Eq. 3. An inherent limitation of this topology is the requirement to recharge the energy storage brick by recovering energy from the magnet load, primarily during the current ramp down (since a grid connection is not available in storage bricks). This implies that enough energy must be stored by the load in order to compensate the storage brick's semiconductor power losses.

VIII. CONCLUSION

This paper presents the optimal design of a scalable and modular power converter that is assembled from a number

of smaller DC-DC converter bricks with independent storage and grid-connected units. The performance and cost benefits of such a converter for a certain application have been demonstrated. It has been shown that up to 28% cost savings can be achieved by using less converter hardware in comparison with a conventional modular converter.

A control scheme that is agnostic to the loads mission profile is demonstrated using a full-scale converter prototype. Two scalability options were examined with different system configurations; the first employed half of the energy storage capability than the second and greater grid-supply ratings. Both of the configuration options operated correctly with the proposed energy management control. The second scalability option allowed for a better utilisation of the energy storage element and a better RMS current balance among different bricks.

The flexibility of the scalable converter enables more choices for optimising for large industrial projects or power converter-based distributed grids, all with a single fundamental power electronic brick.

The design and operating advantages of the proposed modular converter can be found beneficial for a wide range of applications, requiring a relatively low average power draw and high peak power for short time intervals. In these applications, utilising the proposed converter with separated storage, enables peak-shaving strategies in order to limit the constraints for installed capacity. Such an application example is reconfigurable charging infrastructure for electric vehicles (EVs) [17], that can deliver various charging modes (e.g., slow, fast or super-fast charging) by optimising the power drawn from the grid or the local energy-storage system. Moreover, keeping the concept of fundamental brick and combining them in various ways, the charging voltage can configured depending on the EV's battery requirements.

Another application that can benefit is railway traction with on-board energy-storage capability. In this case, the proposed modular converter can control and optimise the energy delivered from the on-board storage or the grid, based on the operating constraints (e.g., lack of overhead supply or higher loads). Finally, grid balancing can also be advanced using the modular converter presented in this paper. In this application, the energy-storage system is used to absorb the excessive power in the grid and deliver it back when there is a lack of power. An example is power grids with large amounts of intermittent renewable energy generation. Depending on the total energy requirements, the response time, the power required from the storage, and spatial constraints, different types of storage can be used. Typical examples of energy storage are super-capacitors, mechanical flywheels, batteries or other novel energy storage systems.

REFERENCES

[1] S. Maestri, R. G. Retegui, D. Carrica, S. Rossini, G. Le Godec, and K. Papastergiou, "Figures of merit for the evaluation of regenerative power converters," *2016 18th European Conference on Power Electronics and Applications, EPE 2016 ECCE Europe*, pp. 1–9, 2016, publisher: Jointly owned by IEEE-PELS and EPE Association ISBN: 9789075815245.

[2] G. Kniegl, R. Weber, F. Bordry, and A. Dupaquier, "Four-quadrant converter [±600 A, ±12 V] prototype for LHC," in *Proceedings of the IEEE Particle Accelerator Conference*, vol. 5. IEEE, 1999, pp. 3740–3742.

[3] Y. Thurel, D. Nisbet, B. Favre, and G. Switzerland, "FOUR QUADRANT 120 A, 10 V POWER CONVERTERS FOR LHC," CERN, Geneva, Tech. Rep., 2007.

[4] A. Lesnicar and R. Marquardt, "An innovative modular multilevel converter topology suitable for a wide power range," *2003 IEEE Bologna PowerTech - Conference Proceedings*, vol. 3, pp. 272–277, 2003, iSBN: 0780379675.

[5] G. J. Kish, "On the emerging class of non-isolated modular multilevel DC-DC converters for DC and hybrid AC-DC systems," *IEEE Transactions on Smart Grid*, vol. 10, no. 2, pp. 1762–1771, 2019, publisher: IEEE.

[6] S. M. Goetz, A. V. Peterchev, and T. Weyh, "Modular multilevel converter with series and parallel module connectivity: Topology and control," *IEEE Transactions on Power Electronics*, vol. 30, no. 1, pp. 203–215, Jan. 2015, publisher: IEEE.

[7] B. L. M. Lamaille, F. Dragoni, S. Evrard, F. J. Harden, E. Harrouch, M. Lazzaroni, R. Lopez, and K. D. Papastergiou, "Study of the Energy Savings Resulting From the East Area Renovation," *10th Int. Partile Accelerator Conferance*, pp. 4023–4025, 2019, iSBN: 9783954502080.

[8] S. Rocca, F. Boattini, and L. M. De Paco Soto, "Development of a control strategy for the 18 MW power converter of the CERN PS Booster accelerator," in *2018 IEEE 19th Workshop on Control and Modeling for Power Electronics, COMPEL 2018*. Institute of Electrical and Electronics Engineers Inc., Sep. 2018.

[9] M. Parchomiuk, R. Strzelecki, K. Zymmer, and T. Sak, "Modular high precision high current source for special applications-Simulation and verification," *Proceedings - 2016 10th International Conference on Compatibility, Power Electronics and Power Engineering, CPE-POWERENG 2016*, pp. 422–427, 2016, publisher: IEEE ISBN: 9781467372930.

[10] F. Boattini, J.-P. Burnet, and G. Skawinski, "POPS: The 60MW power converter for the PS accelerator: Control strategy and performances," in *2015 17th European Conference on Power Electronics and Applications (EPE'15 ECCE-Europe)*. Geneva: IEEE, Sep. 2015, pp. 1–10. [Online]. Available: http://ieeexplore.ieee.org/document/7309267/

[11] F. H. Khan and L. M. Tolbert, "A multilevel modular capacitor-clamped DC-DC converter," *IEEE Transactions on Industry Applications*, vol. 43, no. 6, pp. 1628–1638, Nov. 2007.

[12] S. Choudhury, M. Bajaj, T. Dash, S. Kamel, and F. Jurado, "Multilevel inverter: A survey on classical and advanced topologies, control schemes, applications to power system and future prospects," *Energies*, vol. 14, no. 18, 2021.

[13] A. Dekka, B. Wu, R. L. Fuentes, M. Perez, and N. R. Zargari, "Evolution of Topologies, Modeling, Control Schemes, and Applications of Modular Multilevel Converters," *IEEE Journal of Emerging and Selected Topics in Power Electronics*, vol. 5, no. 4, pp. 1631–1656, 2017.

[14] M. A. Perez, S. Bernet, J. Rodriguez, S. Kouro, and R. Lizana, "Circuit topologies, modeling, control schemes, and applications of modular multilevel converters," *IEEE Transactions on Power Electronics*, vol. 30, no. 1, pp. 4–17, Jan. 2015. [Online]. Available: http://ieeexplore.ieee.org/lpdocs/epic03/wrapper.htm?arnumber=6757004

[15] T. Soong and P. W. Lehn, "Internal power flow of a modular multilevel converter with distributed energy resources," in *IEEE Journal of Emerging and Selected Topics in Power Electronics*, vol. 2. Institute of Electrical and Electronics Engineers Inc., Dec. 2014, pp. 1127–1138, issue: 4 ISSN: 21686785.

[16] A. M. Abbas and P. W. Lehn, "A unified power delivery solution for integrating DER into distribution networks through VSC based DC system," in *2009 IEEE Power and Energy Society General Meeting, PES '09*, 2009.

[17] K. N. Kumar, R. Miskiewicz, P. Trochimiuk, J. Rabkowski, and D. Peftitsis, "Performance Evaluation of SiC-based Isolated Bidirectional DC/DC Converters for Electric Vehicle Charging," *2022 24th European Conference on Power Electronics and Applications (EPE'22 ECCE Europe)*, p. 11, 2022.

[18] K. L. Haugen, K. Papastergiou, P. Asimakopoulos, and D. Peftitsis, "On dimensioning the fundamental brick for a scalable DC-DC converter with energy recovery," in *2021 23rd European Conference on Power Electronics and Applications (EPE'21 ECCE Europe)*. Ghent, Belgium: IEEE, Sep. 2021, pp. P.1–P.10. [Online]. Available: https://ieeexplore.ieee.org/document/9570676/

[19] M. Arazi, A. Payman, M. B. Camara, and B. Dakyo, "Energy management in a Multi-source System using isolated DC-DC resonant

converters," in *2020 22nd European Conference on Power Electronics and Applications, EPE 2020 ECCE Europe*, 2020, pp. 1–7.

[20] J. Fang, Z. Li, and S. M. Goetz, "Multilevel Converters with Symmetrical Half-Bridge Submodules and Sensorless Voltage Balance," *IEEE Transactions on Power Electronics*, vol. 36, no. 1, pp. 447–458, 2021.

[21] P. Asimakopoulos, K. Papastergiou, T. Thiringer, M. Bongiorno, and G. Le Godec, "On Vce Method: In Situ Temperature Estimation and Aging Detection of High-Current IGBT Modules Used in Magnet Power Supplies for Particle Accelerators," *IEEE Transactions on Industrial Electronics*, vol. 66, no. 1, pp. 551–560, 2019.

[22] D. R. Brown and W. D. Chvala, "Flywheel energy storage: An alternative to batteries for ups systems," *Energy Engineering: Journal of the Association of Energy Engineering*, vol. 102, no. 5, pp. 7–26, 2005.

[23] R. Magdalena Stephan, R. de Andrade Jr., and G. Gonçalves Sotelo, "Third Generation Of Flywheels: A Promising Substitute To Batteries," *Eletrônica de Potência*, vol. 13, no. 3, pp. 171–176, 2008.

[24] G. Wang, G. Konstantinou, C. D. Townsend, J. Pou, S. Vazquez, G. D. Demetriades, and V. G. Agelidis, "A review of power electronics for grid connection of utility-scale battery energy storage systems," *IEEE Transactions on Sustainable Energy*, vol. 7, no. 4, pp. 1778–1790, Oct. 2016. [Online]. Available: http://ieeexplore.ieee.org/document/7506096/

[25] T. M. Masaud, K. Lee, and P. K. Sen, "An overview of enrgy storage technologies in electric power systems: What is the future?" *North American Power Symposium 2010, NAPS 2010*, 2010, publisher: IEEE ISBN: 9781424480463.

[26] L. Ängquist, A. Antonopoulos, D. Siemaszko, K. Ilves, M. Vasiladiotis, and H. P. Nee, "Open-loop control of modular multilevel converters using estimation of stored energy," *IEEE Transactions on Industry Applications*, vol. 47, no. 6, pp. 2516–2524, 2011.

[27] K. Ilves, L. Harnefors, S. Norrga, and H. P. Nee, "Analysis and operation of modular multilevel converters with phase-shifted carrier PWM," *IEEE Transactions on Power Electronics*, vol. 30, no. 1, pp. 268–283, 2015.

[28] G. L. Rodal, A. B. Acharya, and L. E. Norum, "Analysis and Evaluation of Repetitive Controllers for Circulating Current Suppression in Modular Multilevel Converters," *2018 20th European Conference on Power Electronics and Applications, EPE 2018 ECCE Europe*, pp. 1–10, 2018, iSBN: 9789075815283.

[29] K. L. Haugen, K. Papastergiou, P. Asimakopoulos, and D. Peftitsis, "Energy flow control in a modular DC-DC converter with energy recovery," in *2021 IEEE 12th International Symposium on Power Electronics for Distributed Generation Systems (PEDG)*. Chicago, IL, USA: IEEE, Jun. 2021, pp. 1–8. [Online]. Available: https://ieeexplore.ieee.org/document/9494229/

Article III

K. L. Haugen, K. Papastergiou, P. Asimakopoulos, and D. Peftitsis,

High precision scalable power converter for accelerator magnets

Published by Journal of Instrumentation, March 2022.

Published by IOP Publishing for Sissa Medialab

Received: *October 22, 2021*
Accepted: *January 24, 2022*
Published: *March 16, 2022*

Topical Workshop on Electronics for Particle Physics 2021
20–24 September, 2021
Online

High precision scalable power converter for accelerator magnets

K.L. Haugen,[a,b,*] **K. Papastergiou,**[b] **P. Asimakopoulos**[b] **and D. Peftitsis**[a]

[a] *Department of Electric Power Engineering, Norwegian University of Science and Technology (NTNU), Trondheim, Norway*
[b] *Accelerator Systems Department, CERN, Geneva, Switzerland*

E-mail: krister.leonart.haugen@cern.ch

Abstract: The lower conduction power losses and the positive temperature coefficient that favours parallel connections, make Silicon Carbide (SiC) Metal Oxide Semiconductor Field-Effect Transistors (MOSFETs) to be an excellent replacement of existing Silicon Insulated Gate Bipolar Transistors (IGBTs) technology. These characteristics combined with high switching frequency operation, enables the design of high-accuracy DC-DC converters with minimised filtering requirements. This paper investigates the design for a converter with high-accuracy current (0.9 ppm) supplying a 0.05 H electromagnetic load, aiming to achieve the accuracy without the use of active filters, by using SiC MOSFETs and a scalable module-based converter design.

Keywords: Modular electronics; Performance of High Energy Physics Detectors; Power recycling; Pulsed power

ArXiv ePrint: 2201.10824

*Corresponding author.

https://doi.org/10.1088/1748-0221/17/03/C03021

Contents

2022 JINST 17 C03021

1 Introduction

A primary objective of the powering in particle accelerator is the precision and reproducibility of the experiments. Scalable converters enable sub-ppm current precision with minimal filtering requirements by using multiple modules in interleaved operation [1]. In order to reach the <1 ppm level which is required for some applications, active filters are often used [2]. However, they require relatively large reactors, contribute to power losses and their control is not trivial. With the introduction of Silicon Carbide (SiC) Metal Oxide Semiconductor Field-Effect Transistors (MOSFETs) as a commercial alternative to silicon Insulated Gate Bipolar Transistors (IGBTs) for switch-mode converters, it is now feasible to utilise SiC semiconductor technology in the world of high-energy particle physics as well. This paper demonstrates a case study for a 0.05 H electromagnet with high accuracy requirement of 0.9 ppm and investigates the performance improvements to the design and operation of such converters when using SiC MOSFETs compared to IGBTs. The benefits of the SiC MOSFET are two-fold. Firstly, the reduced conduction on-state losses and positive on-state temperature coefficient and secondly, the reduced switching losses, enabling operation at higher switching frequencies. And since the SiC based technology is emerging with lower current ratings than the IGBTs, parallel connection is necessary to take advantage of the SiC MOSFETS.

The reduced on-state losses of SiC MOSFETs enables high-efficiency operation. Besides, their positive temperature coefficient facilitates a robust and more reliable parallel connection, as the positive temperature coefficient leads to natural balance of the current. If the parallelisation required to handle the current is achieved by parallel connecting H-bridges, introducing a number of parallel connected DC-DC converter enables the use of interleaving to achieve a lower current ripple.

The current these power converters are designed to supply, will often be a series of trapezoid current pulses. These are supplied by power converters with built in energy recovery to reduce the overall energy consumption of the experiments [3, 4]. An example of such a current train is shown in figure 1(a). Since the ramping and energy recovery often will require negative voltage

to be applied across the magnet during ramp-down, such as in figure 1(b), the power converters are required to have 4-quadrant operation and a energy storage facility. Taking into account the advantages of SiC based MOSFETs, and taking the need for parallelisation as an opportunity, some interesting possibilities emerge with regards to reducing the ripple of the current supplied to magnets.

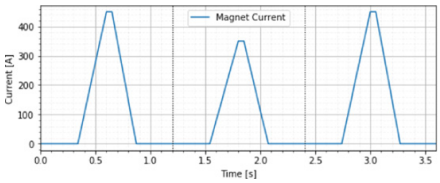

(a) Typical current cycle sequence, dotted lines indicate division between cycles.

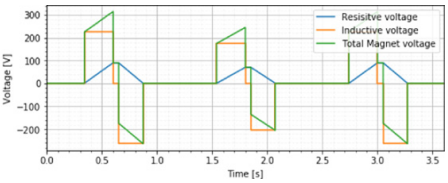

(b) Typical voltage requirement for the cycles.

Figure 1. Examples of load which the DC-DC converters have to be designed for.

2 The modular power converter

Considering the constraints mentioned in the introduction, the magnets are normally supplied by an H-bridge with an electrolytic capacitor bank as energy storage [4]. The converter is such that often one converter is sufficient, perhaps combining 2 or 4 in series, parallel or series-parallel combination to achieve the required outputs, depending on the specific magnet. By opting for a parallel connection of power converters, the size and power ratings of each power converter can be reduced. The converter is now consisting of smaller identical modules, which will be named bricks, and for this paper the brick size has been chosen as 100 V and 100 A. This choice is based on previous work relating to the sizing system and operating cost of such modular power converters [5].

The proposed topology employs several bricks and assumes different functionality for them; some of them are connected to energy storage for the recovery of the magnet B-field energy, while other bricks are connected to a power source (i.e. the grid). The grid connected bricks supply the power losses due to the magnet resistance and the circuit self-consumption, and the option to reduce the front-end peak-load and greater utilisation of the storage [6]. More specifically in the example of figure 2, four of the bricks are connected to storage while just one brick is connected to the power grid via a 3-phase diode rectifier.

This paper ends up with the topology shown in figure 2, with each brick able to supply 100 V and 100 A. Four of the bricks are connected to storage, and supply the reactive power to the magnet, and the 5th brick is connected to the grid via a 3-phase diode rectifier. Normally the power converter would be connected to the magnet via an active filter, which ensures the requirement for current accuracy. However, this filter is omitted in this paper in an effort to achieve the same accuracy by simply interleaving several bricks and operate them at higher switching frequencies. In this converter configuration and also in the modelling and simulations the arm inductance and

2022 JINST 17 C03021

the intrinsic inductances were considered small compared to the inductance of the load, meaning they don't need to be compensated for by the converter control.

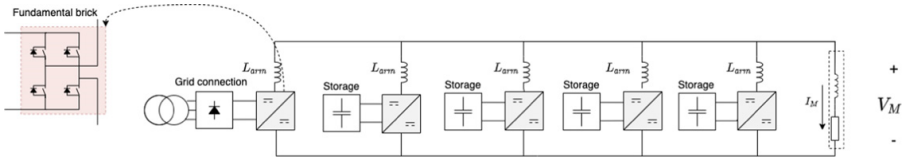

Figure 2. A possible configuration of the parallel connected bricks.

3 Simulating the interleaving

To investigate the performance of the parallel connected bricks, a PLECS model based on the topology in figure 2 was developed and simulated, where the number of parallel connected bricks was varied from 1 up to 25, to investigate the effect of using SiC MOSFETs with relatively small current rating to supply a large current with interleaving. The single brick compares to the conventional case where the current is supplied by a single power converter. This was done to understand how the interleaving would influence the current ripple to the inductive load of a magnet. All simulations were performed without considering power losses, apart from the resistance in the magnet, or relevant limits in dv/dt for the power semiconductor devices and the magnets. The interleaving was achieved by phase-shifting each of the bricks evenly, i.e., the phase-shift of brick N_i is $N_i = 360\frac{1}{N_{\text{bricks}}}$. Where N_{bricks} is the total number of bricks, and N_i is one of the bricks.

4 Effect of parallelisation and frequency on the current ripple

Using the voltage and current results shown in figure 3, it is possible to estimate the ripple of the current through the magnet. If the number of interleaved bricks is larger than one ($N_{\text{bricks}} > 1$), the voltage switches between zero and a positive value V_{M}, which is different to the bus voltage V_{bus}. And as the number of parallel connections increases, the number of pulses increases proportionally and the magnitude of the voltage is inversely proportional. The current in the magnet is ramped up when the voltage is positive, and slowly discharges through the resistor when the voltage is zero. This voltage is determined by $V_{\text{M}} = \frac{V_{\text{arm}}}{N_{\text{arms}}}$, and the duration of the applied voltage is controlled by the duty cycle of the bricks. The current is in the flat-top phase, so the average current over one cycle is equal to the DC-current applied, where the duty cycle m gives the following average voltage: $\widehat{V}_{\text{M}} = V_{\text{M}}m$. This is the voltage driving the ramp-up of the current. The voltage $\widehat{V}_{\text{M}}$ is also equal to the average DC-voltage required to sustain the current in the resistor component of the magnet, thus $\widehat{V}_{\text{M}} = I_{\text{flat}}R_{\text{M}}$.

2022 JINST 17 C03021

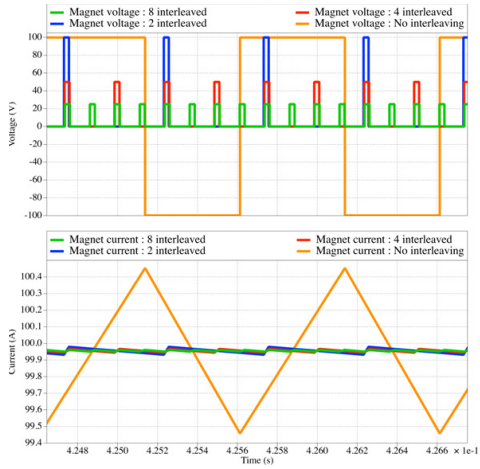

Figure 3. A plot showing the wave-forms of the interleaved voltage and current supplied to the magnet.

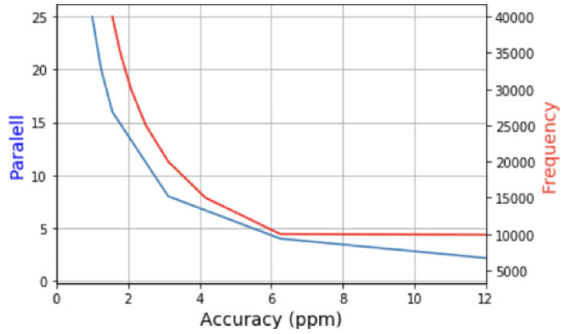

Figure 4. Effect of interleaving on magnet voltage (and current) precision (blue line: varying number of bricks with a fixed frequency of 40 kHz. Red line: varying the frequency with a fixed number of 16 interleaved bricks).

Using the fundamental relationship of an inductor in (4.1), and considering the delta current during the increasing of the ripple, the increasing current $\mathrm{d}i_{\mathrm{M}} = \Delta I_{\mathrm{ripple}}$ can be expressed in terms of the voltage V_{M}, inductance L_{M} and time $\mathrm{d}t = m\frac{1}{f_{\mathrm{sw}}}$.

$$V_{\mathrm{M}} = L_{\mathrm{M}}\frac{\mathrm{d}i_{\mathrm{M}}}{\mathrm{d}t}. \tag{4.1}$$

Using (4.1) and expressing for the $\Delta I_{\mathrm{ripple}}$ the ripple can be expressed as in eq. (4.2). This finding closely matches the observed results from the simulations as shown in figure 4 for the case where $N_{\mathrm{arms}} > 1$. Using the results obtained in eq. (4.2), the estimate is that 4.44 parallel strains should give the required accuracy at 50 kHz. This result has been achieved with only a

2022 JINST 17 C03021

moderate increase of the switching frequency that becomes possible with a SiC technology device. In practice, 5 parallel interleaved bricks are sufficient to achieve the ripple accuracy of 0.9 ppm. This topology is shown in figure 2.

$$\Delta I_{\text{ripple}} = \frac{V_{\text{M}}\,\mathrm{d}t}{L_{\text{M}}} = \frac{\frac{\widehat{V}_{\text{M}}}{mN_{\text{arms}}}\frac{m}{f_{\text{sw}}}}{L_{\text{M}}} = \frac{I_{\text{flat}}R_{\text{M}}}{L_{\text{M}}f_{\text{sw}}N_{\text{arms}}} \Longrightarrow \Delta I_{\text{ppm}} \approx \frac{R_{\text{M}}}{L_{\text{M}}f_{\text{sw}}N_{\text{arms}}}. \tag{4.2}$$

5 Summary

The current ripple from a single converter can be approximated by (5.1), where the ripple is inversely proportional to the switching frequency of the DC-DC converter. By using SiC MOSFETs it becomes possible to increase the switching frequency from 5 kHz that is currently used, up to 60 kHz and beyond. This gives an increase in accuracy by an order of magnitude or more. In addition, higher switching frequency results in a higher frequency on the ripple, reducing the size of any filters if they are still required. Thus, the anticipated cost and losses of filters are reduced. It is also possible to consider 3-level modulation (unipolar switching), reducing the ripple even further.

$$\Delta I_{\text{ppm}} \approx \frac{R_{\text{M}}}{L_{\text{M}}f_{\text{sw}}N_{\text{arms}}}. \tag{5.1}$$

Introducing parallel connected devices leads to an increased investment cost for the devices, but it can reduce the device losses, cooling requirements, filter requirements and filter losses. In addition to being a more scalable topology, which enables it to cover a large range of loads with minimal overcapacity and the possibility to have redundancy in the converter. It also introduces more segmentation for the storage in the case of pulsed loads with storage requirements for the DC-DC converter. By taking a complete view and considering lifetime costs, SiC MOSFETs seem to be very suitable technology for this application [5]. Using the topology in figure 2 with interleaving, it is possible to achieve the sub ppm filter requirement without using active filters for this particular load. The results in figure 4 shows the effect of interleaving and switching frequency on the current ripple. At relative small number of parallel connected bricks, the sub-ppm accuracy seems achievable. Combining with SiC MOSFETs this solution compares well to a conventional converter with IGBTs and active filters.

References

[1] S.A. Gorji, H.G. Sahebi, M. Ektesabi and A.B. Rad, *Topologies and control schemes of bidirectional DC-DC power converters: an overview, IEEE Access* **7** (2019) 117997.

[2] M. Parchomiuk, R. Strzelecki, K. Zymmer and T. Sak, *Modular high precision high current source for special applications-simulation and verification, Proceedings — 2016 10th International Conference on Compatibility, Power Electronics and Power Engineering, CPE-POWERENG 2016* (2016), pp. 422–427.

[3] B.L.M. Lamaille et al., *Study of the energy savings resulting from the east area renovation, 10th Int. Partile Accelerator Conference* (2019), pp. 4023–4025.

2022 JINST 17 C03021

[4] P. Asimakopoulos, K. Papastergiou, T. Thiringer, M. Bongiorno and G. Le Godec, *On V_{ce} method: in situ temperature estimation and aging detection of high-current IGBT modules used in magnet power supplies for particle accelerators,* *IEEE Trans. Ind. Electron.* **66** (2019) 551.

[5] K.L. Haugen, K. Papastergiou, P. Asimakopoulos and D. Peftitsis, *On dimensioning the fundamental brick for a scalable DC-DC converter with energy recovery,* in *2021 23rd European Conference on Power Electronics and Applications, EPE 2021 ECCE Europe,* EPE Association (2021), pp. 1–10.

[6] K.L. Haugen, K. Papastergiou, P. Asimakopoulos and D. Peftitsis, *Energy flow control in a modular DC-DC converter with energy recovery, Proceedings of the 2021 IEEE 12th International Symposium on Power Electronics for Distributed Generation Systems, PEDG 2021* (2021).

2022 JINST 17 C03021

Article IV

K. L. Haugen, K. Papastergiou, P. Asimakopoulos, and D. Peftitsis

Energy flow control in a modular DC-DC converter with energy recovery

Submitted to International Symposium on Power Electronics for Distributed Generation Systems (PEDG), June 2021.

2021 IEEE 12th International Symposium on Power Electronics for Distributed Generation Systems (PEDG) | 978-1-6654-0465-5/21/$31.00 ©2021 IEEE | DOI: 10.1109/PEDG51384.2021.9494229

Energy flow control in a modular DC-DC converter with energy recovery

Krister Leonart Haugen
Department of Electric Power Engineering
NTNU, Trondheim, Norway
krister.l.haugen@ntnu.no

Konstantinos Papastergiou
Medium Power Converters Section
CERN, Geneva, Switzerland
k.papastergiou@cern.ch

Panagiotis Asimakopoulos
Medium Power Converters Section
CERN, Geneva, Switzerland
panagiotis.asimakopoulos@cern.ch

Dimosthenis Peftitsis
Department of Electric Power Engineering
NTNU, Trondheim, Norway
dimosthenis.peftitsis@ntnu.no

***Abstract*—This paper proposes an energy management control scheme for controlling the energy flow in a modular and scalable DC/DC converter design with energy recovery, based on a fundamental building block structure. The overall design in terms of control, number and configuration of the building blocks for optimised electrical operation is presented. Series and parallel connection of a low voltage and current building block are used to achieve the required current and voltage. This flexibility allows for a converter design with different operating characteristics and enhanced degree of reconfigurability, while keeping the same design of the fundamental building blocks. This combination results in a more scalable and flexible converter for efficient maintenance, with modularised storage for increased safety. In addition, a strategy of redundancy is implemented, which gives increased up-time and enhances the possibility for hot-swapping.**

***Index Terms*—Power Supply, DC-DC power converter, Modular Converter, Energy Storage**

I. Introduction

The ultimate technology to supply large electromagnets used to control the beam of particles in large physics experiments is power electronic converters [1]. At CERN there are particle transfer lines used in circular accelerators facilities [2], where the electromagnets are operated in cycling mode implying a significant energy flow to and from the electromagnet in every cycle. In particular, they receive a current pulse as shown in Fig. 1, typically trapezoidal, ramping from zero to a certain flat-top value, before ramping down again to zero and remaining at zero until the next pulse is requested [3]. This process requires a high power for a short time, in particular as the current ramps up, to supply both the power losses, as well as changing of the magnetic field. An example of the required power is plotted in Fig. 2.

Currently the power converters are of a high and medium power level, with the benefits and challenges this includes. The storage consisting of units storing large amounts of energy, which has to be dealt with in case of a fault. Starting from the point low power bricks and relatively small storage has benefits for operation and safety, but implies that several bricks has to work together to reach the target power. Segmentation of the energy storage makes is more likely to interrupt the current in case of failure, and there is less energy to manage. Using a low voltage and current building-block to construct a medium power converter implies a series and parallel connection of multiple bricks to achieve the required current/voltage. These bricks can, in principle, be connected in different ways and they are either connected to interface storage elements or the grid as illustrated in Fig. 3. This flexibility allows for a scalable converter with different characteristics, while keeping the same fundamental components. Which in turn allows for efficient maintenance with modularised storage for safer management of the stored energy. In addition, a strategy of redundancy can be implemented when required.

This concept of modular converters has been used for DC-DC converter for years [4] and with integrated storage can be used in DC grids for integrating fast response power in DC-DC converters, traction or automotive application with

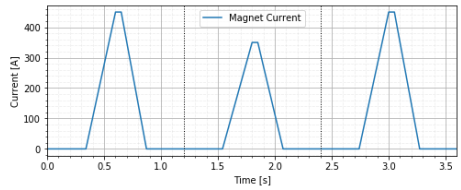

Fig. 1. Typical current pulse sequence, dotted lines indicate division between cycles.

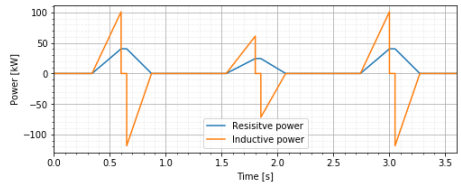

Fig. 2. Typical power requirement for the cycles.

978-1-6654-0465-5/21/$31.00 ©2021 IEEE

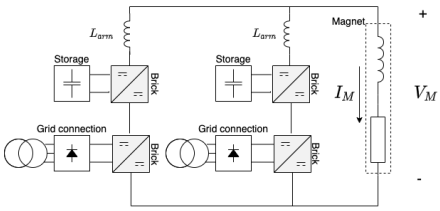

Fig. 3. Block diagram of the combined series and parallel connected bricks including the arm inductance used to control the current sharing.

TABLE I
SIMULATION PARAMETERS

	Grid Connected Brick	**Energy Storage Brick**
Max Voltage	200V	200V
Max Current	200A	200A
Energy Storage	N/A	8.1kJ @900V
Load inductance	40mH	
Load resistance	20mΩ	

regenerative breaking or similar applications [5], where there is a need for extracting energy from the system and reusing it [6]–[10]. The converter can be compared to a Modular Multilevel Converter (MMC) [4], [11], while taking advantage of a full bridge module to ensure 4-quadrant operation [12]. It integrates storage on some of the modules, which allows the converter to serve as a power balance compensator of short-term power imbalance [13]–[16]. It can also be used to deliver power to a highly inductive load requiring pulsed current, enabling the recovery of the energy stored in the inductors magnetic field, reducing the power consumed as in the case described in this paper.

With a modular system of converters, there are many possibilities for how each of these bricks should be used to ensure the highest utilisation in terms. Such as utilisation of the stored energy, optimising for lifetime, efficiency, precision (current regulation precision required on the current flat-top) [17] and front-end size for both transformer and rectifier. This paper investigates these relationships, to understand when it is beneficial to use separated storage bricks and how their energy can be managed to ensure reliability and selectivity.

In principle any number of storage types can be used, such as batteries, capacitors, mechanical flywheel [18], [19] or super-capacitors depending on the amount of stored energy required, delivered power and storage time [20]. This paper focuses on the use of capacitors to take advantage of the high power capability and their ability to handle a large number of cycles ($\gg$ 1e6). Using capacitors introduces some challenges in the regulation since the energy is a function of the voltage, however this also allows for relatively easy monitoring of the state of charge.

This paper will start from the basis that a scalable converter can be optimal, and then discuss how the energy in the storage and the power supplied from the different bricks can be shared. Starting from a simple simulation showing the behaviour of the energy controller.

II. The converter topology

In the case of a converter supplying a large electromagnet with a large current, the converter effectively has to supply two forms of energy; the joule losses and the magnetic field energy. The latter is possible to recover and use for the next current cycle [2]. Certain accelerator applications such as the particle storage rings require longer time/higher RMS magnetic current cycles with comparatively low recoverable energy, while others such as particle transfer lines require the opposite. A scalable converter is one that integrates a variable number of dedicated energy storing bricks (for the recoverable energy) and dedicated grid-connected bricks (that provide the joule losses). The system costs and benefits have been discussed in another paper [21] while this work discusses a scalable energy management controller that is required to manage the energy flow among the different types of bricks.

In order to investigate the possibilities of a modular power converter a relatively simple topology is proposed for further investigation. It consists a total of 5 fundamental bricks in parallel, shown in Fig. 4. In order to supply the losses in the particular magnet described in this paper only one grid connected brick is needed. The electromagnet this converter is designed to supply is a 40mH and 20mΩ magnet requiring 600A for 50ms every 1.2s. Similar to the current pulse shown in Fig. 1. The brick and load parameters are collected in Table I, the energy storage is calculated from the nominal bus voltage at 900V.

While other combinations remain possible, the chosen configuration allows an examination of the possible effects of combining modular bricks. One of the advantages of having modular converter design is to allow the power flow to be distributed in different ways among bricks according to the energy management objectives (grid power shaving, energy storage depth of discharge etc).

III. Fundamental brick and energy controller description

The purpose of an energy controller is to distribute the energy flow among the grid-connected and the energy storage bricks of a converter to fullfil an objective such as to limit the grid-current, to control the capacitor voltage fluctuation, or to achieve a certain regulation precision in the output. As a result such a controller impacts the peak and RMS loading of each brick. Additionally, the power flow among different bricks may be optimised for smaller temperature variations of the semiconductors and thus, improving the expected lifetime of power modules.

To fulfil these requirements three levels of control have been implemented; a voltage controller on each series connected brick, an arm-level current controller for the current control in different arms and a system level energy-controller. Significant work has been done on MMC to control and manage the energy stored in the cells [22]–[25]. However, this concerns

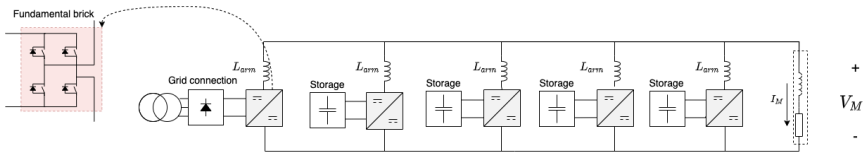

Fig. 4. Block diagram of the topology used in the simulations.

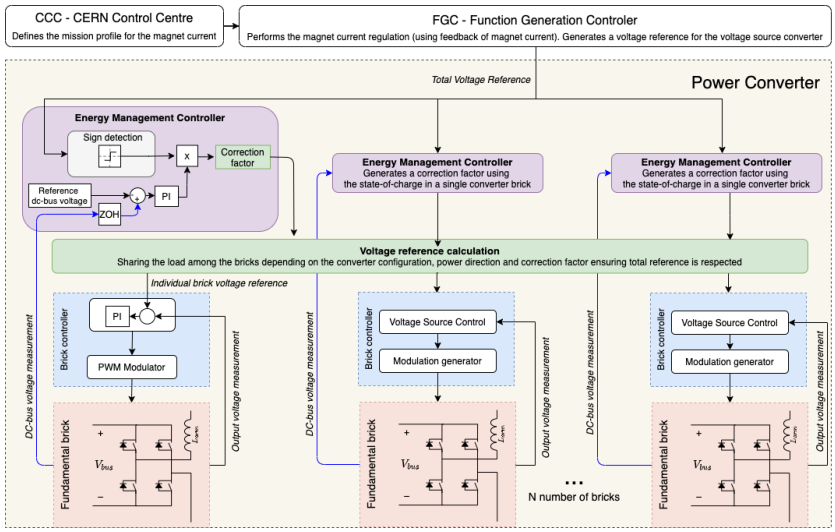

Fig. 5. High level controller of the converters at CERN. Showing where the energy controller is inserted into the control chain.

AC/DC applications and not a DC/DC converter. The controller hierarchy discussed in this paper is shown in Fig. 5. The controller uses the energy storage state-of-charge information, and relies on the use of circulating currents to balance the energy in the blocks.

The configuration shown is for the case where the current is shared among parallel bricks, a similar approach can be used for the series connected bricks. At the highest level, a system controller used in CERN applications, the function generation controller (FGC) performs the current control at the load level. The energy controller is regulating the voltage on the storage bus and modifies accordingly the references to keep the correct energy stored in the bricks. It is interjected between the references given by the system and before being passed to the individual converter bricks and is also responsible for dividing the total current and voltage references into the individual references for each brick. For a series connected system this correction will be added to the voltage reference for the bricks and subtracted from the corresponding grid brick reference. For a parallel connected system the correction will be added to the *current* reference, and subtracted from the grid reference. Subtracting from the grid reference ensures that the total current reference is always respected. In a system with both parallel and series, while it is possible to do both, it is probably best to manage the energy within a single arm first, before redistributing across several arms, but this is not covered by this paper. Through controlling the functioning of each brick, it can also control the power flow between the bricks. The converter bricks are in essence managed as separate converters, with independent power flow control and independent voltage loops.

IV. Simulation Results

The simulations were performed using PLECS® using a simple trapezoidal current pulse, similar to a single pulse shown in Fig. 1, the load profile is a pulse train of 10 identical such pulses. The topology used in the simulations is shown in Fig. 4. The topology with bricks in parallel was chosen as the parallel connection seems to exhibit the largest benefits for the applications at CERN. The objective of the energy management controller is to recharge the DC-link of each storage brick to an initial reference voltage while supplying the magnet current. The number of grid and storage bricks is determined by the chosen load and has a n+1 redundancy, all chosen to reflect the characteristics of the system in a good way. It was also considered since controlling the current in the

bricks causes the most challenges for the current references. This is due to that the grid brick has to reverse the current in some circumstances, this will be discussed in a later section. The case where grid and storage bricks are series connected is a much simpler case in terms of the concept and managing the energy flow.

A. Operation of the energy controller

The first set of results shows the system responding to a small error with respect to the grid current reference, this illustrates how the energy controller applies the correction. In the case of this small error of the grid current reference, the energy controller increases the power supplied from the storage bricks as the voltage after the pulse is completed is higher than the nominal. And correspondingly decreases the current from the grid. Fig. 6 illustrates the simulation results for the four storage bricks, all four bricks have identical results in this case as the capacitance of the storage is the same. The green line is the correction value supplied to the brick. Within 5-6 pulses the voltage has been recovered to within 2V of the nominal, and the new current for the brick is established. If the bus voltages are to high, the references for the storage bricks are increased during the ramp-up and flat-top phases, and decreased for the recovery phase. The voltage obtained by the controller is shown in Fig. 7. No detectable influence on delivered current to the magnet load is observed, even if the voltage on the bus is dropping.

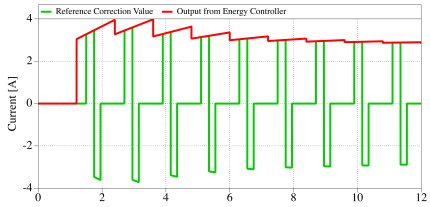

Fig. 6. Simulation results showing the current correction over time supplied from the energy controller all four of the energy storage bricks.

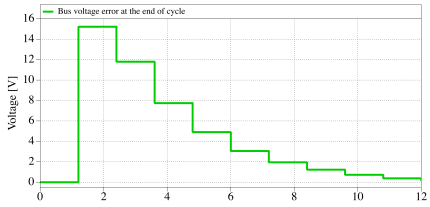

Fig. 7. Simulation results showing the bus voltage error over time for the four storage brick.

B. Effect of varying capacitance

Another challenge with using capacitors as energy storage is the slight variation in the capacitance of the capacitors. In theory the different storage modules have the exact same capacitance, and if the power loads are balanced they should all have the same voltage on the DC-bus. However, slight variation in the capacitance and losses occurring in the brick H-bridge can result in a small variation in the energy stored in each brick. Small as this effect might be, after hundreds of cycles it may become significant, so the energy controller needs to take this into account. This must be done to ensure that the voltages are kept at the correct value independently for the storage bricks. In Fig. 8 the bus voltage for the 4 storage bricks are plotted, showing how the controller can adjust the power individually for the 4 bricks. In this simulation the storage was set to +/- 10% to exacerbate the effect of uneven capacitance. The capacitance for the 4 storage bricks was 0, +5%, +10% and -10% respectively with reference to the nominal value chosen for the capacitor banks (10 mF). This indicates that the controller is able to keep the energy balance even as the capacitance of the storage is initially different, drifts over time or is influenced by other effects.

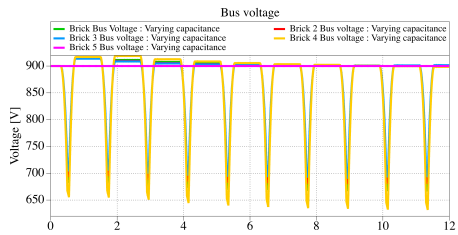

Fig. 8. Bus voltage on the 4 bricks with variation on the voltages over time from the different capacitances

C. Single brick failure

The second set of simulations investigates the open-circuit failure of a single storage brick. It is assumed that the remaining storage bricks are sized to be able to compensate by increasing their power output and with the variance in capacitance as described in the previous section. The failed brick is deactivated and left in a blocking state, and the controller can adapt and continue to deliver the required current to the load as long as the remaining bricks have the current capability and storage energy to comply.

Fig. 9 shows the current and voltage output from the bricks. It is shown that the voltages for the bricks are naturally the same as they are all connected in parallel, until Brick 1 fails as shown by the blue line. The remaining bricks are still operating as normal as long as no short-circuit is introduced by the failure and the modules' ratings are sufficient. The top plot in Fig. 9 shows the voltages on the other bricks as they recover to nominal value. The difference in the bus voltages is because the capacitances in the network are different as described in the previous section.

Prior to the fault, each of the bus voltages varies between 900V and 700V for each cycle, and after the fault the remaining 3 bricks cycle down to about 600V in order to compensate

for the energy that is no longer available from the failing brick. From the currents in Fig. 9 it is visible that after the fault, the 3 remaining bricks have to increase their supplied current in order to reach the total magnet current, while the grid brick does not change since the losses in the magnet are unchanged.

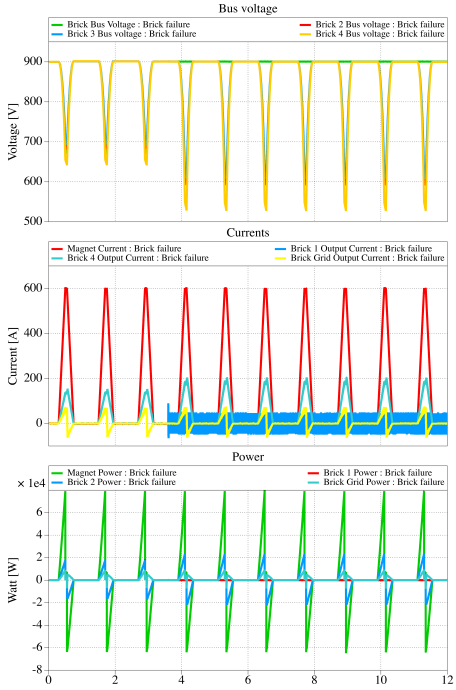

Fig. 9. Simulation results showing the bus voltage for the 4 storage bricks and the grid brick over time. As well as the current and power for the different types of bricks, failure of brick occurs at 3.6s.

D. Grid current control strategies

In the simulations above, the grid bricks have been given a trapezoidal current shape current to supply to the magnet (red line in Fig. 10). The grid bricks try to supply the losses in the magnet and the system. Notice the negative value in the ramp-down phase, this is necessary to keep a positive power delivery during the ramp-down for the grid brick, as the magnet voltage is negative in this phase.

It is possible to give the grid brick a shaped reference in any shape. A trapezoidal shape, similar to the system current reference in Fig. 1, is used as the initial shape, which allows the current to be most equally shared between the storage and the grid bricks. These are shown in Fig. 10, where the red line describes the current pulse case used in the results above. The red and green describes trapezoidal voltage shapes which shares more evenly the peak current stress between the bricks and the green has the grid brick delivering positive power during the recovery phase of the magnet. The current has

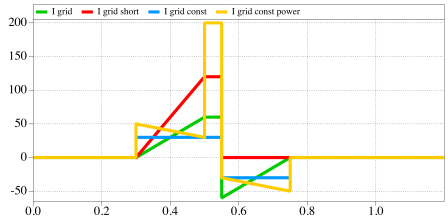

Fig. 10. Possible grid brick reference shapes.

to be reversed to keep a positive power, since the recovery voltage is negative in order to recover the energy stored in the magnet. The yellow is a linear approximation of a constant power shape, limited by the max current capability of the bricks. The blue shape is delivering a constant current for the duration of the pulse. The advantage and disadvantage of each is discussed in the sections below. It should be noted that these different shapes are only of significance when the flat-top are relatively short compared to the ramping-up and down. As the flat-top increases compared to the ramps, all shapes eventually approximates the blue shape in Fig. 10, i.e. a square wave. The following sections will describe the four strategies and the results in the simulations. A comparison of the four strategies in two selected key metrics are presented in Table II.

1) Sharing current stress: Letting the Grid current have a trapezoidal shape shares the current between the storage and grid bricks during ramping, while the grid supplies almost the full power during flat-top. It has a higher peak current for the grid brick and a higher current supplied from the grid. It also has an abrupt change after the flat-top in the current reference for the grid brick, as the grid brick has to reverse its current direction to continue positive power delivery during the ramp-down, as shown in Fig. 11.

The yellow line in the middle plot in Fig. 11 shows the current supplied by the grid brick, the ramping as the direction of the current is reversed is caused by the arm inductor for the grid brick. This disadvantage in reversing the current direction of the grid current forces the storage bricks to absorb extra energy at a time when then the current stress is all ready at its highest. However it does allow the grid brick to supply power during the entire current pulse, reducing the peak power for the grid brick and thus the front-end rectifier and grid.

2) Sharing current stress - without current reversal: Using the same shape as for the trapezoidal current, but excluding the ramp-down phase shares the current stress between the bricks for the ramp-up phase and flat-top of the pulse, referred to as *trapezoidal current short* in the plots. However the Grid brick does not supply anything during ramp-down, this saves the grid bricks from having to reverse their current direction. The storage bricks are actually recovering energy during flat-top, since they have to supply the losses during ramp-down. It has the minimal drop in voltage on the storage capacitors on

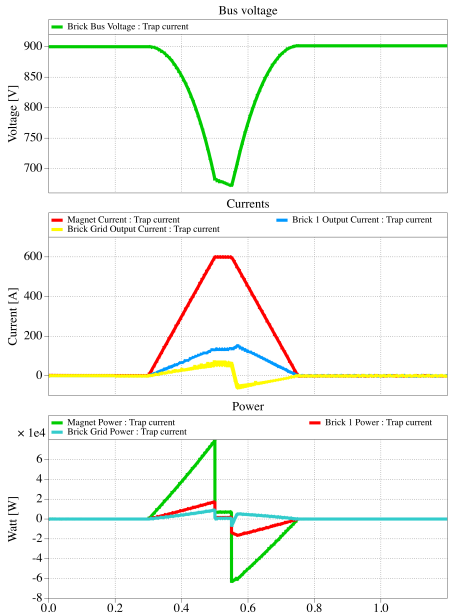

Fig. 11. Simulation results showing the output current, bus voltage and output power for the bricks, the grid brick using the trapezoidal current reference.

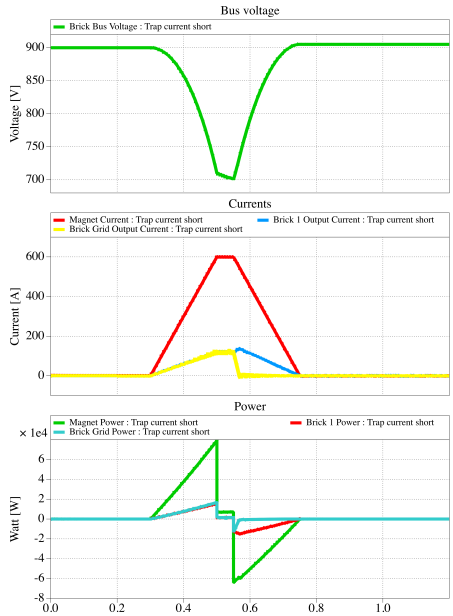

Fig. 12. Simulation results showing the output current, bus voltage and output power for the bricks, the grid brick using the short trapezoidal current reference.

the storage bricks, meaning that it uses the least of the stored energy in the capacitors.

The results are plotted in Fig. 12. The top plot shows the bus voltage for one of the storage brick and how it is only dipping down to 700V during the pulse, corresponding to the least use of energy stored in the capacitors of the strategies proposed in this paper. Since the grid brick have a shorter time to supply the losses occurring in a cycle, it has a higher peak-power than the previous current shape.

3) Minimal grid current RMS: The constant current shape tries to supply a constant current from the grid brick. This results in a significantly lower peak stress for the grid brick. However the storage bricks now have to do most of the work during the pulse and have to absorb energy in the first moments of the pulse before the current reference value reaches the grid reference value, notice how the grid brick current is higher than the magnet current in the very first moments of the pulse in Fig. 13. This results in the storage bricks also has to reverse their current direction in the very first moments, and also increasing the voltage on the storage above the nominal. For a magnet with higher losses, the grid current will be relatively higher, and the increase of the bus voltage at the beginning of the pulse will be more significant.

The results are plotted in Fig. 13, the bus voltage shows this strategy is one of the strategies utilising most of the storage. Since the current from the grid is lower than the reference, the storage have to supply more current during the flat-top. This becomes a significant limitation as the duration of the flat-top increases, since supplying a magnet with current from a capacitor bank requires very large energy storage capability.

4) Minimal peak grid power: The final strategy tries allow the grid brick to draw a constant power from the grid. The current is calculated from an approximation of constant power dictated by the voltage on the magnet. In principle, the initial voltage would go to infinity if this shape was to follow the power law directly, so a linear averaging approximation is used. This shape has the storage brick supplying the most power during flat-top and thus has the lowest voltage on the storage bus. It minimises front-end power requirements at the cost of larger storage requirements and higher storage brick losses. It also has the problem of the constant current approach, where in the storage bricks has to absorb energy at the beginning of the pulse and reverse their current direction at the beginning of the cycle.

The results are plotted in Fig. 14. The yellow line in the middle plot shows the output current from the grid brick, which have to change significantly several times during the pulse. In particular the high current during flat-top reversing into a negative current during ramp-down results in a dip in the supplied power from the grid brick and a step the storage bricks have to compensate for. In the simulations the grid brick actually goes down into negative power for a short time, i.e. the grid brick is absorbing power, before the current in the arm inductance have been reversed. This type of strategy is more feasible in the case where the losses in the magnet are higher

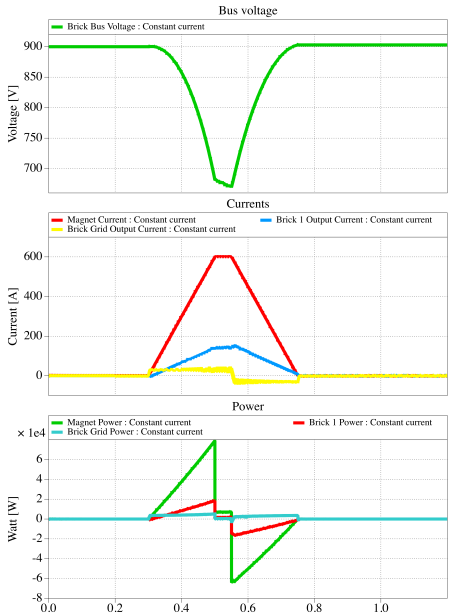

Fig. 13. Simulation results showing the output current, bus voltage and output power for the bricks, the grid brick using the constant current reference.

Fig. 14. Simulation results showing the output current, bus voltage and output power for the bricks, the grid brick using the approximated constant power current reference.

compared to the stored energy or the pulses are much longer. However, this also increases the problem with a negative current direction for the storage bricks at the beginning of the cycle. Perhaps a hybrid approach can be considered, wherein the current shape is limited to always be below the magnet current to avoid the reversals of the current for the storage bricks.

E. Summary of grid current control strategies

A comparison of the four strategies in selected key metrics are presented in Table II. This tables shows a comparison of some key parameters for the different proposed strategies, the delta voltages and energy are referenced to the nominal bus voltage of 900V and corresponding energy. As discussed above, the difference in strategy 1 and 2 is the increase in peak current and reduced utilisation of the storage since less of the energy in the storage can be recovered as it is used for losses during the ramp-down. Strategy 3 on minimal grid RMS current, enables a lower RMS current for the grid brick compared to strategy 1. However, the biggest difference using strategy 3 is the much lower peak current for the grid bricks, while the other parameters are fairly similar to strategy 1. Except for the difference that the storage bricks are changing the direction of the power flow several times during a single pulse. Strategy 4 imposes a significant peak current on the grid brick, which is slightly above the capability of the brick due to the ripple in the arm current. The high current occurs as the voltage during the flat-top is very low compared to the ramping, this also results in a higher grid brick current RMS as well. For all the cases the storage bricks changes very little, as it has constraints to supply the power to the load within a very short time interval and this is the dimension load for the storage bricks. Ultimately, the choice of the most optimal strategy is influenced by the flat-top duration, the L/R-ratio of the magnet load and the availability/cost of front-end peak power capability. The advantage of such a modular design is that the strategy can be adapted to the individual load.

V. Conclusion

An energy flow control scheme for modular DC-DC converters has been proposed, modelled and simulated. It has been shown that the controller can respond efficiently under various operating scenarios, such as cycling loads, variable capacitance among the bricks and it is also able to handle a simple open-loop brick failure. The 5 bricks can also manage different types of grid brick power strategies shapes internally, allowing it to achieve different targets for optimisation. Such targets are the minimal front-end current, cycling depth of the storage or thermal stability. The energy flow in the system, meaning the energy exchange among the load the storage bricks and the grid connected bricks, is controlled in an optimised way by choosing the appropriate current reference shape for the grid brick. By having a shape which follows the current to the load, i.e., trapezoidal, the current stresses in the brick switches and losses are shared most equally among the bricks.

TABLE II
COMPARISON OF GRID BRICK POWER SHARING STRATEGIES

Strategy	Key metric	Grid Brick	Storage Brick
1. Sharing current stress	$I_{RMS-out}$	22.9A	56.8A
	I_{peak}	70.3A	152.4A
	ΔV_{bus}	-	228.0V
	ΔE_{str}	-	3.58kJ
2. Sharing current stress - short	$I_{RMS-out}$	38.4A	50.9A
	I_{peak}	128.3A	138.3A
	ΔV_{bus}	-	198.9V
	ΔE_{str}	-	3.18kJ
3. Minimal grid current RMS	$I_{RMS-out}$	18.3A	57.9A
	I_{peak}	41.0A	151.4A
	ΔV_{bus}	-	229.5V
	ΔE_{str}	-	3.60kJ
4. Minimal peak grid power	$I_{RMS-out}$	44.6A	53.3A
	I_{peak}	208.2A	144.2A
	ΔV_{bus}	-	217.6V
	ΔE_{str}	-	3.44kJ

Two additional strategies, aiming to reduce the front-end peak power have also been shown. These strategies are most suited for relatively short pulses in inductive loads, with a large amount of recoverable energy compared to the losses. It shows the possibility to have any number of bricks connected in series and parallel, and within their current and voltage ratings, the power-flow can be individually controlled.

Starting from this basis, it is possible to improve the converter's lifetime, overall reliability and the peak power required from the grid. This is achieved by optimising the utilisation of the sub-modules to balance the current stressing and therefore the thermal stress among the storage bricks. Using this modelling as a basis, the lifetime and temperatures of a specific type of semiconductor module could be investigated in the future.

REFERENCES

[1] S. Maestri, R. G. Retegui, D. Carrica, S. Rossini, G. Le Godec, and K. Papastergiou, "Figures of merit for the evaluation of regenerative power converters," *2016 18th European Conference on Power Electronics and Applications, EPE 2016 ECCE Europe*, pp. 1–9, 2016.

[2] B. L. M. Lamaille, F. Dragoni, S. Evrard, F. J. Harden, E. Harrouch, M. Lazzaroni, R. Lopez, and K. D. Papastergiou, "Study of the Energy Savings Resulting From the East Area Renovation," *10th Int. Partile Accelerator Conferance*, pp. 4023–4025, 2019.

[3] P. Asimakopoulos, K. Papastergiou, T. Thiringer, M. Bongiorno, and G. Le Godec, "On Vce Method: In Situ Temperature Estimation and Aging Detection of High-Current IGBT Modules Used in Magnet Power Supplies for Particle Accelerators," *IEEE Transactions on Industrial Electronics*, vol. 66, no. 1, pp. 551–560, 2019.

[4] A. Lesnicar and R. Marquardt, "An innovative modular multilevel converter topology suitable for a wide power range," *2003 IEEE Bologna PowerTech - Conference Proceedings*, vol. 3, pp. 272–277, 2003.

[5] Y. Yang, L. Dorn-Gomba, R. Rodriguez, C. Mak, and A. Emadi, "Automotive Power Module Packaging: Current Status and Future Trends," *IEEE Access*, vol. 8, pp. 160126–160144, 2020.

[6] T. M. Masaud, K. Lee, and P. K. Sen, "An overview of enrgy storage technologies in electric power systems: What is the future?," *North American Power Symposium 2010, NAPS 2010*, 2010.

[7] J. M. Carrasco, L. G. Franquelo, J. T. Bialasiewicz, E. Galvan, R. C. Portillo Guisado, M. A. M. Prats, J. I. León, and N. Moreno-Alfonso, "Power-electronic systems for the grid integration of renewable energy sources: A survey," *IEEE Transactions on Industrial Electronics*, vol. 53, no. 4, pp. 1002–1016, 2006.

[8] S. A. Khan, M. R. Islam, Y. Guo, and J. Zhu, "A New Isolated Multi-Port Converter With Multi-Directional Power Flow Capabilities for Smart Electric Vehicle Charging Stations," *IEEE Transactions on Applied Superconductivity*, vol. 29, no. 2, pp. 1–4, 2019.

[9] P. Peng, Y. Li, Z. Li, Y. Shao, X. Luo, Y. Wang, and N. Zhang, "Analysis of Advantage of the Connection of Energy Storage System to Distribution Network and the Impact on the Voltage Quality," *2nd IEEE Conference on Energy Internet and Energy System Integration, EI2 2018 - Proceedings*, no. 1, pp. 2018–2021, 2018.

[10] M. Parchomiuk, R. Strzelecki, K. Zymmer, and A. Domino, "Modular power converter topologies for energy storage and electric power distribution systems," *2017 Progress in Applied Electrical Engineering, PAEE 2017*, 2017.

[11] G. J. Kish, "On the emerging class of non-isolated modular multilevel DC-DC converters for DC and hybrid AC-DC systems," *IEEE Transactions on Smart Grid*, vol. 10, no. 2, pp. 1762–1771, 2019.

[12] S. M. Goetz, A. V. Peterchev, and T. Weyh, "Modular multilevel converter with series and parallel module connectivity: Topology and control," *IEEE Transactions on Power Electronics*, vol. 30, pp. 203–215, 1 2015.

[13] M. N. Raju, J. Sreedevi, R. P. Mandi, and K. S. Meera, "Modular multilevel converters technology: A comprehensive study on its topologies, modelling, control and applications," *IET Power Electronics*, vol. 12, no. 2, pp. 149–169, 2019.

[14] M. Vasiladiotis and A. Rufer, "Analysis and control of modular multilevel converters with integrated battery energy storage," *IEEE Transactions on Power Electronics*, vol. 30, no. 1, pp. 163–175, 2015.

[15] I. Stoppa, J. Lundin, N. Lima, and J. G. Oliveira, "Dual voltage/power system by battery/flywheel configuration," *2015 IEEE 13th Brazilian Power Electronics Conference and 1st Southern Power Electronics Conference, COBEP/SPEC 2016*, pp. 1–6, 2015.

[16] T. Ise, M. Kita, and A. Taguchi, "A hybrid energy storage with a SMES and secondary battery," *IEEE Transactions on Applied Superconductivity*, vol. 15, no. 2 PART II, pp. 1915–1918, 2005.

[17] M. Parchomiuk, R. Strzelecki, K. Zymmer, and T. Sak, "Modular high precision high current source for special applications-Simulation and verification," *Proceedings - 2016 10th International Conference on Compatibility, Power Electronics and Power Engineering, CPE-POWERENG 2016*, pp. 422–427, 2016.

[18] D. R. Brown and W. D. Chvala, "Flywheel energy storage: An alternative to batteries for ups systems," *Energy Engineering: Journal of the Association of Energy Engineering*, vol. 102, no. 5, pp. 7–26, 2005.

[19] R. Magdalena Stephan, R. de Andrade Jr., and G. Gonçalves Sotelo, "Third Generation Of Flywheels: A Promising Substitute To Batteries," *Eletrônica de Potência*, vol. 13, no. 3, pp. 171–176, 2008.

[20] G. Wang, G. Konstantinou, C. D. Townsend, J. Pou, S. Vazquez, G. D. Demetriades, and V. G. Agelidis, "A review of power electronics for grid connection of utility-scale battery energy storage systems," *IEEE Transactions on Sustainable Energy*, vol. 7, pp. 1778–1790, 10 2016.

[21] K. L. Haugen, K. Papastergiou, P. Asimakopoulos, and D. Peftitsis, "On dimensioning the fundamental brick for a scalable DC-DC converter," in *To be published at EPE*, pp. 1–8, 2021.

[22] L. Ängquist, A. Antonopoulos, D. Siemaszko, K. Ilves, M. Vasiladiotis, and H. P. Nee, "Open-loop control of modular multilevel converters using estimation of stored energy," *IEEE Transactions on Industry Applications*, vol. 47, no. 6, pp. 2516–2524, 2011.

[23] K. Ilves, L. Harnefors, S. Norrga, and H. P. Nee, "Analysis and operation of modular multilevel converters with phase-shifted carrier PWM," *IEEE Transactions on Power Electronics*, vol. 30, no. 1, pp. 268–283, 2015.

[24] M. A. Perez, S. Bernet, J. Rodriguez, S. Kouro, and R. Lizana, "Circuit topologies, modeling, control schemes, and applications of modular multilevel converters," *IEEE Transactions on Power Electronics*, vol. 30, pp. 4–17, 1 2015.

[25] G. L. Rodal, A. B. Acharya, and L. E. Norum, "Analysis and Evaluation of Repetitive Controllers for Circulating Current Suppression in Modular Multilevel Converters," *2018 20th European Conference on Power Electronics and Applications, EPE 2018 ECCE Europe*, pp. 1–10, 2018.

Article V

K. L. Haugen, K. Papastergiou, and D. Peftitsis

Adaptive system control of a modular converter with energy storage to optimise for different key metrics

Submitted to in IET Journal of Power Electronics, September 2023. Currently under review.

Received: Added at production | Revised: Added at production | Accepted: Added at production

DOI: xxx/xxxx

ORIGINAL RESEARCH PAPER

Adaptive System Control of a Modular Converter With Energy Storage Optimising Different Key Metrics

Krister Leonart Haugen[1,2] | **Konstantinos Papastergiou**[2] | **Dimosthenis Peftitsis**[1]

[1]Department of Electric Energy, Norwegian University of Science and Technology (NTNU), NO-7491 Trondheim, Norway

[2]Medium Power Converters Section, European Organisation for Nuclear Research (CERN), 1211 Geneva 23, Switzerland

Correspondence

Corresponding author Krister Haugen.
Email: krister.haugen@ntnu.no

JEL Classification: ejlje

Abstract

Using modularized power converters with scalable energy storage enables the use of controls that can be adapted to optimise different design targets, such as to minimise the front-end current, the cycling depth of discharge of energy storage units or the thermal cycling of semiconductors. Such a scalable converter has the capability of individually adjusting the power flow of the modules, and this can be used to achieve the different target, it also allows a separation of storage and grid connection even under rapid cycling, enhancing scalability. The paper briefly recapitulates the characteristics of the modular converter and then presents four alternative strategies and simulations demonstrating their behaviour. The four control strategies have been validated experimentally on a 800 kW laboratory prototype of a modular and scalable converter. It is shown that applying each strategy, the corresponding design objectives can be achieved, for example, optimal utilisation of the energy storage systems or minimised current stress in the semiconductors.

KEYWORDS

AC-DC converters, Adaptive control, Energy balance control, Modular converter, Pulsed power supplies, Scalability.

1 | INTRODUCTION

Modularisation is currently an emerging trend in the design of modern power electronic converters[1–3]. Modularised converters exhibit many benefits, in terms of redundancy under fault conditions, parallel connection to reduce losses, standardisation etc. They can also incorporate storage in order to improve the voltage quality and stability of grids[4,5] and this is a key requirement to ensure successful integration of renewable energy sources into the grid[6].

The storage component can be any type of electrical energy storage, such as batteries, capacitors, mechanical flywheel[7,8] or supercapacitors, depending on the amount of stored energy required, delivered power and storage time[9]. Other works[10] demonstrated the use of inductive storage in conjunction with battery storage, to compensate for the difference in power demand and supply from a wind farm. Significant work has been done on modular multilevel converters (MMC) to control and manage the energy stored in the cells with the additional constraint of keeping each cell's voltage constant[11–14].

All of the converters discussed in the aforementioned literature are designed to be flexible, have high peak-power and be scalable. Such scalable solutions are also popular as renewable energy interconnectors with grid-forming requirements and integrated storage[6,15–18] or in rail application with similar bi-directional power flow requirements[19].

In the niche application of power supply for particle accelerators, reliable powering and energy efficiency are increasingly important. In particular, recycling and reusing of the magnetic field stored energy has given significant energy savings in the past[20].

More specifically, DC/DC converters are used for the precise regulation of the current supplying electromagnets in high-energy physics experiments[21,22]. These electromagnets are operated in a repetitive manner[20], which results in a cycling power flow, shown in Fig. 1 and this leads to technical challenges that have been discussed in[23]. In certain applications the load mission profile is unknown[24], while at CERN, the European Organisation for Nuclear Research, the powering requirements of electromagnets are often well defined, and the designer can take this into account for optimising electrical and thermal performance of the converters.

Furthermore, in modular converters the energy recovery in storage bricks requires a topology with 4-quadrant operating capability to handle the bidirectional power flow. While the topics of control[2,3,25,26] and power flow[27–30] of DC-DC converters have been

Abbreviations: MMC, modular multilevel converter; SiC, Silicon Carbide; MOSFET, metal oxide semiconductor field-effect transistors.

discussed elsewhere, this paper focuses on the challenge of a power converter where the energy available in some of the bricks is inherently limited. [31] manages to optimise the control of a converter for several parameters at the same time, but this converter is not pulsing, which introduces several challenges addressed here.

The scalability advantage of DC-DC converters for highly inductive loads has been investigated before, both with [27] and without [22] energy storage. This paper investigates a particular scenario where the converter operates with a pre-defined (known) cycling current shape. Unlike in a conventional modular converter, the discussed control concept commands each one of the converter modules with a different modulation index, that corresponds to the desired mission profile (which is different for energy storing and grid-connected bricks). The goal of this work is to optimise the power converter's performance for different key metrics by flexibly utilising its energy storage as much as possible and recover the energy at the end of the cycle. These key metrics can be related to power losses and efficiency, current stress of power semiconductors, utilisation of the storage system and grid-supply requirements. The proposed energy-flow control strategies can offer financial benefits as well [32], in particular if Silicon Carbide (SiC) metal oxide semiconductor field-effect transistors (MOSFETs) are utilised. The contribution of this paper is to demonstrate the advantage of utilising the planned strategies on a full-scale prototype.

The paper is organised as follows. Section 2 presents the operating constraints and load requirements for such a converter. Then in Section 3 the concept for this modular converter is briefly presented. In Section 4 the adaptive control strategy is analysed and the different optimisation strategies are explained. Section 6 shows the laboratory prototype and experimental validation of the proposed scheme. Finally, the conclusions of this work are summarised in Section 7.

2 | OPERATING CONSTRAINTS AND LOAD REQUIREMENTS

Typical magnet waveforms encountered in the transfer lines in particle accelerators are shown in Fig. 1. The different magnet loads across the length of an accelerator vary considerably in inductive and resistive values. For one single experimental area the range of current required varies between 100 A to 2 kA, hence the benefit of having a flexible converter design [32,33]. In addition, during the ramp down phase of the current, there is a potential to have a negative power flow, i.e. a fraction of the energy can be recovered and used in the next cycle, which is very beneficially from an energy consumption perspective [20]. Hence the need for built-in energy storage in the power converters.

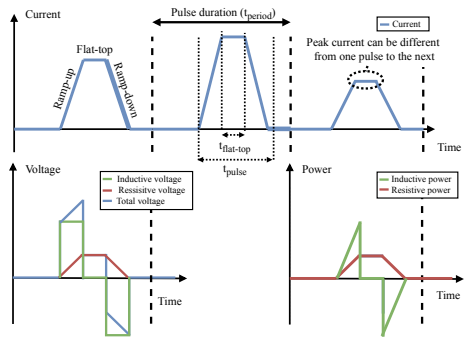

FIGURE 1 Typical current cycle sequence, dotted lines indicate division between cycles. t_{period} is typically 1.2 s, $t_{flat-top}$ is typically 50 ms and t_{pulse} can vary from 300 ms-800 ms depending on the load and flat-top current.

The maximum value of energy stored in the electromagnet field, E_{magnet} is given by Eq. 1, where L_{magnet} is the inductance of a particular electromagnet and I_{magnet} is the current through the magnet at any given time.

$$E_{magnet} = \frac{1}{2} L_{magnet} I_{magnet}^2 \tag{1}$$

By integrating adequate energy storage (e.g. capacitors) in the system, and with the power capability to deliver this energy in the relatively short time (<1 s) of the current ramp-up and ramp-down processes, the stored energy can be reused.

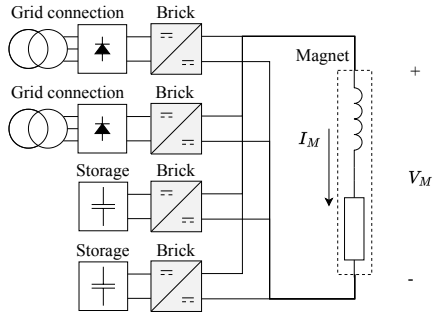

FIGURE 2 Schematic diagram showing of grid bricks and storage bricks can be combined in parallel connection of bricks. The fundamental brick in the grey box contains a full-bridge circuit with an arm inductor.

Since the voltage and the rate of change of voltage, dV/dt, that can be applied to the magnets are limited by design, there are limitations on how fast the current can be ramped. This voltage is often considered as a ramping voltage, shown as inductive voltage in Fig.1.

The load voltage constraint determines the power converter output requirements.

3 | FUNDAMENTAL BRICK CONCEPT

This paper is based on the converter design and operation published by the authors in [32], where a more detailed description of the function and control are shown. The proposed power converter topology comprises two types of power modules or bricks; one or more *storage bricks* handle the magnetic field energy recovery while one or more *grid bricks* supply the resistive losses of the load. Each of these bricks have a certain output current and voltage capability, so the number of bricks required to meet the converter's capabilities will depend on the load requirements. As discussed in Section II, the required currents span over a wide range and the ability to easily connect bricks in parallel makes it possible to scale the current. The required voltage for the electromagnets also spans in a wide range, which impose the need for connecting bricks in series.

The proposed structure (an example can be seen in Fig. 2), enables a converter design where the resistive and inductive power can be scaled independently. An investigation of the optimal output characteristics of these bricks has been presented in [32], such that the converter can be scaled to each magnet in an optimal way.

Each one of the grid and storage bricks is implemented using a full-bridge output stage [26,34–36] with a brick inductance L_{HF} which allows the output voltage to be independently controlled.

3.1 | Storage brick

The storage brick has the primary task of supplying the inductive power flow of the load. It features no grid-connection, and thus its operation relies on a controller that manages balanced supply and recovery of energy during each of the load cycles (in particular during the ramp-up and the ramp-down of the current). The ramp-down phase is described in Fig. 1. The storage brick will connect to the load using the fundamental brick described above, and will store energy using electrolytic capacitors connected to a DC-bus on the input side of the full-bridge in the fundamental brick.

Since the peak power by these converters is only delivered during ramp-up and ramp-down, the storage components need to deliver the majority of their energy in less than one second. Thus, capacitors have been chosen as appropriate storage elements [37]. This, in turn, means that the bus voltage in the storage bricks depends on the state-of-charge of the storage capacitors. In order to maximise the utilisation of the capacitors, the nominal bus voltage has been chosen to be the highest voltage the power semiconductor devices can safely manage.

The storage capacitors and the nominal voltage determine the amount of energy stored in the storage bricks. Given the need to use H-bridges to supply the magnets, it is only possible to step down the voltage from the DC bus. This limits the lowest voltage the storage bus can accept, since there has to be sufficient voltage left on the bus to deliver the full output voltage. The minimum requirement for the voltage on the capacitors reduces the amount of usable energy in the capacitors. Eq. 2 expresses the usable energy in the storage brick, E_{brick}, as a function of the capacitance of the storage brick, C_{str}, nominal DC-bus voltage, V_{bus} and the lowest allowable voltage on the bus, V_{out}, in order to deliver the required output voltage for the brick.

$$E_{brick} = \frac{1}{2} C_{str} (V_{bus}^2 - V_{out}^2) \tag{2}$$

This is where the complexity of designing the storage bricks emerges. If the output voltage is selected to be relatively high, then the usable energy in the capacitors is somewhat limited for a given capacitance in the storage bricks. This implies that either a large number of storage bricks is needed to achieve the required storage for supplying the inductive stored energy in the magnet, which increases the cost of semiconductors and capacitors; or that each storage brick needs a large number of capacitors, making them more costly and storing more energy, increasing the short-circuit energy. However, if the output voltage is selected to be relatively low, then the storage capacitors are utilised at a larger degree, and fewer capacitors are needed overall to satisfy the storage requirements. In this design scenario, the number of bricks starts to increase, in order to achieve the voltage requirement of the individual magnet. This trade-off has been discussed in detail in a previous publication and based on the findings there [32], a brick size of 200V and 400A has been specified.

3.2 | Grid brick

The grid bricks will use the same bus and output voltage as the storage bricks. This is the condition to ensure re-usability of the design and components. Since the grid bricks in principle only need to supply the power losses in the magnet, there is no need to consider bi-directional power flow or the state-of-charge of the storage, making it a more simple component to scale. The grid brick is supplied by a diode rectifier connected to a three-phase AC grid, hence no power shall ever flow back to the grid.

While the grid bricks and storage bricks could be dimensioned in terms of voltage ratings independently, for the sake of standardisation and to allow the bricks to be freely connected in series and parallel, the output voltage of the grid bricks was chosen to be the same as for the storage bricks.

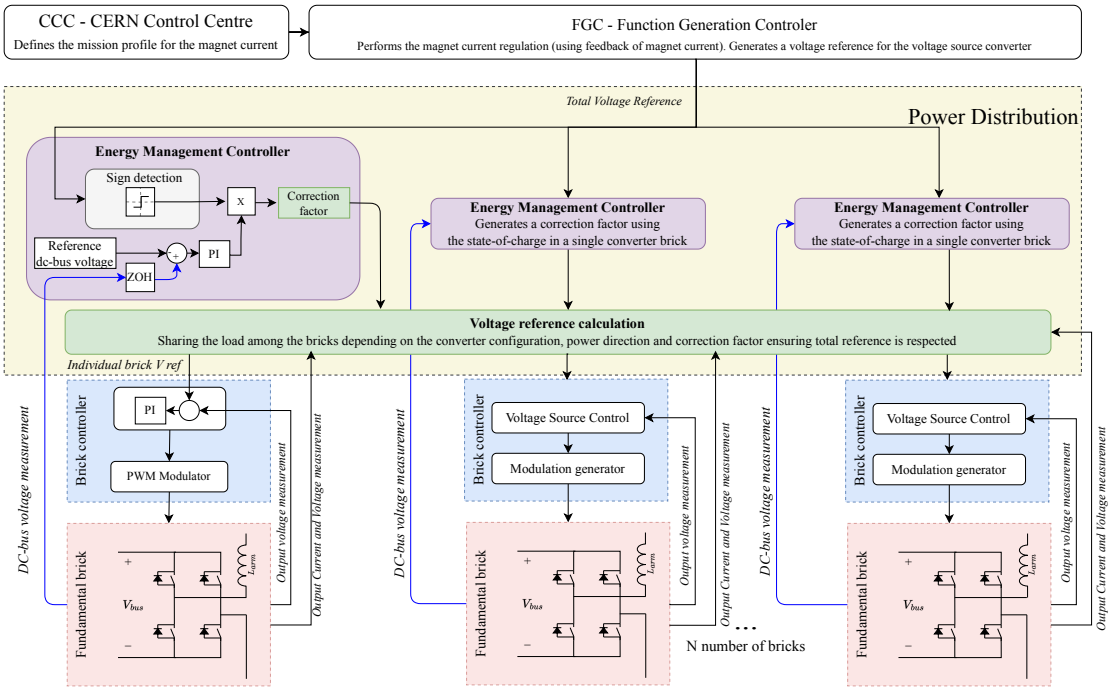

FIGURE 3 High level controller of the converters at CERN. The proposed energy controller that inserted in the control chain is shown in the yellow shaded area.

4 | SYSTEM CONTROL IMPLEMENTATION

The scalable converter is controlled by a central energy controller. This controller is responsible for distributing the energy flow between the grid-connected and the energy-storage bricks of the converter. The primary target is to respect the total voltage and current references and to ensure that the energy in the storage bricks are maintained at the desired level. A principle sketch of the controller structure of the converter used in this paper is shown in Fig. 3, the yellow shaded area shows where the code is inserted into the existing control structure. The controller uses the storage state-of-charge information and regulates the power flow between the bricks to maintain the state-of-charge at the end of each supplied pulse, taking advantage of the power supplied to the load and circulating currents to replenish the storage.

While the primary targets poses some limitations on the range of operation, there is normally still quite a lot of room left to have a secondary target. This is used in this paper to optimise for different targets such as to limit the grid-current, to increase the usage of the storage, or to achieve a certain regulation precision in the output current. By regulating the power flow, the controller adjusts the peak and RMS current loading of each brick. Additionally, the power flow among different bricks may be optimised for smaller temperature variations of the power semiconductors modules and thus, improving their expected lifetime.

The configuration discussed in this work is four parallel-connected bricks; two of them are storage bricks connected to capacitive energy storage and two of them are grid bricks connected to the power grid.

When a higher voltage is required to supply the load, the bricks need to be connected in series, but the principle of distributing the power supplied by the different bricks remains. This approach is made easier by the fact that the current can be considered the same for all series connected bricks, and the voltage of the individual bricks regulated to supply the desired power. The function generation controller (FGC) acts as the system controller, receiving the mission profile from the CERN Control Centre and controlling the current at the load level. The reference is then passed on to the energy regulator in the converter, which regulates the bus voltage in the storage bricks by calculating the energy available and dispatching a modified current reference for each of the bricks independently.

The calculation depends on the configuration on the bricks in the converter. If all bricks are connected in parallel, then the output voltage is necessarily always the same, but the energy management

controller can distribute the current between the bricks, while always respecting the total current. This modifies the reference given to the voltage loops in the individual bricks, using the added inductance in each brick to regulate the current. If the bricks are connected in series, the voltage to each brick can be controlled more directly, but the energy management controller must take the current into account in order to correctly anticipate the delivered and recovered energy. The theoretical background for this implementation strategy has been presented in [27], including the redistribution of power flow during a fault condition.

5 | GRID CURRENT CONTROL STRATEGIES

In a conventional converter topology with four parallel connected bricks, all of them receive the same trapezoidal current reference and supply their part of the total current (this reference is represented with a grey colour line in the graphs of Fig. 4). The proposed control scheme produces different reference shapes for the grid bricks to satisfy different objectives. The results shown in this section extend on the work presented in [27] (some of the findings are reported here to provide the necessary context for the laboratory verification).

It is reminded that the role of the grid bricks is to supply the losses in the magnet and the system. Besides, it should be noticed that the current contributed by grid bricks may exhibit negative values in the ramp-down phase (red, pink and green curves in Fig. 4). This negative current, and the corresponding negative voltage delivered by the brick, are necessary to keep a positive power flow during the ramp-down phase for the grid brick (the grid brick cannot absorb energy).

Tab. 1 summarizes the key objectives of the different strategies and the corresponding equations used to calculate the grid current references in the green box in Fig. 3. The storage brick current references are then calculated to ensure that the total magnet current reference is respected, and some checks are done to ensure the maximum allowable current for the bricks are respected. It should be noted that the total current control is performed by the FGC exclusively. The controller is utilising measured values for the magnet current and voltage, to overcome limitations in the control structure. The output of the Energy Management Controller (C_{PI}), the purple box in Fig. 3, is updated only after every cycle to avoid stability issues in the controller.

The initial value of C_{PI} has to be calculated in each case to account for the magnet current profile, resistance and inductance. The PI-controller is then able to compensate for unbalances in the capacitance on the DC-bus, losses due to parasitic in the cables and losses in the switches. In the case where the load is purely resistive, the value of C_{PI} is equal to 1 for Strategy 1 and 2 and equal to the magnet current RMS in Strategy 3 and the magnet instantaneous losses in Strategy 4.

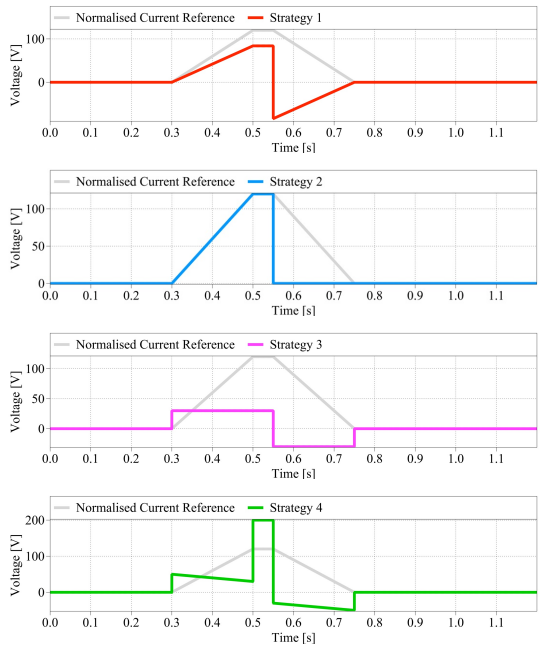

FIGURE 4 Possible grid brick reference shapes for the implementation of the different energy management strategies described in Section IV.

Figure 4 illustrates the modified current reference shapes generated for the grid brick by the proposed controller. The storage bricks receive as reference the difference between the original current reference and the grid brick reference. The four control strategies and corresponding current shapes in this figure are discussed in detail in the following paragraphs.

5.1 | Strategy 1: Current sharing among bricks

The objective of this control strategy is to ensure that the storage brick provides the recoverable (magnetic) energy throughout the cycle. This operation is illustrated with a blue line in Fig. 5. The strategy often yields optimal current sharing among the bricks when the (recoverable) magnetic energy is comparable with the thermal losses of the inductive load during a cycle.

In general, this strategy results in a relatively high peak current for the storage brick, which reaches 150 A for a short duration during the ramp down. This is caused by the reversal of the grid brick happening at the same time. The sudden current reversal of

Strategy	Current stress sharing	Grid load	Storage utilisation	Stability	Equation used to calculate grid brick reference
1	✓				$I_{grid,ref} = I_{mag} C_{PI} \frac{P_{dir}}{N_{grid}}$
2	✓			✓	$I_{grid,ref} = I_{mag} C_{PI} \frac{P_{dir}}{N_{grid}}, If(P_{dir} == -1) -> I_{grid,ref} = 0$
3		✓	✓	✓	$I_{grid,ref} = C_{PI} \frac{P_{dir}}{N_{grid}}$
4		✓	✓		$I_{grid,ref} = C_{PI} \frac{1}{V_{mag} N_{grid}}$

TABLE 1 Summary of key objectives and equation for the grid current strategies used in the green box in Fig. 3, where I_{mag} is the measured current, C_{PI} is the output of the energy management controller PI, P_{dir} is the direction of power flow (either 1 or -1), N_{grid} is the number of grid bricks and V_{mag} is the measured voltage on the load

the grid brick current just after the flat-top duration, is caused by the arm inductor for the grid brick. This disadvantage in reversing the current direction of the grid current forces the storage bricks to absorb extra current at a time when the current stress is already at its highest, shown as the small peak on the blue line in Fig. 5. The size and magnitude of this spike can be significantly depending on the specific load and current sharing between the two types of bricks. However, it does allow the grid brick to supply power during the entire current pulse, reducing the peak power for the grid brick and thus the good utilisation of the front-end rectifier and grid peak power.

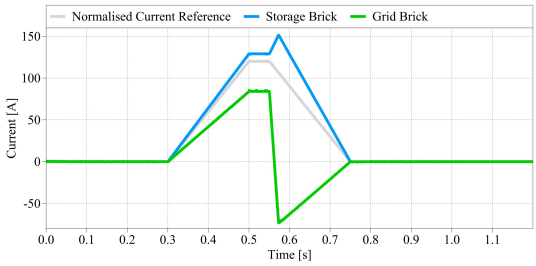

FIGURE 5 Simulation results showing the normalised output current (grey line), the grid brick current (green line) and the resulting storage brick current (blue line) by applying Strategy 1. This strategy results in a balanced RMS loading among converter bricks.

5.2 | Strategy 2: Sharing current stress among bricks - without current reversal

This strategy employs the same shape as for the trapezoidal current supplied from the grid brick in the previous section, but excluding the ramp-down phase, allows for current sharing stress between the bricks for the ramp-up phase and flat-top of the pulse shown in Fig. 6, referred to as *trapezoidal current short* in the plots.

However, the grid brick does not supply any power during ramp-down, which saves the grid bricks from having to reverse their current direction. This adds voltage stability as it avoids large current gradients and in theory the grid bricks can be considered 1Q, which ensures that they never recovery any energy. The other strategies requires some check of the dc-bus voltage for the grid bricks to avoid over voltage. This forces the storage bricks to absorb this negative current, to keep the load current inline with the reference. The storage bricks are actually supplying very little energy during flat-top, since they have to supply the losses during ramp-down phase. This strategy exhibits the minimal drop in voltage on the storage capacitors on the storage bricks, meaning that it uses the least of the stored energy in the capacitors and therefore has the smallest energy storage requirement. Since the grid brick has a shorter time to supply the losses occurring in a cycle, it has to supply a higher peak power than the previous current shape strategy.

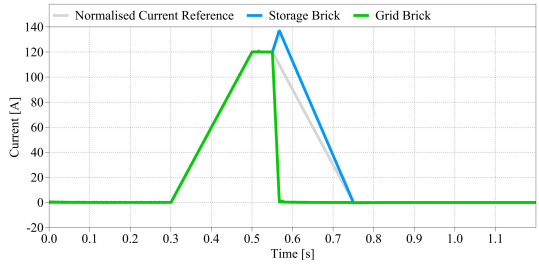

FIGURE 6 Simulation results showing the normalised output current (grey line), the grid brick (green line) using the short trapezoidal current reference and the storage brick current (blue line) by applying Strategy 2.

5.3 | Strategy 3: Minimal grid peak current

The objective of this strategy is to draw a constant current from the grid brick. Therefore, the anticipated peak current stress of the grid

bricks is reduced significantly in comparison to Strategy 1 and Strategy 2. By using Strategy 3, however, the storage bricks are forced to to do most of the work during the pulse, while they also absorb energy during the first instants of the pulse and before the current reference reaches the grid reference value. Fig. 7 shows typical simulation results for the currents when Strategy 3 is applied. From this figure it is observed that the current of the grid brick is larger than the magnet load current at the beginning of the pulse. Hence, it becomes apparent that under this operating mode, the storage bricks must reverse their current direction, and also increasing the voltage on the storage above the nominal value. For a magnet exhibiting higher losses, the grid current will be relatively higher, and the increase of the bus voltage at the beginning of the pulse will be more significant.

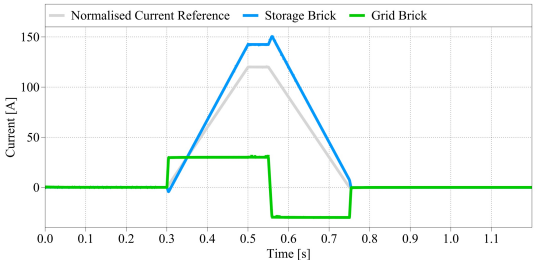

FIGURE 7 Simulation results showing the output current, the grid brick using the constant current reference (Strategy 3).

Strategy 3 utilises most of the installed storage in the scalable converter. This is basically due to the fact that the peak values of the grid-bricks current are lower than in the other strategies. Hence, the storage bricks supply a larger amount of current during the flat-top period of the pulse. Under the situation that the duration of the flat-top increases, a significant limitation emerges. Supplying a magnet with current from a capacitor bank requires very large energy storage capability, which eventually increases the installation cost of the converter.

5.4 | Strategy 4: Minimal peak grid power

The objective of the last strategy (Strategy 4), is to provide a constant power from the grid. In this strategy, the current reference is estimated based on an approximation of constant power dictated by the voltage on the magnet. With this strategy, the storage bricks supply the majority of the power during flat-top, which eventually forces the storage bus to reach the lowest voltage. Moreover, Strategy 4 enables minimisation of the front-end power requirements at the cost of larger storage requirements and higher power losses in the storage bricks. Similarly to Strategy 3, by applying Strategy 4, the storage bricks have to absorb energy and reverse their current direction during the first instants of the pulse, which is still challenging. The constant current changes require the arm level current regulator to adjust the dI/dt against the total dI/dt, which impose the risk for instabilities in the controller. As a result, the current regulator is limited in its available voltage and every step change in the reference will require time to correct.

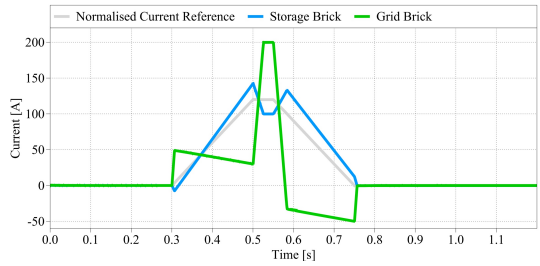

FIGURE 8 Simulation results showing the output current, the grid brick using the approximated constant power current reference (Strategy 4).

Figure 8 shows simulation results when applying Strategy 4. In this figure, the green line presents the output current from the grid brick. It is observed that the grid brick current changes significantly several times during the duration of the pulse. During the flat-top interval, the grid current has a very high value, while during the ramp-down phase this current reverses into a negative value. As a result, a power dip in the supplied power from the grid brick occurs, for which the storage bricks have to compensate. Strategy 4 would be very beneficial for the converter's performance in the case where the magnet's power losses are larger than the stored energy in the capacitors or where the pulses are much longer. However, this also worsens the issue with a negative current for the storage bricks at the start of the cycle. A possible solution to this is to develop a hybrid approach, where the current shape is continuously limited to be below the magnet's current in order to eliminate reverse currents in the storage bricks. Nevertheless, such an approach would approximate the minimal grid RMS current approach (Strategy 3), depending on the load requirements.

6 | LABORATORY EXPERIMENTAL RESULTS

For the experimental validation, an existing 800 kW power converter in the CERN laboratory was used. A photograph of the test setup is included in Figs. 9 and 10, with the schematics of the topologies shown in Fig. 11. The grid bricks are brick A and B, and the storage bricks are brick C and D. The storage bricks have a large

capacitor bank used for the energy storage, while the grid bricks are supplied from the electrical grid via a transformer, a diode rectifier and a DC/DC boost converter stage. This enables the grid brick to supply the losses of the grid bricks, storage bricks and the losses in the load. The storage bricks are designed to supply power as long as the voltage is between 600 V and 900 V, and the corresponding usable energy can be calculated from Eq. 2 and is 13.5 kJ per storage brick.

TABLE 2 Converter IGBT parameters

CM1200DC-34N	Voltage	Current
Rated value	1700 V	1200 A
Max designed	450 V	450 A

The converter is controlled by a Texas Instrument DSP. It is integrated with a CERN developed current measurement system and uses LEM sensors for voltage measurements (LV 25-P/SP5 both on the output and the DC-bus). The CERN developed current measurement system (DCCT) has the ability to measure current with a significant accuracy in the parts-per-million (ppm) range. With the parameter of the IGBT used listed in Table 2, it is clear that these devices are significantly de-rated in their designed operation. This is to achieve lifetime requirements due to the thermal impact of cycling loads. Also the parallel connection of IGBT devices might impose current imbalances if the collector-emitter saturation voltages, Vce, of the IGBTs differ significantly. Extensive differences in Vce might cause load current imbalances, causing uneven thermal effects [23], which was taken into account when this converter was designed.

The existing converter, used in the CERN East Experimental Area [20] been modified as illustrated in Fig. 11 by disconnecting the grid connection (via a transformer, a diode rectifier and a DC/DC boost converter) of two out of four bricks. The converter parameters used by the converter in the test setup are summarised in Table 3. With the connection to the grid disconnected, the storage bricks are simply a full-bridge DC/DC converter switching at 6.5 kHz with a large capacitive dc-link connected on the front. A minimum of capacitors on the grid bricks are kept to form the necessary dc-link. Since the storage bricks do not have their own source of energy, the grid bricks shall supply the losses for the complete system, as well as for the load. By separating the grid connection and storage, it is possible to scale the converter for storage and grid connection independently, and by using the same brick to connect to the load, the system complexity is kept to a minimum.

The load used in this paper is four parallel-connected accelerator electromagnets with solid iron core that are commonly used in accelerator facilities. Its key parameters are listed in Table 4.

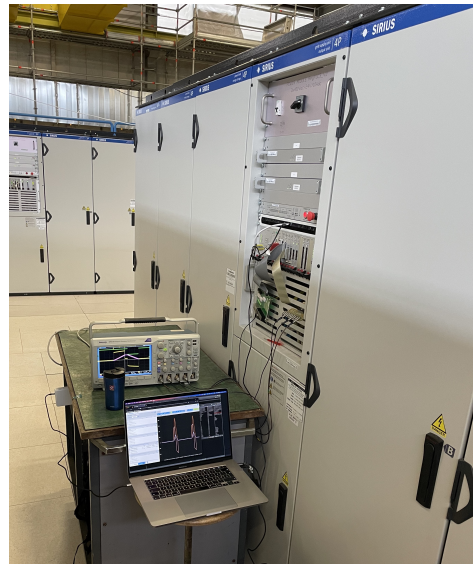

FIGURE 9 Photograph of the laboratory setup.

FIGURE 10 Photograph of the laboratory setup, showing the power stack, gate drivers and DC-bus filter capacitors integrated into the cabinet. The storage capacitors can be seen at the bottom.

6.1 | Strategy 1

Using the strategy described in subsection 5.1, the current sharing between the storage and grid bricks are shown in Fig. 12a. The storage bricks supply approximately 200 A (bricks C and D), during the current ramp and flattop, and recover a peak of 440 A during the ramp-down phase. It is interesting to note that when the current

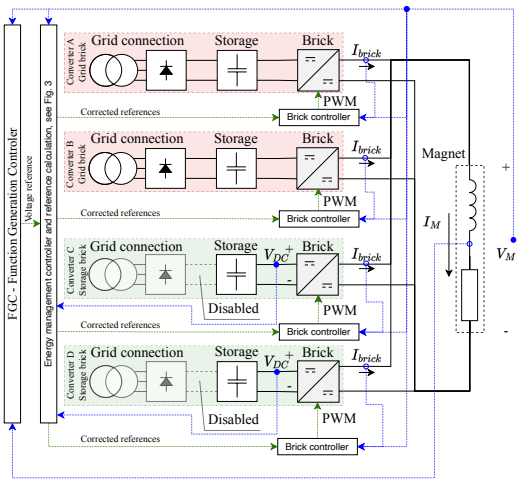

FIGURE 11 Schematic diagram of the converter topology used in the lab setup and configured with two grid and two storage bricks, only one set of measurement signals shown. The shaded area illustrates the hardware that is removed as a result of the proposed control scheme.

TABLE 3 Converter parameters

	Grid Connected Brick	Energy Storage Brick
Max Voltage	200 V	200 V
Max Current	450 A	450 A
Energy Available	N/A	56.4 kJ @900 V

TABLE 4 Parameters of the load used for the experimental setup

Load parameter	Value
Inductance	430 mH
Resistance	83 mΩ
Max current	916 A
Pulse current flat-top	700 A
Peak stored energy at @700 A	105.35 kJ
RMS power	8 kW
Peak power	175 kW

supplied by the grid-brick reverses the storage brick is forced to compensate with an additional equivalent current, which increases its peak current contribution. This however results in more energy recovery due to the negative output voltage during this time.

The DC-link voltage plots in Fig. 12b demonstrate the energy recovery performed by the storage bricks throughout the cycle which guarantees that enough energy will be available for the next load cycle.

A summary of the performance indicators are listed in Table 5. The storage bricks use the energy recovered during the ramp-down phase to cover the losses of the storage bricks, as well as contributing to the current delivered during ramp-up and flat-top intervals.

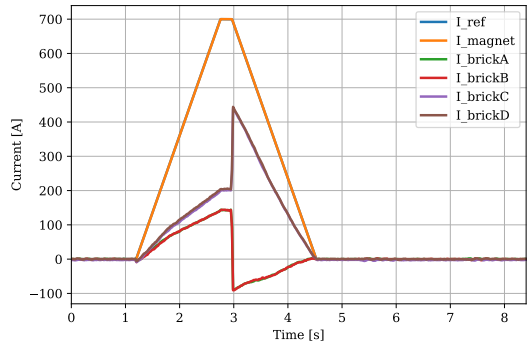

(a) Experimental measurements of the magnet and bricks currents

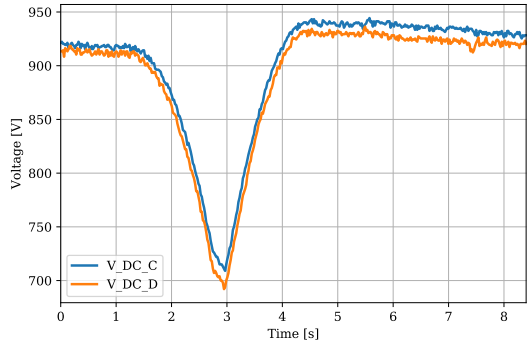

(b) Experimental measurements of the DC-dus voltages for the storage bricks V_{DC_C} and V_{DC_D}

FIGURE 12 Experimental results for Strategy 1: Sharing current stress

6.2 | Strategy 2

This strategy is similar to the previous one with the difference that the grid brick current is not allowed to reverse. As described in subsection 5.2, the grid bricks (A and B) are effectively delivering zero current during the ramp-down phase, as shown in Fig. 13a. The storage bricks (C and D) recover the totality of the energy into the storage element. This is fairly typical for this approach, and the more energy the storage bricks can recover, the higher current they can supply during the ramp-up and flat-top of the next cycle. Again Fig. 13b shows that the energy in the storage bricks maintained

at the end of the cycle; thus, the energy controller has found the optimal distribution of currents using this strategy.

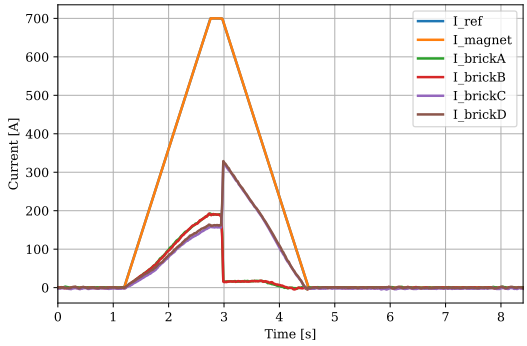

(a) Experimental measurements of the magnet and bricks currents

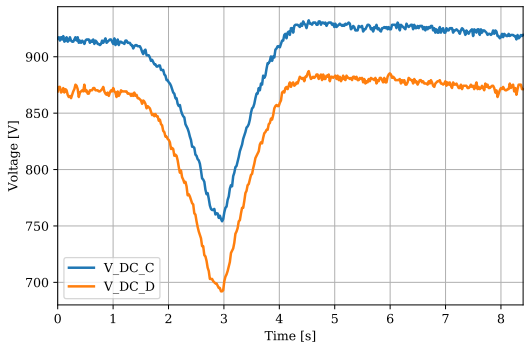

(b) Experimental measurements of the DC-dus voltages for the storage bricks V_{DC_C} and V_{DC_D}

FIGURE 13 Experimental results for Strategy 2: Sharing current stress - Short

used during the first 300 ms to absorb energy, enhancing the usage of the storage. The energy used and other key metrics are listed in Tab. 5.

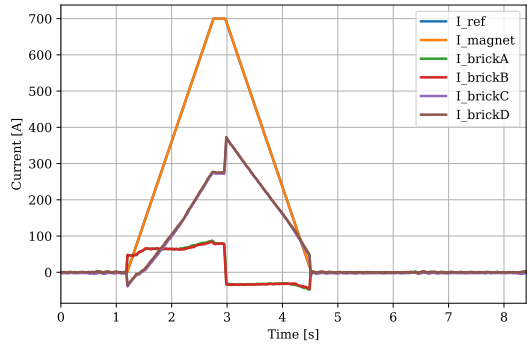

(a) Experimental measurements of the magnet and bricks currents

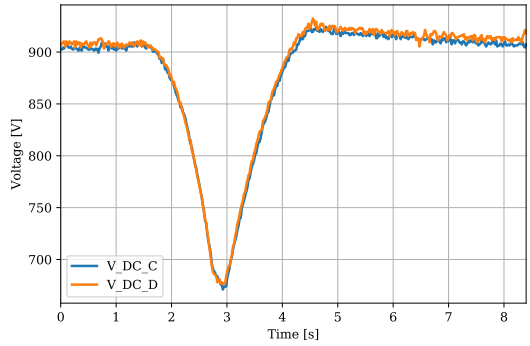

(b) Experimental measurements of the DC-dus voltages for the storage bricks V_{DC_C} and V_{DC_D}

FIGURE 14 Experimental results for Strategy 3: Minimal grid current RMS

6.3 | Strategy 3

With this strategy, as described in subsection 5.3, the grid bricks maintain a constant current during the ramp-up and flat-top, before reversing to the same negative current value during the ramp-down phase. As shown in Fig. 14a for bricks A and B, the grid bricks reach 80 A and maintain this value until the end of the flat-top. Then the current flips to -80 A to keep the power flow from the grid brick positive. The storage bricks (C and D) are left to ensure that the total current reference is respected, and the energy controller has to calculate what the current value for the grid bricks should be, shown as the green and red lines in the plot (Fig. 14a). Similarly to the cases above, it is observed that this strategy also results in the energy being conserved in Fig. 14b; notice also that the storage is

6.4 | Strategy 4

The final strategy is also the most demanding from a regulation perspective, as described in subsection 5.4. Using Strategy 4, the current estimate is now also dependent on the load voltage, and so the references change significantly throughout the pulse. However, as shown in Fig. 15a the regulator is able to follow this varying current quite well, and the storage bricks ensure that the total current reference is always respected. The energy regulator has found a stable grid brick power, sufficient to maintain the energy stored in the storage bricks, as illustrated in Fig. 15b.

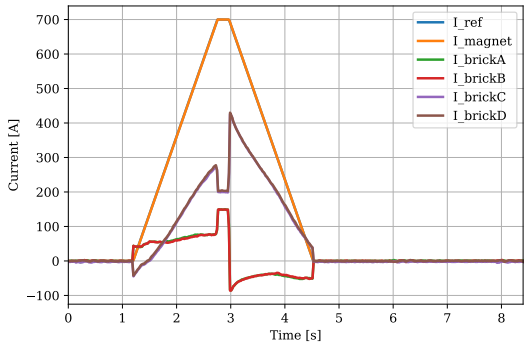

(a) Experimental measurements of the magnet and bricks currents

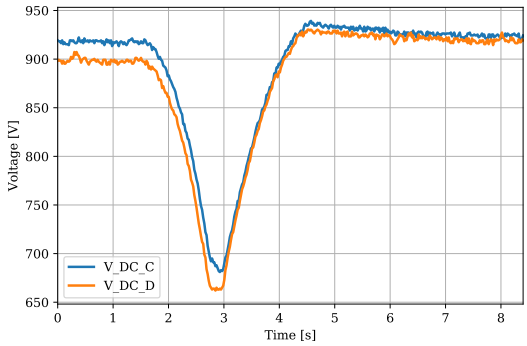

(b) Experimental measurements of the DC-dus voltages for the storage bricks V_{DC_C} and V_{DC_D}

FIGURE 15 Experimental results for Strategy 4: Minimal peak grid power

7 | DISCUSSION

A comparison of the four strategies in selected and key metrics are presented in Table 5. The values presented are the averages of the two bricks of the same type. These metrics highlight the different utilisation of the converter hardware by the four strategies. The total output current and output voltage are always the same regardless of the strategies, as this is defined by the load mission profile. The way energy is dispatched by the converter bricks differs according to the control strategy.

Comparing Strategies 1 and 2 in Table 5 the RMS current values are very similar between the grid brick for Strategy 1 and 2 and storage bricks for strategies 1 and 2. For Strategy 1 approximately 46.8 kJ of the energy cycled per brick, this is equivalent to 89% of the energy stored in the magnet. The storage bricks are also reaching their current limit, during the ramp-down.

While for Strategy 2 the recycled energy is slightly decreased, which indicates that such a strategy allows to reduce the amount of installed energy storage which costs approximately 250 EUR/kJ in this type of converter. The energy recovered is about 72 % of the total stored in the magnet as shown in Tab. 4, after accounting for losses this is close to the maximum which can be extracted. The other strategies uses the grid brick to inject more energy during the ramp-down, enhancing the usage of the storage. Similarly the peak current of the storage bricks is reduced leading to less thermal stress in the semiconductors, maximising the cycling lifetime of the IGBTs. Since the brick and storage bricks use the same full-bridge topology, the second strategy also leads in better utilisation of the grid-brick hardware.

Strategies 3 and 4 are primarily targeted to limiting the cycling impact on the power grid by performing some sort of peak shaving. This reduces the installed power requirement for the grid, and can also be used to limit the peak-power during high demand periods. Strategy 3 in Table 5 introduces a lower RMS current for the grid bricks, compared to strategies 1 and 2. However, there is a corresponding increase for the storage bricks usage; the storage bricks recover some energy during the ramp-up phase, as well as the ramp-down phase, and therefore have more energy available to deliver to the load. In total the storage bricks uses an amount of storage equivalent to 94% of the energy in the magnet. Achieving a reduced grid supply loading and using more energy storage, may be a useful objective in certain applications and these are candidate applications for strategies 1 and 2. However, it should be noted that these strategies load the two types of bricks unequally, which could result in a different lifetime of the two types of bricks (assuming identical ratings).

Finally Strategy 4 aims to reduce the peak grid power, which eventually results in a very different utilisation of the bricks. The storage bricks are carrying most of the current, and also their reference varies considerably throughout the load cycle. In total the storage bricks uses an amount of storage equivalent to 96 % of the energy in the magnet. This strategy is best served if the grid supplying the converter is limited in the available power, or increasing installed power is very costly, so that minimising the installed power requirements is beneficial. It also shows how creative it is possible to be with the currents from the different bricks, without affecting the performance with respect to the output current precision.

Ultimately, the choice of the optimal strategy is impacted by several parameters, including the flat-top duration, the L/R-ratio of the magnet load, cost of cooling and the availability/cost of front-end peak power capability. The advantage of such a modular design is that the utilised strategy can be adapted to the individual load by using the same converter topology. The energy storage or grid-connection costs can be optimised on circuit per circuit basis in a large industrial complex, by modifying the way energy is dispatched to the load.

The energy flow in the system, meaning the energy exchange among the load, the storage bricks and the grid connected bricks, is controlled by an energy controller by choosing the appropriate current reference shape for the grid brick and finding the optimal current distribution between the bricks. By having a shape which

TABLE 5 Comparison of Grid brick power sharing strategies

Strategy	Key metric	Grid Brick	Storage Brick
Strategy 1	$I_{RMS-out}$	45.1 A	115.0 A
	I_{peak}	144.2 A	444.3 A
	ΔV_{bus}	-	240 V
	ΔE_{str}	-	46.8 kJ
Strategy 2	$I_{RMS-out}$	53.3 A	88.9 A
	I_{peak}	193.0 A	329.1 A
	ΔV_{bus}	-	187 V
	ΔE_{str}	-	37.7 kJ
Strategy 3	$I_{RMS-out}$	32.1 A	115.5 A
	I_{peak}	87.4 A	373.2 A
	ΔV_{bus}	-	255 V
	ΔE_{str}	-	49.3 kJ
Strategy 4	$I_{RMS-out}$	39.0 A	120.5 A
	I_{peak}	149.0 A	430.0 A
	ΔV_{bus}	-	263 V
	ΔE_{str}	-	50.6 kJ

follows the current to the load, i.e., trapezoidal, the current stresses in the brick switches and losses are shared most equally among the bricks. Two additional strategies, aiming at reducing the front-end peak power have also been shown. These strategies are mostly suited for relatively short pulses in inductive loads, with a large amount of recoverable energy compared to the losses. It has been shown that it is possible to have any number of bricks connected in series and parallel, and within their current and voltage ratings, the power-flow can be individually controlled.

Since both bricks operate during most of the cycle time, the thermal cycling of semiconductors would probably be very similar. At the same time the re-circulation of energy among bricks to balance the energy, can result in higher RMS current on the bricks, thus potentially increasing the losses.

8 | CONCLUSION

An energy flow control scheme for a modular DC/DC converter has been proposed and experimentally validated in a full-scale 800 kW prototype. It has been shown that the controller can efficiently respond under various operating scenarios, such as cycling loads and deliver the same performance as a conventional converter. The 4 bricks can also deliver very different currents, resulting in different power flow between them, allowing optimisation for different targets, such as minimising the front-end current, cycling depth of the storage or thermal cycling.

Starting from this basis, it is possible to optimise the converter's lifetime, overall reliability and the peak power required from the grid. This is achieved by optimising the utilisation of the submodules to balance the current stressing and therefore the thermal stress among the storage bricks.

The experiments have shown that the RMS current of grid-connected bricks can vary from 32.1 A for the minimal grid current RMS, and up to 53.5 A for the other strategies. On the other hand, the storage utilisation can vary from 37.7 kJ to 50.6 kJ depending on the strategy. The parameter that can be mostly controlled is the peak current, where the storage brick has a peak current between 373.2 A and 444.3 A depending on the strategy. The choice of a scalable control strategy will have an impact on the switching device selection as well as in the cooling requirements, however, it allows reusing a modular power converter in a scalable manner in a large industrial complex with varied load parameters.

REFERENCES

1. Kumar KN, Miskiewicz R, Trochimiuk P, Rabkowski J, Peftitsis D. Performance Evaluation of SiC-based Isolated Bidirectional DC/DC Converters for Electric Vehicle Charging. 2022 24th European Conference on Power Electronics and Applications (EPE'22 ECCE Europe). 2022;p. 11.
2. Vermulst BJD, Duarte JL, Lomonova EA, Wijnands KGE. Scalable multi-port active-bridge converters: Modelling and optimised control. IET Power Electronics. 2017;10(1):80–91.
3. Galeshi S, Frey D, Lembeye Y. Efficient and scalable power control in multi-port active-bridge converters. 2020 22nd European Conference on Power Electronics and Applications, EPE 2020 ECCE Europe. 2020;p. 2–10. ISBN: 9789075815368.
4. Peng P, Li Y, Li Z, Shao Y, Luo X, Wang Y, et al. Analysis of Advantage of the Connection of Energy Storage System to Distribution Network and the Impact on the Voltage Quality. 2nd IEEE Conference on Energy Internet and Energy System Integration, EI2 2018 - Proceedings. 2018;(1):2018–2021. Publisher: IEEE ISBN: 9781538685495.
5. Parchomiuk M, Strzelecki R, Zymmer K, Domino A. Modular power converter topologies for energy storage and electric power distribution systems. 2017 Progress in Applied Electrical Engineering, PAEE 2017. 2017;ISBN: 9781538615287.
6. Ould Amrouche S, Rekioua D, Rekioua T, Bacha S. Overview of energy storage in renewable energy systems. International Journal of Hydrogen Energy. 2016;41(45):20914–20927. Publisher: IEEE ISBN: 9781467378949.
7. Brown DR, Chvala WD. Flywheel energy storage: An alternative to batteries for ups systems. Energy Engineering: Journal of the Association of Energy Engineering. 2005;102(5):7–26.
8. Magdalena Stephan R, de Andrade Jr R, Gonçalves Sotelo G. Third Generation Of Flywheels: A Promising Substitute To Batteries. Eletrônica de Potência. 2008;13(3):171–176.
9. Wang G, Konstantinou G, Townsend CD, Pou J, Vazquez S, Demetriades GD, et al. A review of power electronics for grid connection of utility-scale battery energy storage systems. IEEE Transactions on Sustainable Energy. 2016 Oct;7(4):1778–1790. Available from: http://ieeexplore.ieee.org/document/7506096/.
10. Ise T, Kita M, Taguchi A. A hybrid energy storage with a SMES and secondary battery. IEEE Transactions on Applied Superconductivity. 2005;15(2 PART II):1915–1918.
11. Ängquist L, Antonopoulos A, Siemaszko D, Ilves K, Vasiladiotis M, Nee HP. Open-loop control of modular multilevel converters using estimation of stored energy. IEEE Transactions on Industry Applications. 2011;47(6):2516–2524.
12. Ilves K, Harnefors L, Norrga S, Nee HP. Analysis and operation of modular multilevel converters with phase-shifted carrier PWM. IEEE Transactions on Power Electronics. 2015;30(1):268–283.

13. Perez MA, Bernet S, Rodriguez J, Kouro S, Lizana R. Circuit topologies, modeling, control schemes, and applications of modular multilevel converters. IEEE Transactions on Power Electronics. 2015 Jan;30(1):4–17. Available from: http://ieeexplore.ieee.org/lpdocs/epic03/wrapper.htm?arnumber=6757004.
14. Rodal GL, Acharya AB, Norum LE. Analysis and Evaluation of Repetitive Controllers for Circulating Current Suppression in Modular Multilevel Converters. 2018 20th European Conference on Power Electronics and Applications, EPE 2018 ECCE Europe. 2018;p. 1–10. ISBN: 9789075815283.
15. Carrasco JM, Franquelo LG, Bialasiewicz JT, Galvan E, Portillo Guisado RC, Prats MAM, et al. Power-electronic systems for the grid integration of renewable energy sources: A survey. IEEE Transactions on Industrial Electronics. 2006;53(4):1002–1016.
16. Errigo F, Chedot L, Morel F, Venet P, Sari A. Modelling and Control of an MMC-HVDC Submodule with Energy Storage for Fast Frequency Response. 2021 23rd European Conference on Power Electronics and Applications, EPE 2021 ECCE Europe. 2021;ISBN: 9789075815375.
17. Vasiladiotis M, Rufer A. Analysis and control of modular multilevel converters with integrated battery energy storage. IEEE Transactions on Power Electronics. 2015;30(1):163–175. Publisher: IEEE.
18. Batarseh I, Alluhaybi K. Emerging Opportunities in Distributed Power Electronics and Battery Integration: Setting the Stage for an Energy Storage Revolution. IEEE Power Electronics Magazine. 2020;7(2):22–32.
19. Milovanovic S, Strobl S, Ladoux P, Dujic D. Hardware-in-the-Loop Modeling of an Actively Fed MVDC Railway Systems of the Future. IEEE Access. 2021;9:151493–151506.
20. Lamaille BLM, Dragoni F, Evrard S, Harden FJ, Harrouch E, Lazzaroni M, et al. Study of the Energy Savings Resulting From the East Area Renovation. 10th Int Partile Accelerator Conferance. 2019;p. 4023–4025. ISBN: 9783954502080.
21. Maestri S, Retegui RG, Carrica D, Rossini S, Le Godec G, Papastergiou K. Figures of merit for the evaluation of regenerative power converters. 2016 18th European Conference on Power Electronics and Applications, EPE 2016 ECCE Europe. 2016;p. 1–9. Publisher: Jointly owned by IEEE-PELS and EPE Association ISBN: 9789075815245.
22. Parchomiuk M, Strzelecki R, Zymmer K, Sak T. Modular high precision high current source for special applications-Simulation and verification. Proceedings - 2016 10th International Conference on Compatibility, Power Electronics and Power Engineering, CPE-POWERENG 2016. 2016;p. 422–427. Publisher: IEEE ISBN: 9781467372930.
23. Asimakopoulos P, Papastergiou K, Thiringer T, Bongiorno M, Le Godec G. On Vce Method: In Situ Temperature Estimation and Aging Detection of High-Current IGBT Modules Used in Magnet Power Supplies for Particle Accelerators. IEEE Transactions on Industrial Electronics. 2019;66(1):551–560.
24. Boukettaya G, Krichen L. A dynamic power management strategy of a grid connected hybrid generation system using wind, photovoltaic and Flywheel Energy Storage System in residential applications. Energy. 2014 Jul;71:148–159. Publisher: Pergamon. Available from: https://www.sciencedirect.com/science/article/pii/S0360544214004526.
25. Dekka A, Wu B, Fuentes RL, Perez M, Zargari NR. Evolution of Topologies, Modeling, Control Schemes, and Applications of Modular Multilevel Converters. IEEE Journal of Emerging and Selected Topics in Power Electronics. 2017;5(4):1631–1656.
26. Lesnicar A, Marquardt R. An innovative modular multilevel converter topology suitable for a wide power range. 2003 IEEE Bologna PowerTech - Conference Proceedings. 2003;3:272–277. ISBN: 0780379675.
27. Haugen KL, Papastergiou K, Asimakopoulos P, Peftitsis D. Energy flow control in a modular DC-DC converter with energy recovery. In: 2021 IEEE 12th International Symposium on Power Electronics for Distributed Generation Systems (PEDG). Chicago, IL, USA: IEEE; 2021. p. 1–8. Available from: https://ieeexplore.ieee.org/document/9494229/.
28. Wang C, Li X, Peng H, He L, Xue Y. Segmented Energy Routing for a Modular AC/DC Hybrid System. IEEE Journal of Emerging and Selected Topics in Power Electronics. 2021;6777(c):1–1. Publisher: IEEE.
29. Ma F, Wang X, Deng L, Zhu Z, Xu Q, Xie N. Multiport Railway Power Conditioner and Its Management Control Strategy with Renewable Energy Access. IEEE Journal of Emerging and Selected Topics in Power Electronics. 2020;8(2):1405–1418. Publisher: IEEE.
30. Zhang Z, Jin C, Tang Y, Dong C, Lin P, Mi Y, et al. A Modulized Three-Port Interlinking Converter for Hybrid AC/DC/DS Microgrids Featured with a Decentralized Power Management Strategy. IEEE Transactions on Industrial Electronics. 2021;68(12):12430–12440. Publisher: IEEE.
31. De Castro R, Pereira H, Araujo RE, Barreras JV, Pangborn HC. *qTSL* : A Multilayer Control Framework for Managing Capacity, Temperature, Stress, and Losses in Hybrid Balancing Systems. IEEE Transactions on Control Systems Technology. 2022 May;30(3):1228–1243. Available from: https://ieeexplore.ieee.org/document/9520124/.
32. Haugen KL, Papastergiou K, Asimakopoulos P, Peftitsis D. On dimensioning the fundamental brick for a scalable DC-DC converter with energy recovery. In: 2021 23rd European Conference on Power Electronics and Applications (EPE'21 ECCE Europe). Ghent, Belgium: IEEE; 2021. p. P.1–P.10. Available from: https://ieeexplore.ieee.org/document/9570676/.
33. Haugen KL, Papastergiou K, Peftitsis D. A scalable DC/DC converter topology with modularised energy storage for high energy physics applications. IEEE Journal of Emerging and Selected Topics in Power Electronics. 2023;p. 1–1. Available from: https://ieeexplore.ieee.org/document/10105646/.
34. Haugen KL, Papastergiou K, Asimakopoulos P, Peftitsis D. High precision scalable power converter for accelerator magnets. Journal of Instrumentation. 2022 Mar;17(03):C03021. Available from: https://iopscience.iop.org/article/10.1088/1748-0221/17/03/C03021.
35. Kish GJ. On the emerging class of non-isolated modular multilevel DC-DC converters for DC and hybrid AC-DC systems. IEEE Transactions on Smart Grid. 2019;10(2):1762–1771. Publisher: IEEE.
36. Goetz SM, Peterchev AV, Weyh T. Modular multilevel converter with series and parallel module connectivity: Topology and control. IEEE Transactions on Power Electronics. 2015 Jan;30(1):203–215. Publisher: IEEE.
37. Masaud TM, Lee K, Sen PK. An overview of enrgy storage technologies in electric power systems: What is the future? North American Power Symposium 2010, NAPS 2010. 2010;Publisher: IEEE ISBN: 9781424480463.

Appendix A

Trapezoidal current calculations

A.1 Load profile plots for constant current ramping

In the following section an example of how the different voltages and powers can be calculated and plotted using a specific example. The plots assume a constant current ramping rate. This is the design approach used in this thesis and is often used at early design stages as most of the equations are simpler.

A.1.1 Current

The power converters will be applied to a variety of accelerator magnets and current requirements. In general, the current levels can go up to $2500A$ and the voltage levels up to $1500V$, however for the purposes of this thesis a specific load profile will be considered as a typical load profile. It consists of a trapezoidal current pulse with a period of $1.2s$. After $340ms$ the current starts to rise, with a $\frac{di}{dt}$ of 1730. After $600ms$ the current reaches the flat-top value of $450A$, which is kept for $50ms$. Then, the current is brought back to zero over $222ms$, giving a $\frac{di}{dt}$ of $2030A/s$. The target current is plotted in Figure A.1. A summary of the values for the load profile is listed in table A.1, it is important to note that the minimum and maximum values are selected from the data set, and does not represent a specific magnet load.

Different magnets have different inductance and resistance values, for the purposes of the first part of this thesis a magnet with $R = 200m\Omega$ and $L = 130mH$. This results in a load voltage consisting of the transient contribution from the inductive part of the magnet and a stationary from the resistive part. The voltage over the resistive is trivial from Ohm's law in equation A.1, and the voltage over the inductor is given by the equation in A.2.

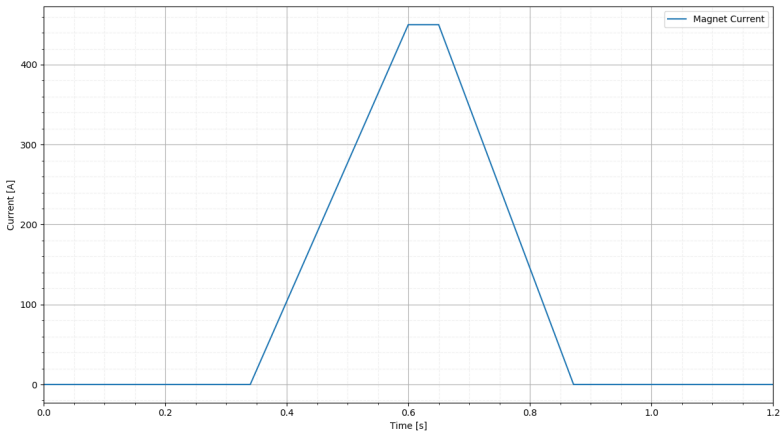

Figure A.1: Reference current for the selected load profile.

$$V = RI \tag{A.1}$$

$$V = L\frac{di}{dt} \tag{A.2}$$

The resulting voltages are plotted in A.2, with the resistive component shown in A.2(a) and the inductive in A.2(b). It is worth noting that the voltage over the resistor, just as the current, will always be positive, while the voltage over the inductor will be negative during the fall time of the current. Whereas the negative voltage over the inductor is larger than the resistor, this will result in a negative power flow, i.e. returning to the source. Normally such reverse power delivery is facilitated by a negative current flow, while the voltage is kept positive. In the scenario where the voltage over the resistor is larger than the negative voltage over the inductor, the total magnet voltage will remain positive and no energy can be recovered. So there is a potential for recovering energy, depending on the load profile, but it requires a way to switch the polarity of the magnet with respect to the source, or a reduction of the voltage to negative values. In the current configuration, CERN is using the former using a full-bridge of IGBTs, used both for inverting polarity and also to control the voltage.

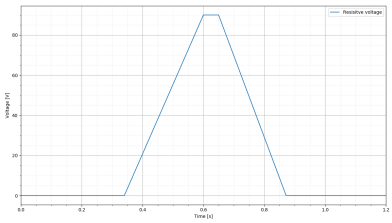

(a) Restive voltage

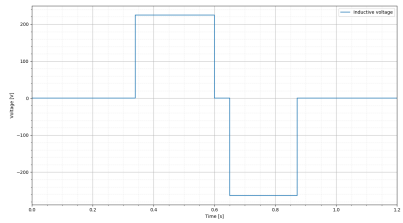

(b) Inductive voltage

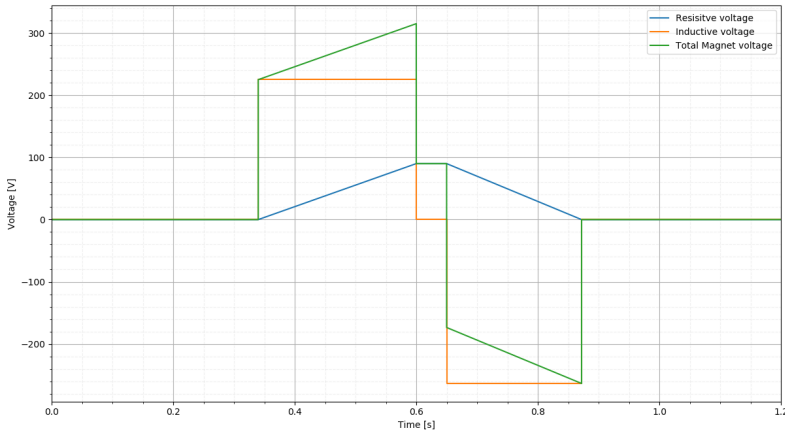

(c) Voltages combined

Figure A.2: Reference voltage for the selected load profile

Taking the two basic voltage equations from A.1 and A.2 it is possible to give a simple relationship for the balance between R, L, I and $\frac{di}{dt}$ which results in the possibility to recover energy as presented in equation A.3. Note that this is based on the balance of power between the two, but since they share the same current, the expression simplifies to setting the two voltages equal to each other during the fall-time of the current. A quick look at the dataset for the North Area magnets at CERN, this holds true for 95% of the magnets given a fall time of 222ms.

$$L\frac{di}{dt} > RI \tag{A.3}$$

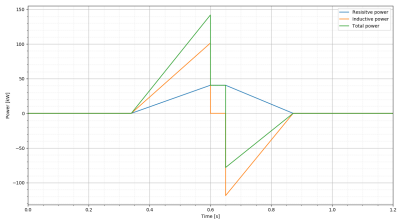

(a) Power required by the magnet

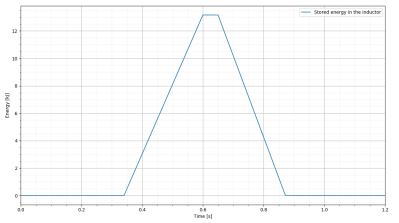

(b) Energy stored in the magnet

Figure A.3: Power and energy for the selected load profile.

A.1.2 Voltage

The approach described in this section assumes the necessity of perfectly following the current trace during rise and fall, giving high peak voltages only used for an infinitely short time. This reduces the utilisation of the voltage rating of the device and could result in higher costs. The most critical phase for the usage of the accelerator magnets is the current during the particle event, as the current directly controls the field strength of the magnet. The particle event is a term used to describe the instant when the particle arrives in a particular device, and in this scenario is when the magnet is used to steer the path of the particle. Using the calculations from the Lorentz force, Equation 1.1. As the particle moves at close to the speed of light, a small error in the direction can lead to the particle leaving the designed path and disappearing from the beam pipe.

Using only the stable current at the particle event and a duration afterwards as the target, it will make more sense to obtain a constant voltage during the rise and fall of the current in the magnet. This will enable better utilisation of the voltage rating of the device.

A.2 Equations for ramping at constant voltage

The second method to approach the ramping phase of the trapezoidal current pulse is to utilise a constant applied voltage. This section shows the calculations for the case where the voltage is constant and are made using the example load in Table A.1.

A.2.1 Positive flank

Starting from the first principles, the first approach is to find an expression for the constant voltage necessary to achieve the desired flat-top voltage within a certain rise time. With this equation it is also possible to do the reverse, calculate the

Parameter	Typical values
Max current	450 A
Current rise-time	260 ms
Current fall-time	222 ms
Restive load	200 mΩ
Inductive load	130 mH
Peak voltage	363 V
Peak power	163 kW
Recoverable energy	13.3 kJ

Table A.1: Typical parameters for a load CERN North Area and TT20

rise-time for a given ramping voltage. Combining equation A.1 and A.2 the total voltage over the magnet can be written as in equation A.4.

$$V = RI + L\frac{dI}{dt} \tag{A.4}$$

Assuming that the current will rise from 0A and increase linearly to $I_{flat-top}$ over the time interval t_{rise} the equation can be expressed as in equation A.5. This does not give a constant voltage, as the current through the magnet is increasing. By assuming a constant voltage, it is possible to find an expression for the increasing current and set it up as an ordinary differential equation as in equation A.6.

$$V = RI + L\frac{I_{flat-top}}{t_{rise}} \tag{A.5}$$

$$Li\dot{(}t) + Ri(t) - V = 0 \tag{A.6}$$

In fact, this equation is a first-order linear ordinary differential equation and has known solutions, on the form in equation A.7, where $a = R/L$, $b = -V/L$.

$$i\dot{(}t) + ai(t) + b = 0 \tag{A.7}$$

This equation has the solution in equation A.8.

$$\begin{aligned} i(t) &= C_1 \cdot e^{-a \cdot t} - \frac{b}{a} \\ &= C_1 \cdot e^{-\frac{R}{L} \cdot t} - \frac{-\frac{V}{L}}{\frac{R}{L}} \\ &= C_1 \cdot e^{-\frac{R}{L} \cdot t} + \frac{V}{R} \end{aligned} \tag{A.8}$$

At time $t_0 = 0$, the current is zero, which means $e^0 = 1$, which makes it possible to find C_1 from equation A.8.

$$\begin{aligned} i(t_0) &= C_1 \cdot e^{-\frac{R}{L} \cdot t_0} + \frac{V}{R} \\ 0 &= C_1 \cdot e^0 + \frac{V}{R} \\ => C_1 &= -\frac{V}{R} \end{aligned} \tag{A.9}$$

Inserting the value of C_1 from equation A.9 into equation A.8 gives A.10.

$$\begin{aligned} i(t) &= -\frac{V}{R} \cdot e^{-\frac{R}{L} \cdot t} + \frac{V}{R} \\ &= \frac{V}{R} \left(1 - e^{-\frac{R}{L} \cdot t}\right) \end{aligned} \tag{A.10}$$

Equation A.10 now gives the expression for the constant voltage. From the fact that at $t = t_{rise}$ the current should be at the constant magnet current I_M.

$$\begin{aligned} i(t_{rise}) &= \frac{V}{R} \left(1 - e^{-\frac{R}{L} \cdot t_{rise}}\right) \\ I_M &= \frac{V}{R} \left(1 - e^{-\frac{R}{L} \cdot t_{rise}}\right) \\ => V &= \frac{I_M \cdot R}{\left(1 - e^{-\frac{R}{L} \cdot t_{rise}}\right)} \end{aligned} \tag{A.11}$$

For the sample load as selected in table A.1. The value of V can be obtained.

$$
\begin{aligned}
V &= \frac{I_M \cdot R}{\left(1 - e^{-\frac{R}{L} \cdot t_{rise}}\right)} \\
V &= \frac{450 \cdot 0.2}{\left(1 - e^{-\frac{0.2}{0.13} \cdot 0.260}\right)} \\
V &= 273
\end{aligned}
\tag{A.12}
$$

Giving the final equation describing the current during the rising flank for the sample load.

$$
i(t) = \frac{273}{0.20}\left(1 - e^{-\frac{0.20}{0.13} \cdot t}\right) \tag{A.13}
$$

A.2.2 Negative flank

The same approach can be used to find the voltage during the fall of the current. Starting from the solution in equation A.8, the value of C_1 for the falling current can be found. Starting from the constant current during the flat-top I_M at t_0.

$$
\begin{aligned}
i(t_0) &= C_1 \cdot e^{-\frac{R}{L} \cdot t_0} + \frac{V}{R} \\
I_M &= C_1 \cdot e^0 + \frac{V}{R} \\
=> C_1 &= I_M - \frac{V}{R}
\end{aligned}
\tag{A.14}
$$

From the C_1 in equation A.14 the equation describing the falling current is given in A.15.

$$
i(t) = \left(I_M - \frac{V}{R}\right) \cdot e^{-\frac{R}{L} \cdot t} + \frac{V}{R} \tag{A.15}
$$

Using this result, the fall time t_{fall} and the final current of 0A can be used to find the voltage during the falling current.

$$
\begin{aligned}
i(t_{fall}) &= \left(I_M - \frac{V}{R}\right) \cdot e^{-\frac{R}{L} \cdot t_{fall}} + \frac{V}{R} \\
0 &= \left(I_M - \frac{V}{R}\right) \cdot e^{-\frac{R}{L} \cdot t_{fall}} + \frac{V}{R} \\
-I_M \cdot e^{-\frac{R}{L} \cdot t_{fall}} &= \left(1 - e^{-\frac{R}{L} \cdot t_{fall}}\right) \frac{V}{R} \\
=> V &= \frac{-I_M \cdot R \cdot e^{-\frac{R}{L} \cdot t_{fall}}}{\left(1 - e^{-\frac{R}{L} \cdot t_{fall}}\right)}
\end{aligned}
\tag{A.16}
$$

Inserting the parameters from the load case in table A.1. The value of V during the negative flank can be found.

$$
\begin{aligned}
V &= \frac{-I_M \cdot R \cdot e^{-\frac{R}{L} \cdot t_{fall}}}{\left(1 - e^{-\frac{R}{L} \cdot t_{fall}}\right)} \\
V &= \frac{-450 \cdot 0.20 \cdot e^{-\frac{0.20}{0.13} \cdot 0.222}}{\left(1 - e^{-\frac{0.20}{0.13} \cdot 0.222}\right)} \\
V &= -221
\end{aligned}
\tag{A.17}
$$

Giving the final equation describing the current during the rising flank for the sample load.

$$
i(t) = \left(450 + \frac{221}{0.20}\right) \cdot e^{-\frac{0.20}{0.13} \cdot t} - \frac{221}{0.20} \tag{A.18}
$$

A.2.3 Voltage during flat-top

Starting from the same equation A.19, finding the voltage during the flat-top is quite simple. As the current should be constant, the di/dt becomes zero and the current is I_M.

$$
\begin{aligned}
V &= R \cdot i(t) + L\frac{di(t)}{dt} \\
&= Ri(t) + 0 \\
&= R \cdot I_M
\end{aligned}
\tag{A.19}
$$

Appendix B

SIRIUS circuit diagram

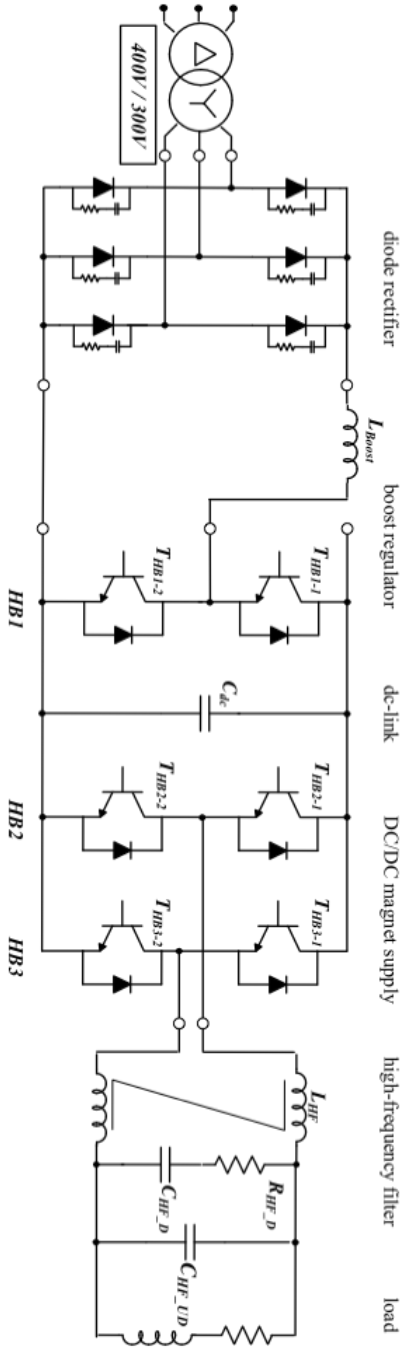

Figure B.1: Circuit diagram of a single SIRIUS converter.

ISBN 978-82-326-7526-5 (printed ver.)
ISBN 978-82-326-7525-8 (electronic ver.)
ISSN 1503-8181 (printed ver.)
ISSN 2703-8084 (online ver.)

NTNU

Norwegian University of
Science and Technology